RESULTS AND DISCUSSION

A. Deformation in Steady Shear Flow

1. Observations of Droplet Deformation

We first consider system A, in which both matrix and droplet phases are highly elastic with a G' ratio of 0.7 at ω = 0.5 rad/s. A shear rate of 0.5 s^{-1} and a droplet size of 75 ($\pm$10%) μm were selected for study at a well-controlled temperature (147°C). We observed that the shape of the deformed drop, Def*, under steady shear flow oscillates before attaining a steady state shape, as shown in Figs. 5 and 6. We divide the transient deformation into 5 regimes. In the first regime, a*, the principle axis projected in the flow direction, shown in Fig. 5 (c), oscillates with a periodicity of around 10 sec, while c, the length of the principle axis in the vorticity direction, shown in Fig. 5 (d), does not change from its initial value until near the end of regime 1. From the absence of a variation in c, we infer that this oscillation may arise from a droplet tilting or rotation around the vorticity (z) axis as shown schematically in Fig. 7. Eventually, near the end of regime 1, while it is still tilting or rotating, the droplet begins to contract in the z-θ plane, and the c axis increases slowly. In the second regime, the drop gradually elongates in the vorticity direction, and after around 500 sec (or 250 strain units) elongation in the vorticity direction reaches its maximum at the end of this regime. At the maximum |Def*| between the regime 2 and 3, as shown in Fig. 5 (a), the c axis is much larger than its initial value so that $c/D_0 \sim 1.35$, while the a axis returns to a length nearly equal to its initial value [Fig. 5 (c)]. From volume conservation, this implies that the droplet is flattened in the z direction, as shown in Fig. 8. However, the deformed drop is not stable at this point because in regime 3, the droplet rapidly contracts in the vorticity direction; see Fig. 5 (d). While contracting in the vorticity direction and stretching occur along the flow direction, cusps emerge out of each side of the droplet along the vorticity axis, as can be seen in Figs. 6 (k) and (l). After 1000 strain units have been imposed, the droplet stretches in the vorticity direction again (regime 4) until a steady-state shape is attained at around 2000 strain units in the fifth regime, as shown in Fig. 5 (b).

These phenomena do not occur in system B, whose droplet and matrix phase elasticities are both lower than in system A, but whose elasticity ratio of droplet to matrix phase is higher than in system A, as shown in Table 3 and Figs. 1 and 2. When a constant shear rate of 0.4 s^{-1} is applied to system B, the deformation parameter rises rapidly from zero to around 0.09, and then slowly and roughly exponentially decreases with time until attaining a steady-state value shown in Fig. 9. This finding is similar to that of Mighri and Huneault (2001) who reported that under a strong shearing flow, an elastic droplet in a Newtonian matrix rapidly stretches along the flow direction, and then gradually contracts in this direction after the first normal stress difference in the droplet has developed sufficiently. Our Fig. 9 is very similar to Fig. 7a of Mighri and Huneault, except that in the latter, the droplet eventually becomes aligned in the vorticity rather than in the shear direction; i.e., the deformation parameter becomes negative. We also obtain negative steady-state values of Def* for system B at higher values of Ca (as will be presented below). The similarity between our results for system B in a torsional plate-plate flow and the results of Mighri and Huneault in a circular Couette flow implies that the unusual oscillatory droplet deformation we observe for system A is not an artifact of our system geometry. We speculate that the oscillations arise only in blends for which both phases are highly elastic, and occur because the different growth periods for the first normal stress differences of the two phases produce time-delayed imbalances in the normal stress conditions on the droplet surface.

2. Effect of Ca on Droplet Deformation.

In this section, the elasticity of the droplet and matrix phases are held constant by holding the shear rate fixed at 0.5 s^{-1}. At this shear rate, where the G' ratio for blend A at ω = 0.5 rad/s is 0.7, we selected various initial droplet sizes to vary the capillary number at a fixed droplet/matrix elasticity ratio. The deformation parameter Def* vs. time from the 2nd to 5th regimes of the 52, 79,110 and 120 μm-drops is shown in Fig. 10 (a). It can be seen in Fig. 10 (b) that between the second and the fourth regimes, droplets with higher Ca show a greater deformation in the

flow direction (larger a^*/D_o). However, for all Ca values in these experiments, nearly the same value of c/D_o is reached at its minimum point at the boundary between regimes 3 and 4, as shown in Fig. 10 (c). For Ca values of 5 and 8, steady shapes are attained at strains around 1300 and 2000 (times of 2600 and 4000 secs), respectively, with larger droplet deformations (more negative Def*) occurring with increasing capillary number. The larger droplets with diameters of 110 and 120 μm (higher capillary numbers of 11 and 12), do not attain steady-state shapes. For these droplets, the vorticity axis, c, rapidly increases for a long period and the axis in the flow direction (a^*) slightly decreases until the drops eventually break [Fig. 10 (b) and (c)].

3. Effect of Elasticity on Droplet Deformation

To investigate the effect of elasticity in system A, the capillary number was kept constant at 8 and the shear rate and drop size were varied inversely with respect to each other. Shear rates of 0.28, 0.5, and 0.8 s^{-1} were chosen and the droplet sizes used for these shear rates were 135 (2 runs), 70-79 (repeated experiments), and 45 μm, respectively. Fig. 11 (a) shows that there is a significant decrease in the maximum value of Def* vs. t (at a strain of around 900) as the shear rate (and hence the elasticity) increases. As shown in Figs. 11 (b) and (c), this decrease results mainly from a decrease in a^*/D_o, rather than an increase in c/D_o. The steady-state value of Def* in regime five is nearly the same for all shear rates.

B. Steady-State Deformation and Droplet Breakup Mechanism

The strains required to attain steady state at each shear rate were determined at shear rates of 0.3 and 0.5 s^{-1} for system A, and at 1 s^{-1} for system B. By increasing the droplet size, the capillary number was varied. As shown in Fig. 12, when Ca increases, the steady-state deformation *in the vorticity direction* increases; i.e., Def* becomes more negative. This contrasts with the behavior of a Newtonian system where the steady-state deformation *in the flow direction* increases *monotonically* with Ca [Taylor (1934), Tsakalos *et al.* (1998), Guido and Villone (1998)]. Fig. 12 shows that a droplet in both systems starts to stretch in the vorticity direction at Ca

around 3. Whereas Mighri and Huneault (2001), using less viscous liquids, found that at Ca less than 10, an elastic droplet in a Newtonian matrix deforms along the flow direction with steady-state deformation increasing with increasing Ca, until Ca reaches roughly 5, above which the droplet starts contracting in the flow direction. At each value of Ca a droplet in our system B deforms less in the vorticity direction than one in system A (lower |Def*|; see Fig. 12). This might be the result of the generally lower elasticity of system B. At the shear rate of 0.5 s^{-1} in system A, for droplets larger than 92 μm do not attain a steady shape, but the droplet eventually breaks up (see Section part A2 above); this size corresponds to a critical value of Ca for breakup of around 9, where the corresponding value of Def^*_c is around –0.27. In addition, the critical capillary number of system A is somewhat comparable to the steady state critical Ca, which was around 6, in Lerdwijitjarud *et al.* (2002). Their system, PS(drop)/HDPE(matrix), like ours, had a viscosity ratio of unity and an N_1 ratio of around 0.7. A droplet in system B breaks at a higher value of Ca (~ 14) than for system A (~ 9). At the viscosity ratio of unity and N_1 ratio of 2, the steady state critical Ca was found to be around 12 in Lerdwijitjarud (2002). This is slightly less than Ca_c of system B. As shown in Fig. 2, the elasticity ratio (G'_r at the selected shear rate) of system B is 3-4 times higher than that of system A, which might account for the difference in critical capillary numbers for systems A and B. An alternative explanation might be that the weaker elasticity of system B produces less deformation in the vorticity direction than that of system A at the same capillary number, and hence a greater shear rate is required to stretch droplets in system B to produce rupture. If this latter explanation is correct, then droplets with intermediate elasticity, high enough to avoid elongation in the flow direction, but low enough to avoid large elongations in the vorticity direction, will be most resistant to rupture and will break at the highest capillary number.

In our more elastic blend A, when a constant shear rate above Ca_c is applied, a spherical drop deforms non-monotonically until regime five is reached and the droplet then elongates continuously in the vorticity direction until breakup occurs as shown in Figs. 10 (a), (b), and (c). The droplet breaks when its two ends are quite far apart and no longer located on nearby streamlines, as shown in Fig. 13. Mighri and

Huneault (2001) found that in a counter-rotating circular Couette cell, a viscoelastic droplet breaks when its two ends separated along the vorticity direction develop unstable motions because of large velocity differences between the two moving layers. A similar instability may occur in our flow.

We note that we could find no clear correlation in the literature or in our data between droplet Weissenberg number and re-orientation or break-up. The effect of elasticity may involve a complicated interplay of the first and second normal stress differences of both phases, and may couple to viscosity ratio, shear thinning, and capillary number. Careful experiments in which all these quantities are carefully controlled, along with numerical simulations of viscoelastic droplet deformation and breakup will be needed to obtain a more quantitative picture of these fascinating phenomena.

CONCLUSIONS

We measured the dynamics of deformation of an elastic droplet in an elastic matrix by selecting two blend systems with viscosity ratio near unity, but of different elasticities of both droplet and matrix phases with the Weissenberg number of matrix phase around 0.1-0.5 and of droplet phase around 0.2-0.5. In start up of a steady shear flow, the different elasticities in the polymer blends produce qualitative differences in the droplet deformations that occur before the droplet attains its steady-state shape. In system A with higher elasticity, the deformation oscillates several times before reaching its steady-state shape. In system B with lower elasticity, the droplet first deforms in the shear direction, and thereafter continuously contacts in the flow direction until it reaches its steady-state shape. When the capillary number is increased at fixed shear rate (and hence fixed elasticity) by increasing the droplet size in system A and B, the steady-state droplet shape becomes increasingly elongated in the vorticity direction and develops cusps along the vorticity axis. In this system A, at still higher capillary number, droplet breakup occurs when two ends of a drop elongated in the vorticity direction are situated on streamlines of different velocity which pull the droplet ends apart, leading to rupture.

ACKNOWLEDGEMENTS

The authors (W.L. and A.S.) would like to acknowledge the financial supports: the Thailand Research Fund (TRF), grants no. BRG/12/2544 and BRG4680015, and the Petroleum and Petrochemical Technology Consortium grant.

REFERENCES

Almusallam AS, Larson RG, Solomon MJ (2000) A constitutive model for the prediction of ellipsoidal droplet shapes and stresses in immiscible blends. J Rheol 44:1055-1083

Bartram E, Goldsmith HL, Mason SG (1975) Particle motions in non-Newtonian media. Rheol Acta 14:776-782

Branrup J, Immergut EH (1989) Polymer Handbook. 3rd Ed., New York

Bentley BJ, Leal LG (1986) An experimental investigation of drop deformation and breakup in steady, two-dimensional linear flows. J Fluid Mech 167:241-283

Grace HP (1982) Dispersion phenomena in high viscosity immiscible fluid systems and application of static mixers as dispersion devices in such systems. Chem Eng Commun 14:225-227

Graebling D, Muller R, Palierne JF (1993) Linear viscoelastic behavior of some incompatible polymer blends in the melt. Interpretation of data with a model of emulsions of viscoelastic liquids. Macromolecules 26:320-329

Guido S, Villone M (1998) Three-dimensional shape of a drop under simple shear flow. J Rheol 42:395-415

Hobbie EK and Migler KB (1999) Vorticity elongation in polymeric emulsions. Phys Rev Lett 82:5393-5396

Larson RG (1999)The structure and rheology of complex fluids. Oxford University Press, New York

Lerdwijitjarud W, Sirivat A, Larson RG (2002) Influence of elasticity on dispersed-phase droplet size in immiscible polymer blends in simple shearing flow. Polym Eng Sci 42:798-809

Lerdwijitjarud W, Larson RG, Sirivat A, Solomon MJ (2003) Influence of weak elasticity of dispersed phase on droplet behavior in sheared polybutadiene/ Poly(dimethylsiloxane) blends. J Rheol 47:37-57.

Levitt L, Macosko CW, Pearson SD (1996) Influence of normal stress difference on polymer drop deformation. Polym Eng Sci 36:1647-1655

Luciani A, Champagne MF, Utracki LA (1997) Interfacial tension coefficient from the retraction of ellipsoidal drops. J Polym Sci, Part B: Polym Phys 35:1393-1403

Mighri F, Ajji A, Carreau PJ (1997) Influence of elastic properties on drop deformation in elongational flow. J Rheol 41:1183-1201

Mighri F, Carreau PJ, Ajji A (1998) Influence of elastic properties on drop deformation and in shear flow. J Rheol 42:1477-1490

Mighri F, Huneault MA (2001) Dispersion visualization of model fluids in a transparent Couette flow cell. J Rheol 45:783-797.

Migler KB (2000) Droplet vorticity alignment on model polymer blends. J Rheol 44:277-290

Palierne JF (1990) Linear rheology of viscoelastic emulsions with interfacial tension Rheol Acta 29:204-214

Rumscheidt FD, Mason SG (1961) Particle Motions in Sheared Suspensions. XII. Deformation and burst of fluid drops in shear and hyperbolic flow. J Coll Sci 16:238-261

Taylor GI (1932) The viscosity of a fluid containing small drops of another fluid. Proc R Soc A138:41-48.

Taylor GI (1934)The formation of emulsions in definable fields of flow. Proc R Soc A146:501-523.

Tsakalos VT, Navard P, Peurel-Disdier E (1998) Deformation and breakup mechanisms of single drops during shear. J Rheol 42:1403-1417

Wu S (1987) Formation of Dispered phase in incompatible polymer blends-interfacial and rheological effects. Polym Eng Sci 27:335-343

Yamane H, Takahashi M, Hayashi R, Okamoto K (1998) Observation of deformation and recovery of poly(isobutylene) droplet in a poly(isobutylene)/poly(dimethyl siloxane) blend after application of step shear strain. J Rheol 42:567-580

TABLE

Table 1 Properties of polymer blend components

Polymer	Suppliers	Grade	M_w*	Melt Flow Index* (g/10min)
PS1	Polyscience	Cat#18544	50,000	-
PS2	Polyscience	Cat#23637	800-5,000	-
HDPE1	Bangkok Polyethylene	1600J	-	14
HDPE2	Aldrich	Cat#42,801-9	-	42

* Quoted by the manufacturers

Table 2 Polymer blend systems

Blend system	Blend components (Drop/Matrix)	Temperature (°C)	Γ (mN/m)
A	PS1/HDPE1	147	5.79
B	PS2/HDPE2	139	5.92

Table 3 The rheological data of blend systems

Blend System	Shear Rate (s^{-1})	Matrix				Droplet			
		η*	N_1†	G'	W_i††	η	N_1	G'	W_i††
A	0.28	2524	403	135	0.38	2426	-	70	0.21
	0.3	2505	435	145	0.39	2425	-	79	0.22
	0.5	2340	772	247	0.42	2340	-	179	0.31
	0.8	2175	1359	400	0.46	2272	936	359	0.40
B	1.0	612	-	34.2	0.11	619	-	64.7	0.21

- not measurable

* η unit is Pa.s

† N_1, G' unit is Pa

†† The Weisenberg number was calculated from the relation $Wi \equiv (2G') / [\eta(\dot{\gamma}).\dot{\gamma}]$

FIGURE CAPTIONS

Figure 1 Viscosity η, storage modulus G', and first normal stress difference N_1 as functions of shear rate and frequency for each pure polymer at the temperatures at which the blend experiments were carried out: (a) matrix phase HDPE1 at 147°C, η (●), G' (o), and N_1 (○), HDPE2 at 139°C, η (■) and G'(□); and (b) droplet phase PS1 at 147°C, η (▲), G' (△), and N( ), PS2 at 139°C: η (◆) and G'(◇).

Figure 2 Values of droplet to matrix ratios of viscosity η (●), storage modulus G' (o), and first normal stress difference N_1 (▲) for (a) system A PS1/HDPE1 at 147°C; and (b) system B, PS2/HDPE2 at 139°C.

Figure 3 Dependence of apparent interfacial tension value on droplet size for: (a) system A; and (b) system B, as inferred from the Palierne formula, Eq. 4.

Figure 4 Schematic drawing of a single drop observed from the "side" and "top" views by optical microscopy, a and b: the long and short axes of the droplet in the flow-gradient plane, a^* : the a axis projected into the flow direction and c: the principal axis in the radial direction.

Figure 5 The time-dependent deformation of 75 (±10%) μm-drops after startup of steady shear at a rate, 0.5 s^{-1}, for system A. (a) Def* vs. time on a log time scale, (b) Def* vs. time on a linear time scale, (c) a^*/D_o vs. time on a log time scale, and (d) c/D_o vs. time on a log time scale. [initial droplet sizes (μm): 76 (●), 68 (⊙), 74 (▼), 69 (▽), 71 (■), 85 (⊡), 76 (◆), 75 (◈), 74 (▲), 70 (◬), and 79 (●)]

Figure 6 Sequence of images of deformed droplets of initial radius 75 (±10%) μm-after startup of a steady shear at a rate of 0.5 s^{-1} for system A; (a)-(f) images of different droplets with lens magnification of 20x [D_o = 69, 69, 71, 76, 75, and 74 μm, respectively]; (g)-(p) images of a single droplet with the lens magnification of 4x [D_o = 79 μm].

Figure 7 Schematic drawing of droplet rotation in the flow-gradient plane.

Figure 8 Sketch of a steady-state deformed droplet.

Figure 9 Time-dependent deformation of a 204 μm-droplet under constant shear rate, 0.4 s^{-1}, for system B.

Figure 10 Time-dependent droplet deformation at different values of Ca, controlled by changing the droplet diameter D_o [D_o = 52 μm; Ca = 5 (●), D_o = 79 μm; Ca = 8 (o), D_o = 110 μm; Ca = 11 (▼), D_o = 120 μm; Ca = 12 (v)] at the same shear rate 0.5 s^{-1} (and therefore the same elasticity) for system A: (a) Def*, (b) a^*/D_o, and (c) c/D_o.

Figure 11 Time-dependent droplet deformation at different shear rates (and therefore different elasticities), at a capillary number Ca of 8, held fixed by varying the initial droplet diameter inversely with the shear rate for system A: (a) Def* vs time, (b) a^*/D_o vs time, and (c) c/D_o vs time. Three different shear rates were used. (1): $\dot{\gamma}$ = 0.28 s^{-1}, with D_o = 135 μm (▲) and a repeat run at this shear rate with the same droplet size, D_o = 135 μm (△)]. (2): $\dot{\gamma}$ = 0.5 s^{-1}: D_o = 70 μm (●), and a repeat run with a slightly larger droplet, D_o = 79 μm (o). (3) $\dot{\gamma}$ = 0.8 s^{-1}, D_o = 45 μm (■)].

Figure 12 Dependence of steady-state deformation parameter on Ca for system A: shear rate 0.3 s^{-1} (○), shear rate 0.5 s^{-1} (▲), and for system B: shear rate 1 s^{-1} (□)].

Figure 13 Sequence of images during droplet breakup in system A, D_o= 120 μm, at a shear rate of 0.5 s^{-1} (Ca=12). The flow direction is horizontal, and the vorticity direction vertical.

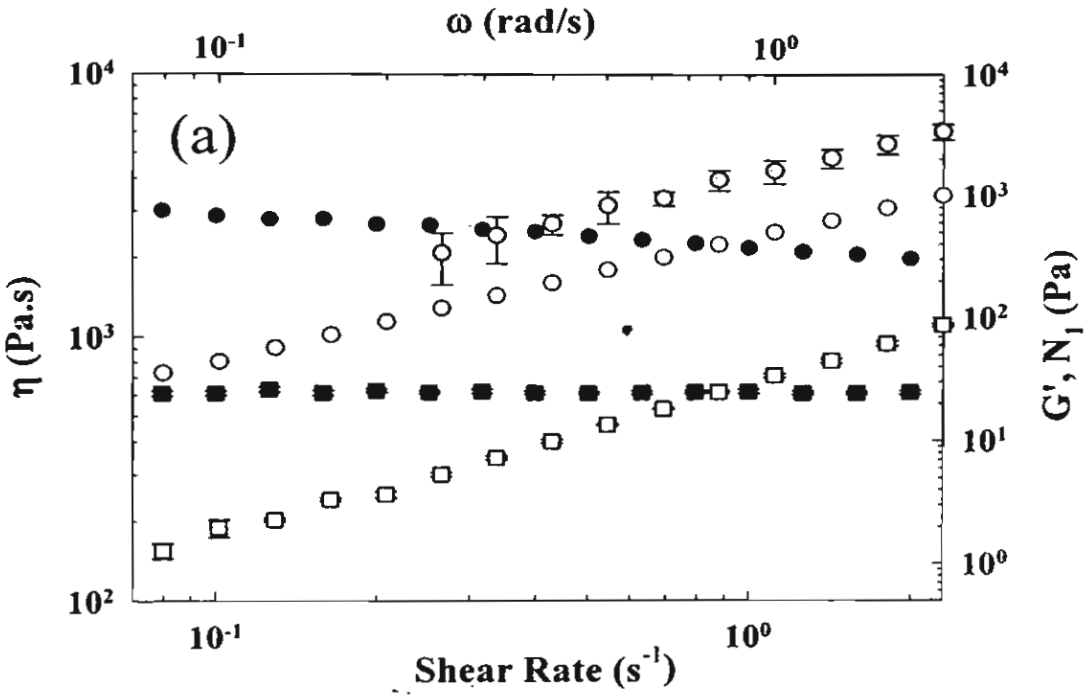

Figure 1 (a)

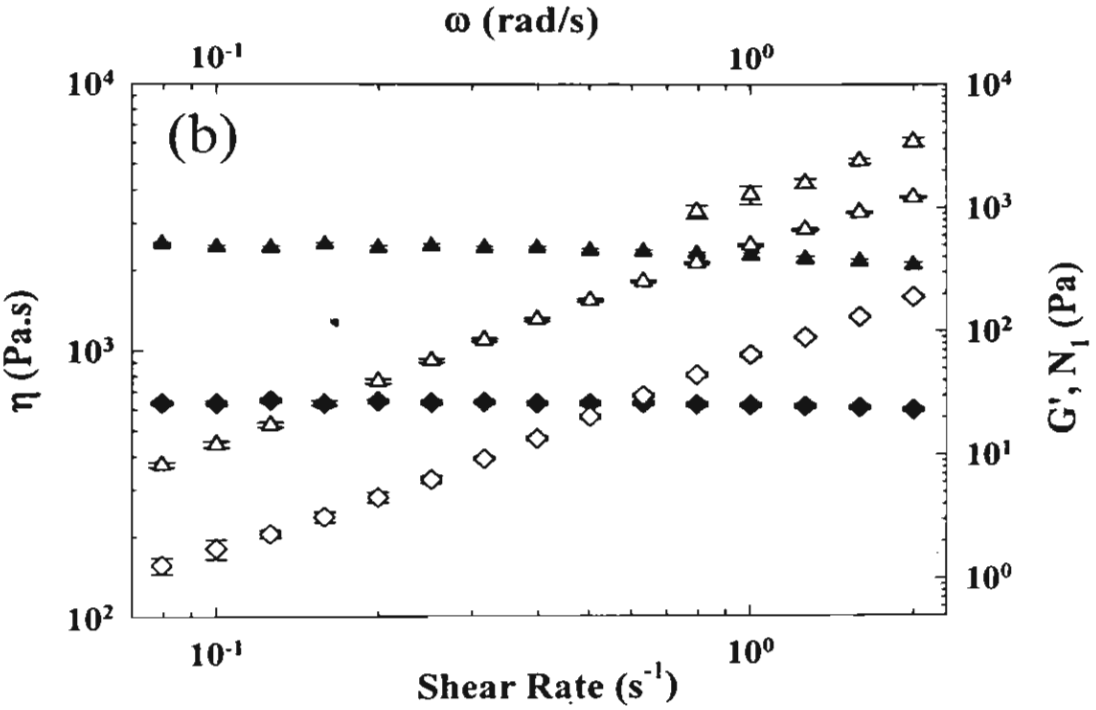
ω (rad/s)
10⁻¹
10⁰
10⁴
10³
10²
(b)
η (Pa.s)
G', N₁ (Pa)
10⁴
10³
10²
10¹
10⁰
10⁻¹
10⁰
Shear Rate (s⁻¹)

Figure 1 (b)

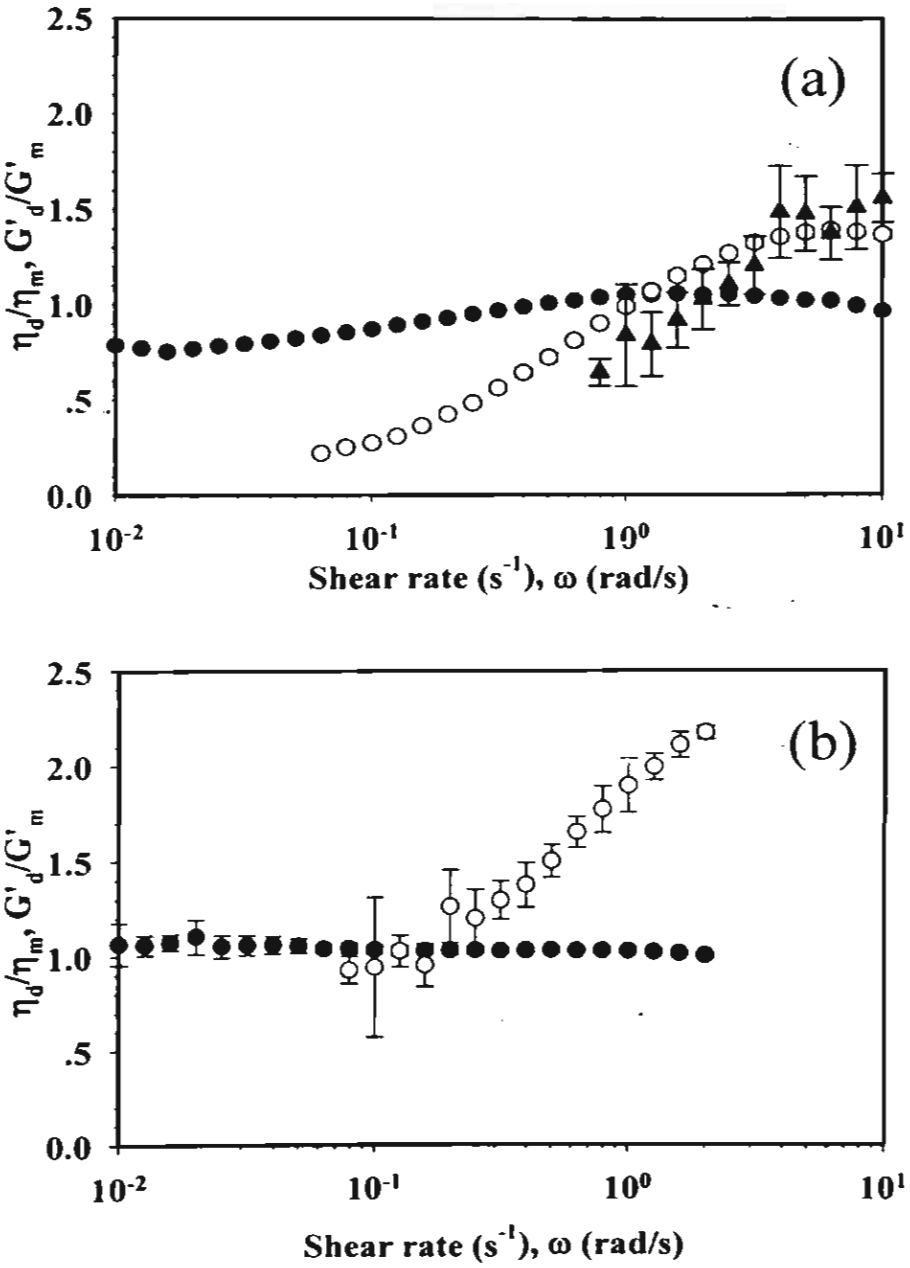

Figure 2 (a) and (b)

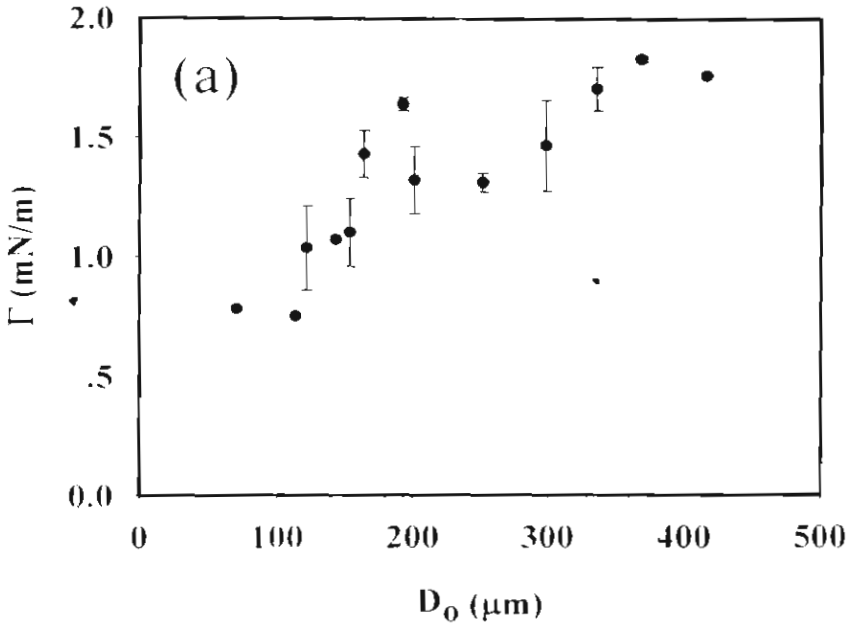

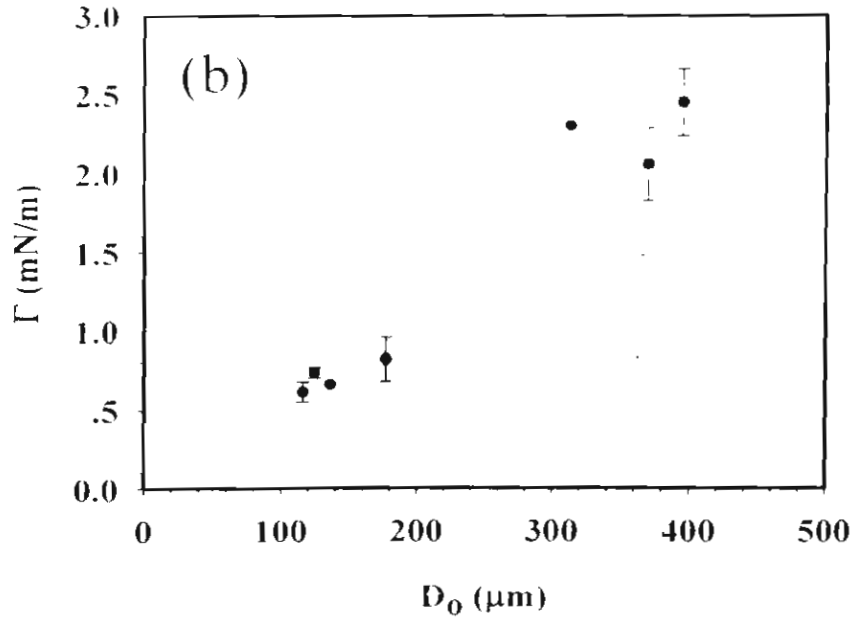

Figure 3 (a) and (b)

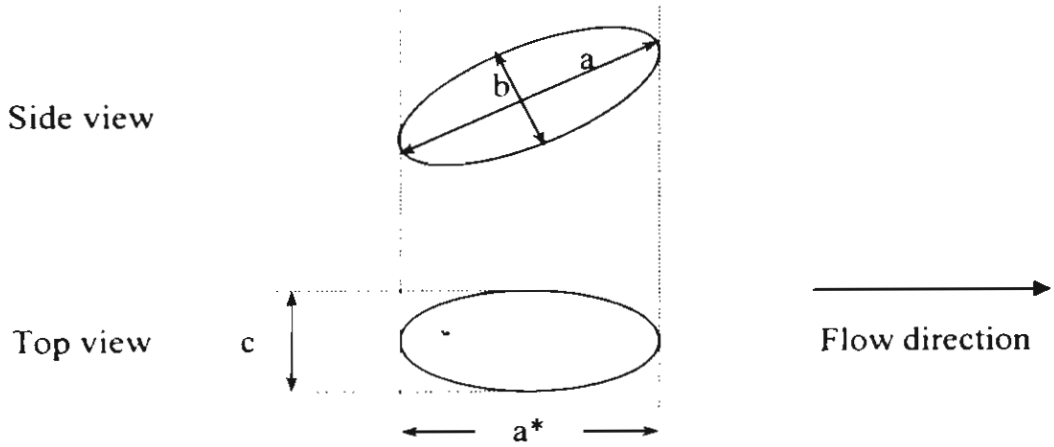

Figure 4

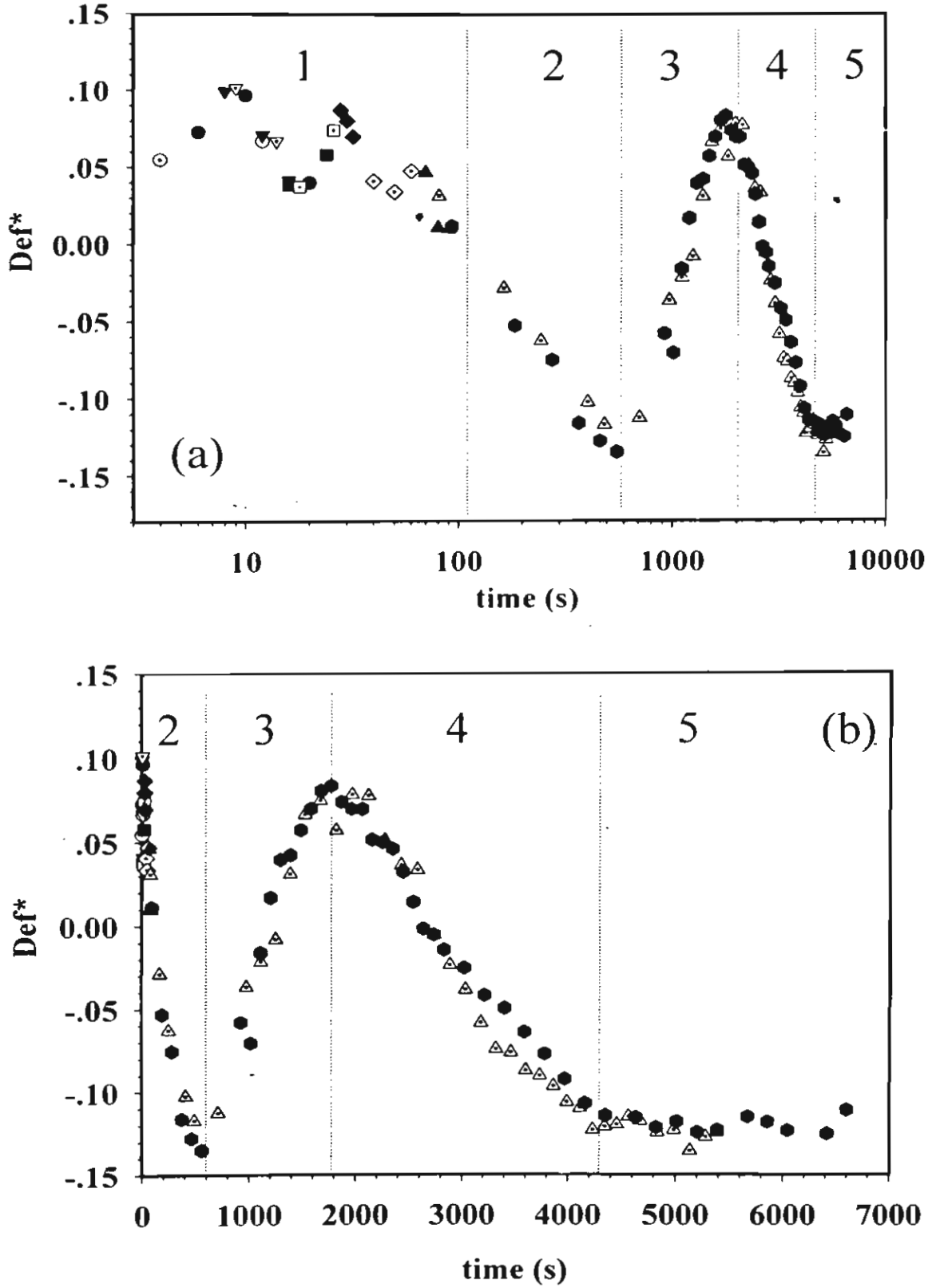
.15
.10
.05
0.00
-.05
-.10
-.15
Def*
1
2
3
4
5
(a)
10
100
1000
10000
time (s)
2
3
4
5
(b)
0
1000
2000
3000
4000
5000
6000
7000
time (s)

Figure 5 (a), (b)

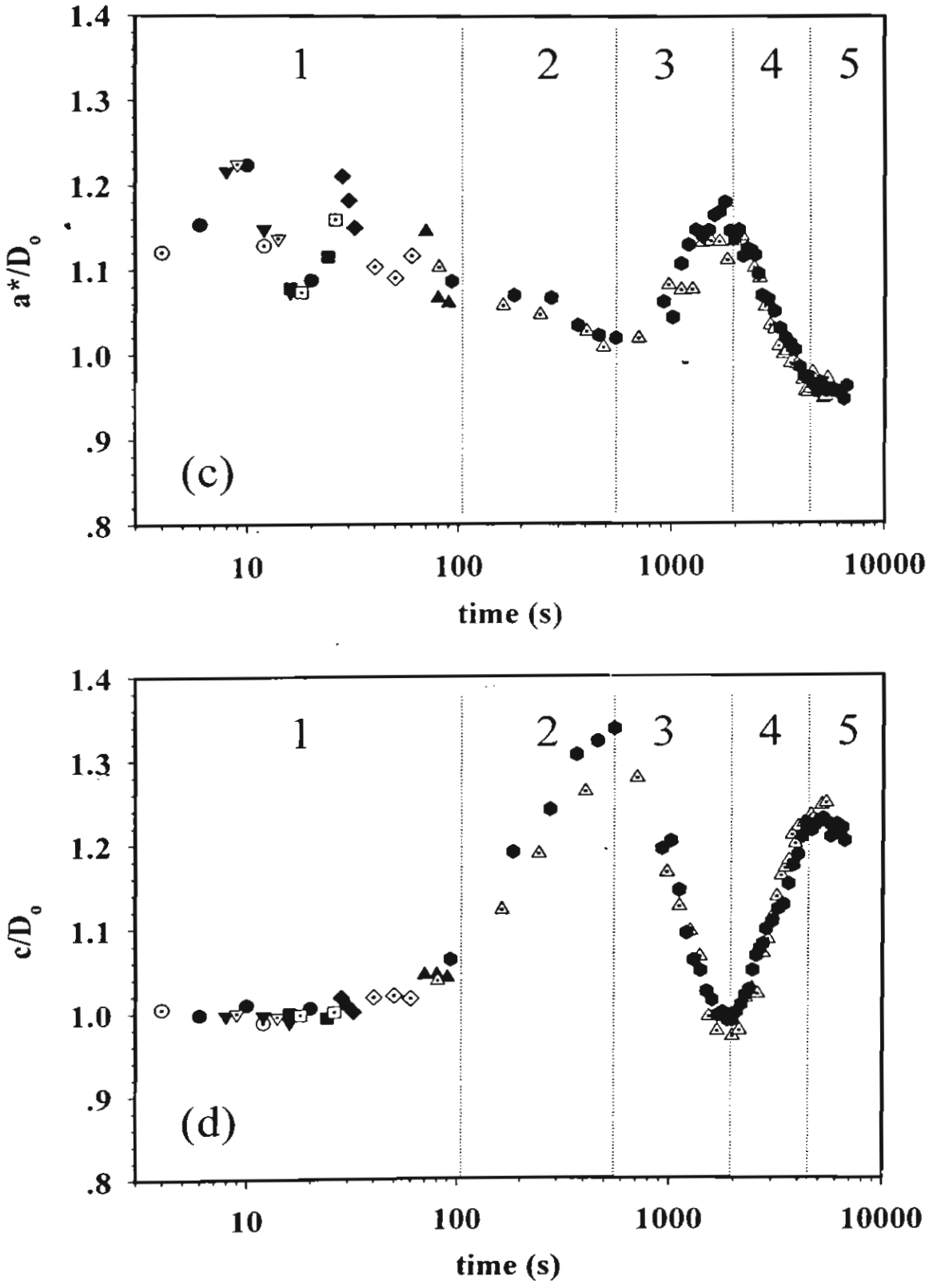

Figure 5 (c), (d)

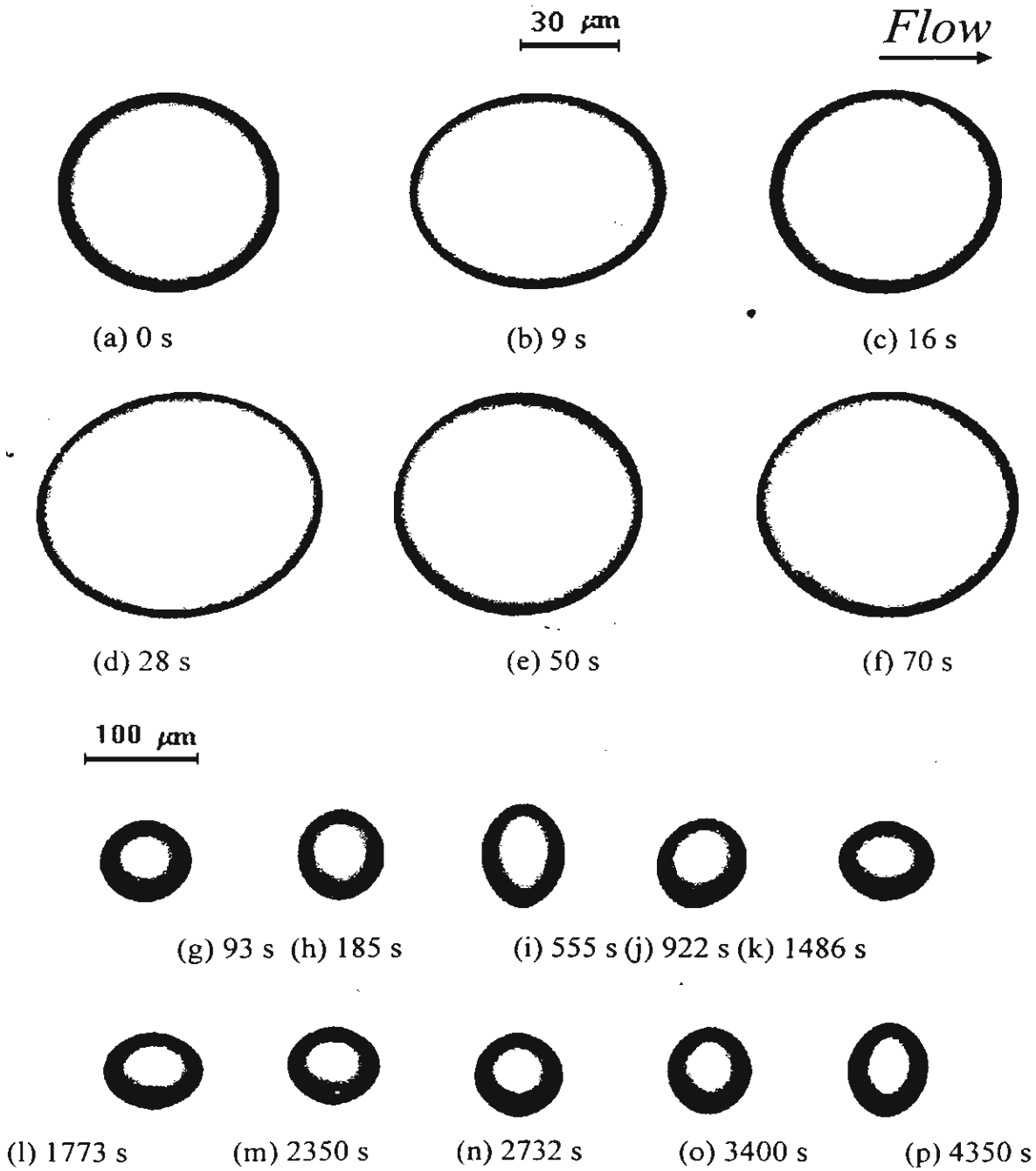
30 μm
Flow
(a) 0 s
(b) 9 s
(c) 16 s
(d) 28 s
(e) 50 s
(f) 70 s
100 μm
(g) 93 s
(h) 185 s
(i) 555 s
(j) 922 s
(k) 1486 s
(l) 1773 s
(m) 2350 s
(n) 2732 s
(o) 3400 s
(p) 4350 s

Figure 6

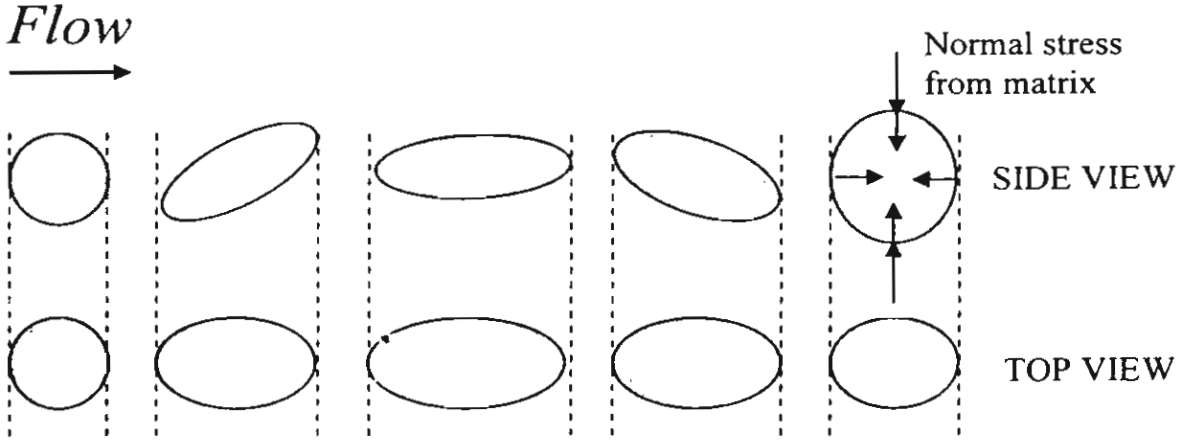

Figure7

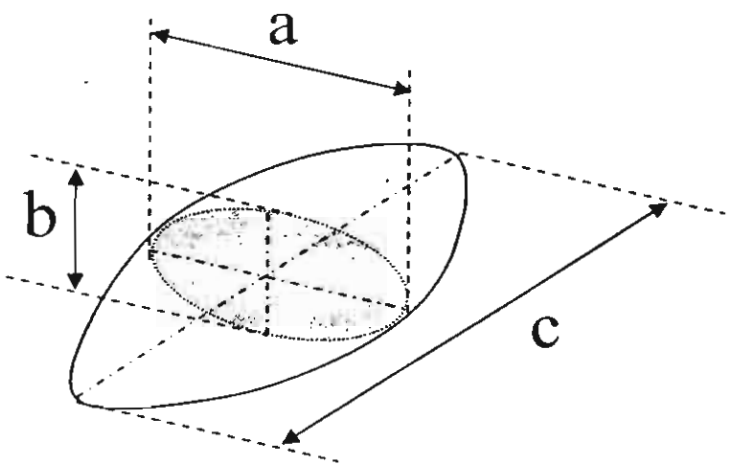

Figure 8

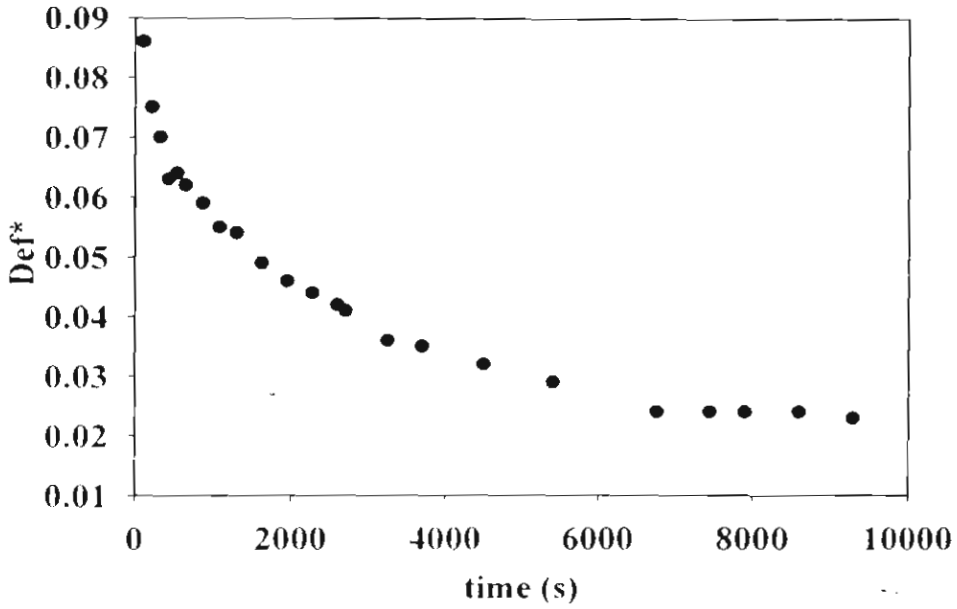
0.09
0.08
0.07
0.06
0.05
0.04
0.03
0.02
0.01
Def*
0
2000
4000
6000
8000
10000
time (s)

Figure 9

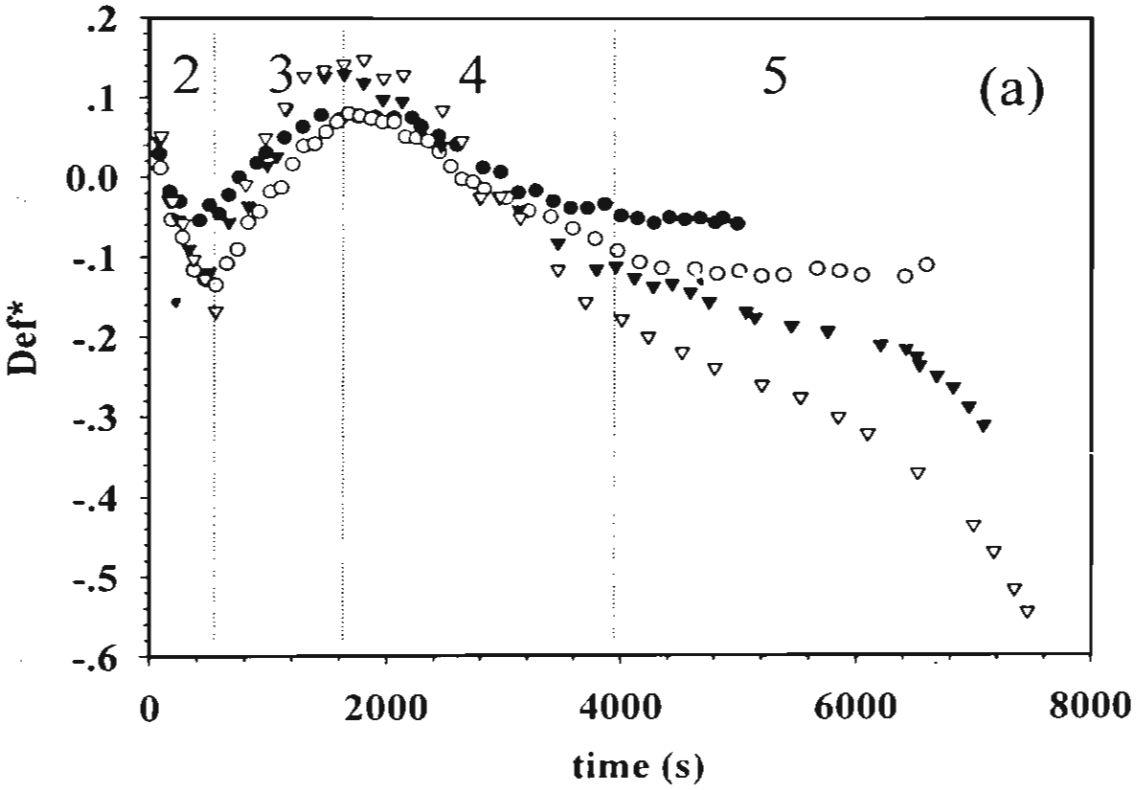

Figure 10 (a)

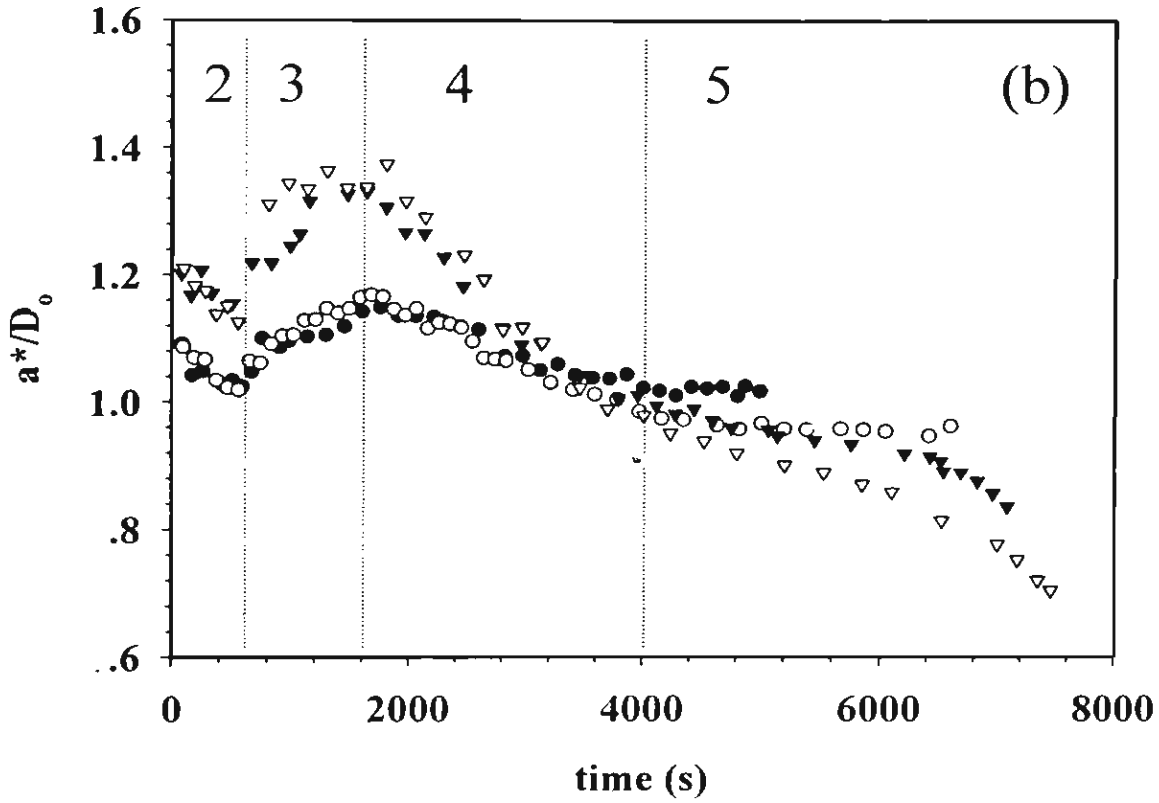
1.6
1.4
1.2
1.0
.8
.6
a*/D0
2
3
4
5
(b)
0
2000
4000
6000
8000
time (s)

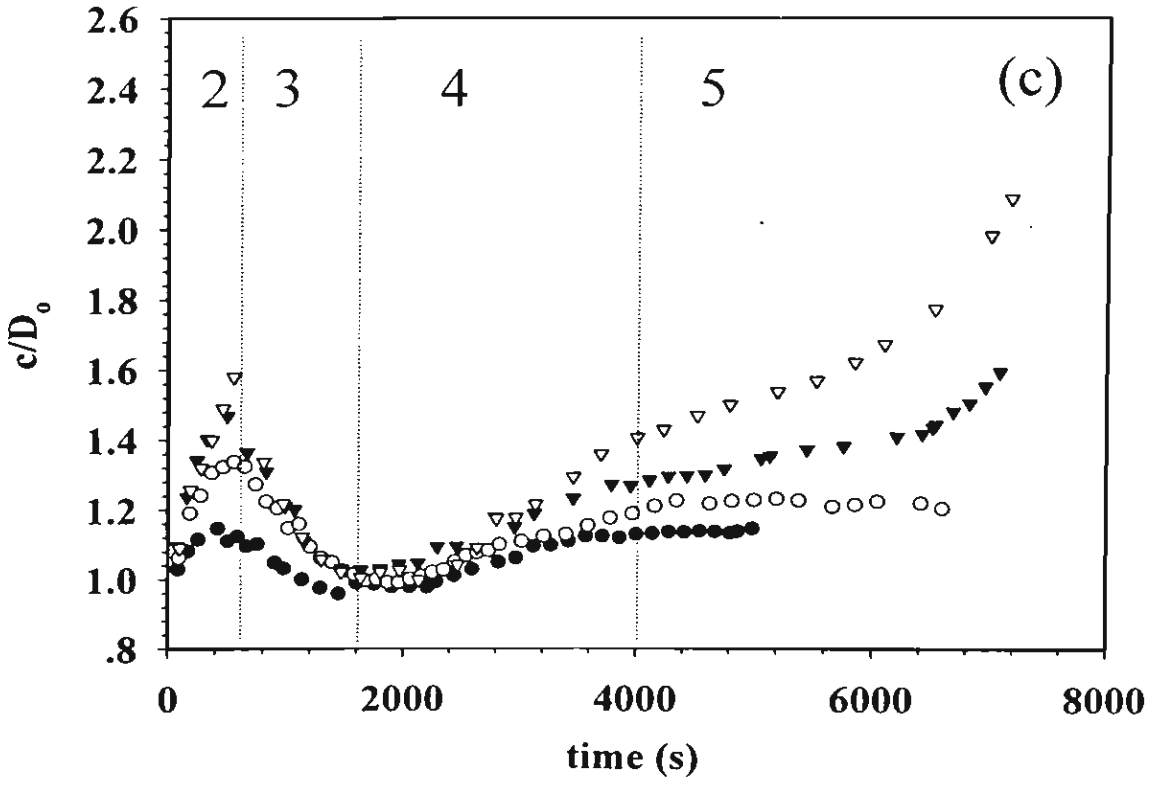
2.6
2.4
2.2
2.0
1.8
1.6
1.4
1.2
1.0
.8
c/D0
2
3
4
5
(c)
0
2000
4000
6000
8000
time (s)

Figure 10 (b), (c)

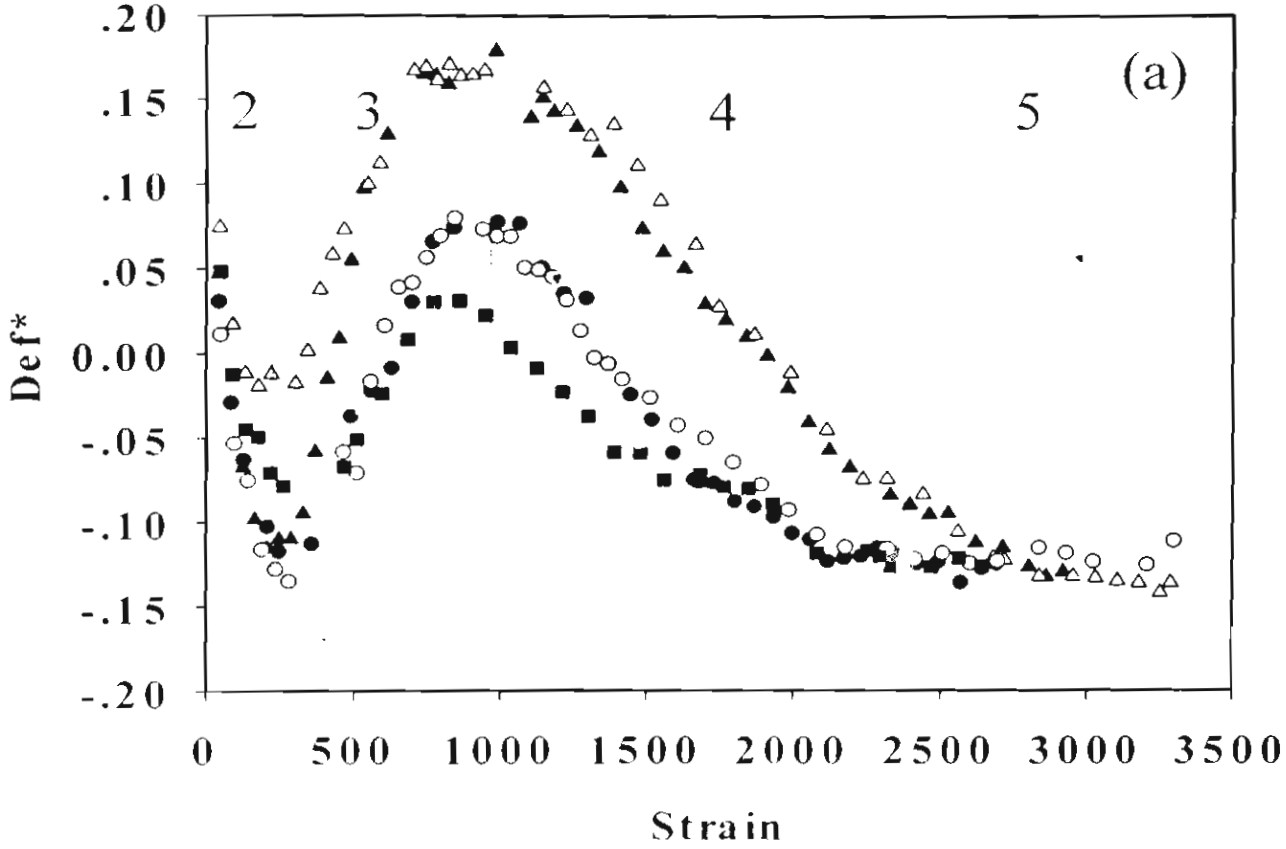
.20
.15
.10
.05
0.00
-.05
-.10
-.15
-.20
Def*
2
3
4
5
(a)
0
500
1000
1500
2000
2500
3000
3500
Strain

Figure 11 (a)

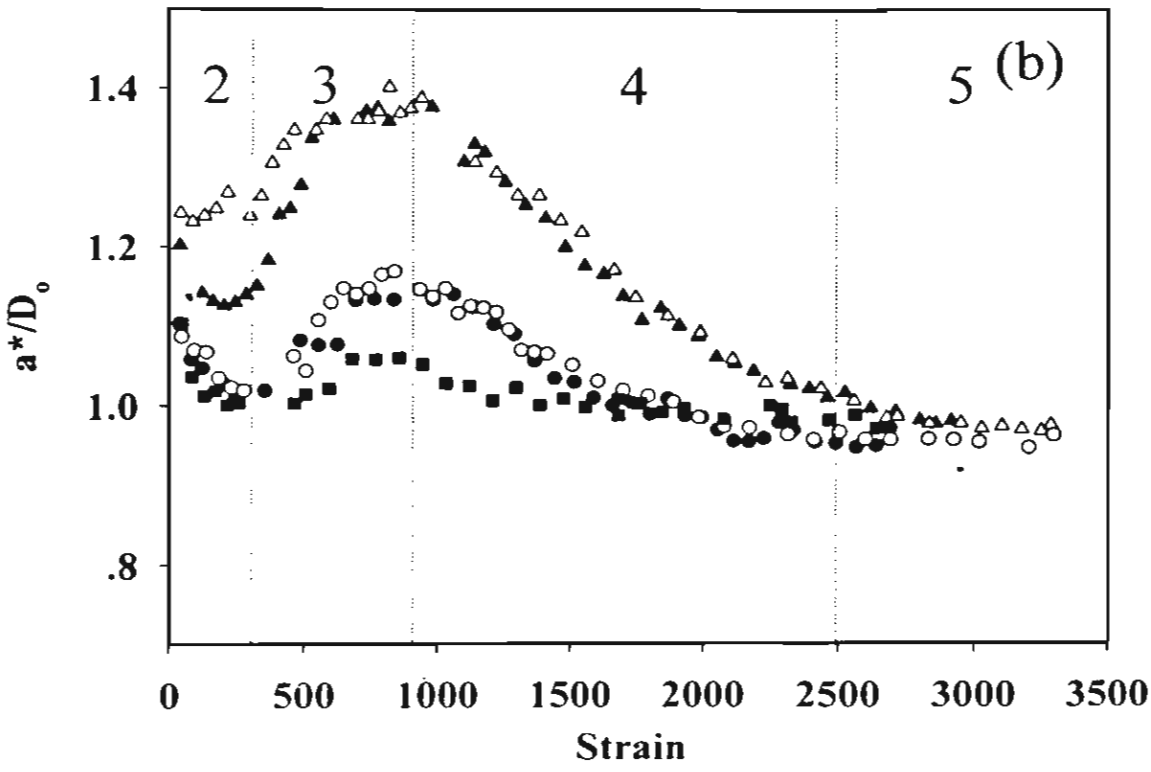
2
3
4
5
(b)
1.4
1.2
1.0
.8
a*/D$_o$
0
500
1000
1500
2000
2500
3000
3500
Strain

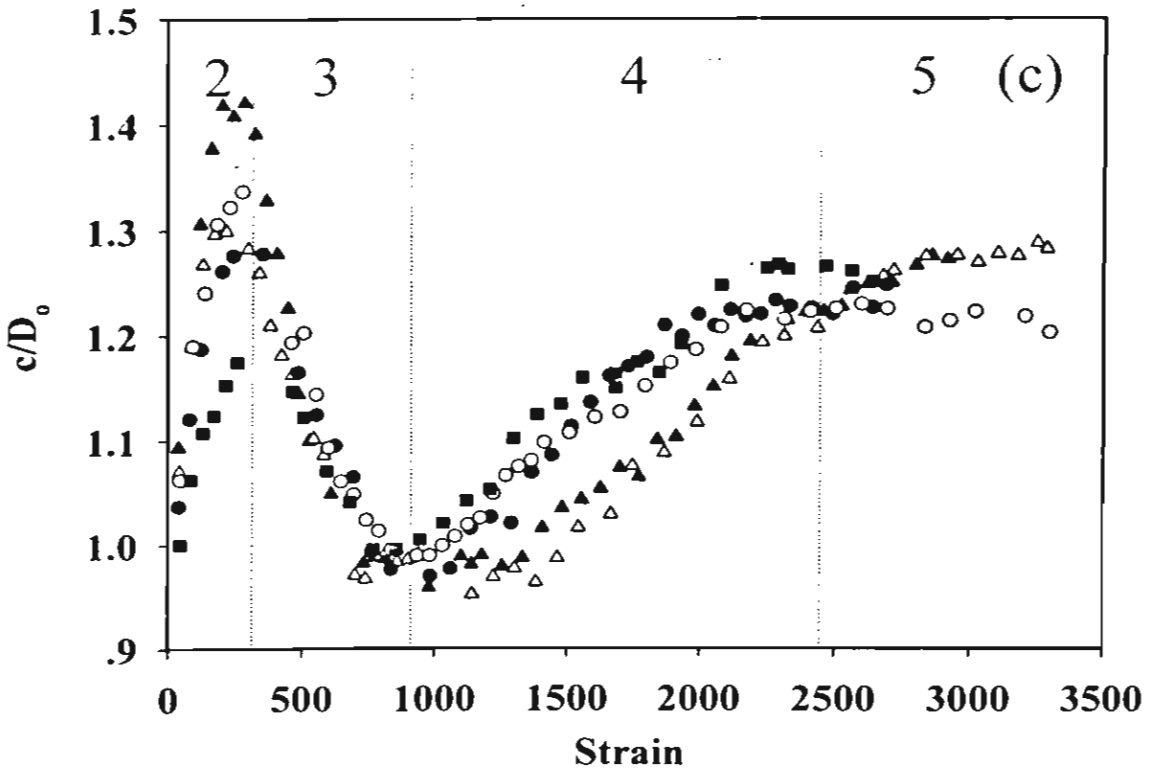
2
3
4
5
(c)
1.5
1.4
1.3
1.2
1.1
1.0
.9
c/D$_o$
0
500
1000
1500
2000
2500
3000
3500
Strain

Figure 11 (b), (c)

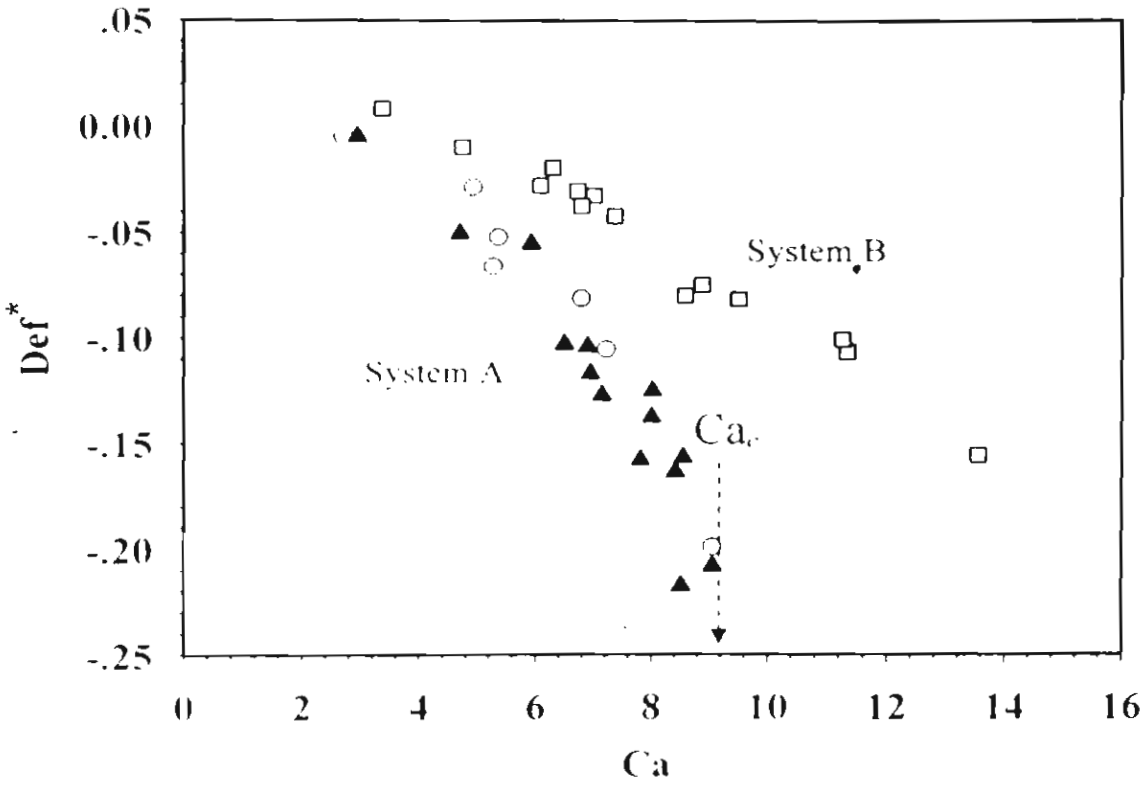
.05
0.00
-.05
-.10
-.15
-.20
-.25
Def*
0
2
4
6
8
10
12
14
16
Ca
System B
System A
Ca_c

Figure 12

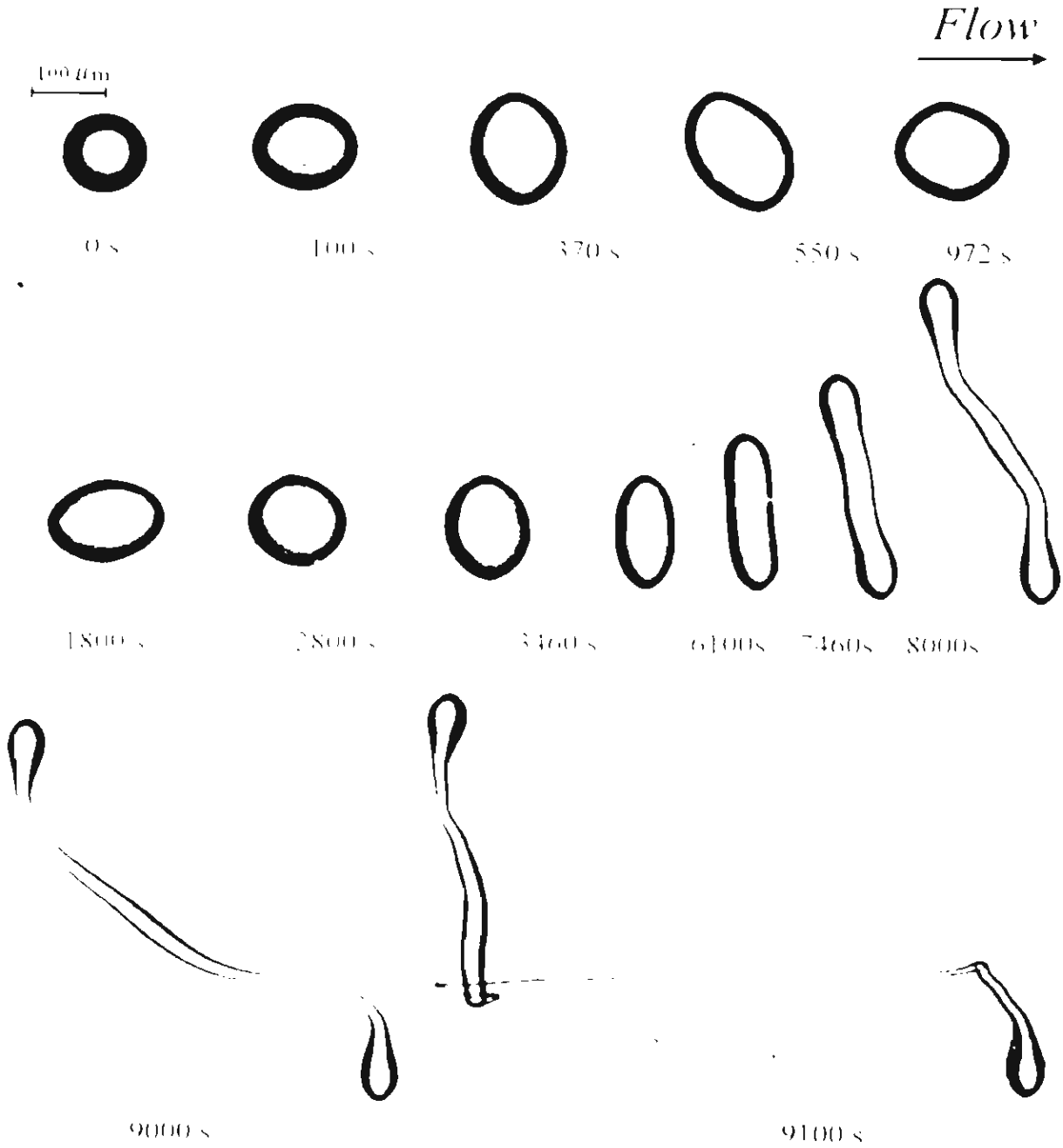
Flow
100 μm
0 s
100 s
370 s
550 s
972 s
1800 s
2800 s
3460 s
6300s
7460s
8000s
9000 s
9100 s

Figure 13

Chapter 4: Transient and Steady State Deformations and Breakup of Dispersed–Phase Droplets of Immiscible Polymer Blends in Steady Shear Flow

Puritat Tanpaiboonkul [a], Wanchai, Lerdwijitjarud [b], Anuvat Sirivat [a #], and Ronald G. Larson [c]

[a] Conductive and Electroactive Research Unit, The Petroleum and Petrochemical College, Chulalongkorn University, Bangkok 10330, Thailand

[b] Department of Materials Science and Engineering, Faculty of Engineering and Industrial Technology, Silpakorn University, Nakhon Pathom 73000, Thailand

[c] Department of Chemical Engineering, University of Michigan, Ann Arbor, Michigan 48109, USA

 # Corresponding author, Email: anuvat.s@chula.ac.th

Transient and Steady State Deformations and Breakup of Dispersed–Phase Droplets of Immiscible Polymer Blends in Steady Shear Flow

Abstract

Transient and steady-state deformations and breakup of viscoelastic polystyrene droplets dispersed in viscoelastic high density polyethylene matrices were observed in a simple steady shear flow between two transparent parallel disks. By separately varying the elasticities of the individual blend components, the matrix shear viscosity, and the viscosity ratio, their effects on the transient deformation, steady-state droplet size, and the breakup sequence were determined. After the startup of a steady shear flow, the viscoelastic droplet initially exhibits oscillations of its length in the flow direction, but eventually stretches preferentially in the vorticity direction. We find that at fixed capillary number, the oscillation amplitude decreases with, increasing droplet elasticity, while the oscillation period depends primarily on, and increases with, the viscosity ratio. At steady-state, the droplet length along the vorticity direction increases with increasing capillary number, viscosity ratio, and droplet elasticity. Remarkably at a viscosity ratio of unity, the droplets remain in a nearly undeformed state as the capillary number is varied between 2 to 8, apparently because under these conditions a tendency for the droplets to widen in the vorticity direction counteracts their tendency to stretch in the flow direction. When a critical capillary number, Ca_c, is exceeded, the droplet finally stretches in the vorticity direction and forms a string which becomes thinner and finally breaks up, provided that the droplet elasticity is sufficiently high. For a fixed matrix shear stress and droplet elasticity, the steady-state deformation along the vorticity direction and the critical capillary number for breakup both increase with increasing viscosity ratio.

I. INTRODUCTION

Because of its importance in polymer processing, there has been considerable work on low Reynolds numbers shear-induced droplet deformation and breakup in blends of immiscible liquids, including blends of polymeric liquids. Taylor (1932, 1934) predicted that for an isolated Newtonian droplet in steady simple shearing flow of a surrounding immiscible Newtonian fluid in the small-deformation limit, two dimensionless parameters control the droplet deformation behavior. The first parameter is the viscosity ratio between the two phases;

$$\eta_r = \eta_d / \eta_m \qquad (1)$$

where η_d and η_m are the viscosities of the droplet phase and the matrix phase, respectively. The second dimensionless parameter is a capillary number, Ca:

$$Ca = \frac{\eta_m \dot{\gamma} r_0}{\Gamma} \qquad (2)$$

where $\dot{\gamma}$ is the applied shear rate, r_0 is the undeformed droplet radius, and Γ is the interfacial tension between dispersed and matrix fluids. Taylor also predicted that the deformation parameter, Def, depends on Ca and η_r according to

$$Def \equiv \frac{a-b}{a+b} = Ca \frac{19\eta_r + 16}{16\eta_r + 16} \qquad (3)$$

where a and b are lengths of the major and minor axes of the deformed droplet, respectively. The capillary number is the ratio of the matrix viscous force ($\eta_m \dot{\gamma}$) to the interfacial stress (Γ/r_0). Correspondingly, for a given droplet and matrix fluid pair, there exists a critical capillary number, Ca_c at which the droplet ruptures in a flow

field. For simple shear flow, the shape of the curve Ca_c vs. η_r is well known; at $\eta_r \approx 1$ Ca is minimumized at $Ca_c \cong 0.5$, while Ca_c becomes infinite at $\eta_r > 4$ so that droplets are stable at all capillary numbers [Taylor (1932,1934); Grace (1982); De Bruijn (1989)]. Other correlations between Ca_{crit} and η_r have also been reported [Rallison and Acrivos (1978); Bentley and Leal (1986)].

The non-Newtonian viscoelastic behavior of common high-molecular-weight polymer blends is expected to influence the droplet deformation and breakup. Working out a quantitative relationship between viscoelasticity and droplet deformation and breakup is a complicated task, however, because viscoelasticity is manifested in various ways, including first and second normal stress differences for both matrix and droplet fluids, and shear thinning in viscous and elastic properties of both fluids. Most experimental studies of droplet deformation and breakup with viscoelastic droplet and matrix fluids have been carried out with little or no systematic control that might allow the influence of one aspect of viscoelasticity to be assessed with others held fixed. However, from many experimental studies one can infer the general behavior that the elasticity of the droplet fluid inhibits droplet deformation causing the droplet to break at a higher capillary number, while elasticity of the matrix phase tends to destabilize the droplet causing it to break at a lower capillary number [De Bruijn (1989); Elmendrop and Maalcke (1985); Varanasri *et al.* (1994); Mighri *et al.* (1997, 1998); Lerdwijitjarud *et al.* (2004)].

In an effort to better control the contributions of fluid viscoelasticity, some studies have chosen only one of the fluids (either matrix or droplet fluid) to be viscoelastic, with the other being Newtonian. Further control can be exerted by choosing for the viscoelastic fluid a so-called "Boger fluid," which is a weakly elastic dilute polymer solution in a Newtonian matrix. Boger fluids have the virtue of

possessing little or no shear thinning in the shear viscosity, and ideally also in the first normal stress coefficient. Studying a blend of a Boger fluid as the droplet phase in a Newtonian matrix fluid at a viscosity ratio of unity, Lerdwijitjarud *et al.* (2004) found that Ca_c increased linearly with Wi_d up to a value of Wi_d of around unity, and thereafter approached an asymptotic value of around unity for high values of Wi_d. Here the dispersed phase Weissenberg number, Wi_d, is defined as $Wi_d(\dot{\gamma}) \equiv [\Psi_{1d}(\dot{\gamma})/2\eta_d(\dot{\gamma})].\dot{\gamma}$, where $\Psi_{1d}(\dot{\gamma})$ is the first normal stress difference coefficient of the dispersed phase at an imposed shear rate $\dot{\gamma}$.

Studies with Boger fluids have generally only revealed rather modest effects of viscoelasticity on the deformation and breakup of droplets, relative to what is seen in Newtonian fluids. Namely one can observe a modest change (a factor of two or so) in Ca_c, but the droplets deform in the flow direction to a similar degree as in blends of Newtonian droplet and matrix fluids. For highly elastic melts, very large increases are observed (more than a decade) in the capillary number required for droplet breakup. Moreover, for some melts, a new mode of droplet deformation, namely transient and steady-state droplet widening or elongation along the vorticity axis, has been observed for viscoelastic droplets sheared in viscoelastic matrices [Levitt *et al.* (1996); Hobbie and Migler (1999); Migler (2000); Mighri and Huneault (2001); Cherdhirankorn *et al.* (2004)]. Experimental work showing this widening phenomenon was reviewed earlier [Cherdhirankorn *et al.* (2004)]. Here it suffices to note that droplet widening has only been observed in blends containing viscoelastic melts, with one exception. Mighri and Huneault (2001) studied the deformation and breakup mechanisms of droplets composed of viscoelastic Boger fluid in a Newtonian matrix (PDMS). At low shear rates, they found that the dispersed drop was oriented along the flow field

and drop deformation increased with shear rate, as expected. However, when a critical shear rate was reached [$Ca_c \approx 5.5$], the deformed drop began to contract in the flow direction. After increasing the shear rate above this critical value, drop contraction occurred, followed by elongation perpendicular to the flow direction. This elongation increased with shear rate until breakup occurred. In our studies with polybutadiene Boger fluids (Cerdwijitjarud *et al.* 2004], we did not observe droplet widening over the range of Weissenberg numbers and capillary numbers we were able to access, despite using very high molecular weight polybutadienes (M_w above one million) at concentrations high enough (1%) to produce significant shear thinning.

In an effort to access more significant effects of elasticity than could be obtained using Boger fluids, Cherdhirankorn *et al.* (2004), studied blends of shear-thinning polymer melts with properties and temperatures chosen to maintain the viscosity ratio near unity at the shear rates used. Viscoelastic modes of transient droplet deformation and droplet extension in the vorticity direction were reported for isolated droplets in two immiscible polymer blends (PS/HDPE) of equal viscosity in a simple shearing flow. In the blend with high elasticity of matrix and dispersed phases, the droplets initially deformed in the flow direction after startup of a steady shear but then began reverting to a spherical shape, and eventually deformed in the vorticity direction. In the second, low-elasticity system, the droplets first deformed in the shear direction, and thereafter continuously contracted in the flow direction until they reached their steady-state shapes. The droplets eventually deformed preferentially along the vorticity direction with increasing capillary number. Above a critical capillary number, breakup occurred whose mechanisms critically depended on the droplet elasticity.

The new work reported here extends the previous study of Cherdhirankorn *et al.* by considering the effect of the viscosity ratio, as well as capillary number and droplet elasticity on isolated droplet deformation and breakup. In addition, we seek to determine if a blend system exists in which droplet deformation does not occur over a certain range of capillary number. Our earlier work [Cherdhirankorn *et al.* (2004)] suggested that such behavior might be exhibited under conditions in which the tendency of the droplet to stretch in the flow direction due to viscous forces is balanced by a tendency to deform in the vorticity direction due to elasticity, leading to a state of almost no deformation over a range of shear rates. Such a condition of shearing flow with no droplet deformation or breakup might be useful if spherical, or unusually large, droplets are desirable under a shearing flow, or might be a condition to avoid if the opposite is true.

II. EXPERIMENTS

A. Materials

The materials used in this study are two grades of high-density polyethylene (HDPE1 and HDPE2) as the matrices. Three grades of polystyrene (PS1 PS2, and PS3) are used as the dispersed phases. The properties of all polymers are tabulated in Table 1. Polystyrene resins were prepared by crushing them into small pieces and their sizes were selected by passing the flakes though a 425 μm sieve. All polymers were heated at 80°C under vacuum for 12 hours to eliminate any volatile substances.

B. Rheological Characterization

The steady-state shear viscosity and the first normal stress difference of each polymer were measured by a cone-and-plate rheometer (ARES, Rheometric Scientific) using a 25-mm diameter plate and a cone angle of 0.1 rad. Figures 1 and 2 show rheological properties of the polymers chosen in our study. Four pairs of polymers and operating temperatures were chosen in our study. Table 2 lists the polymers and the four blend systems (A,B,C, and D) investigated in this work, chosen to have viscosity ratios of somewhat greater than unity (2.6), less than unity (0.5), and unity. The interfacial tension values for the polymer blend systems were taken from the handbook [Brandrup and Imergut (1989)]: 5.84 mN/m for System A at 143°C, 5.60 mN/m for System B at 155 °C, 5.92 mN/m for System C at 139 °C, and 5.79 mN/m for System D at 147 ^{O}C.

C. Observation of an Isolated Droplet in Shearing Flow

1. Shearing Apparatus

To generate a simple shear flow and to observe droplet behaviors, we used a commercial flow cell device (Linkam CSS 450, Linkam Scientific Instruments Ltd., UK) with two quartz parallel disks attached to an optical microscope (Leica DMRPX, Leica Imaging Systems Ltd.). The images were recorded by a CCD camera (Cohu 4910, Cohu Inc., USA). The obtained images were analyzed on a computer using the Scion image software (http://www.scioncorp.com).

2. Sample Preparation

HDPE was melted into a disk 25 mm. in diameter and 0.5-1.0 mm. in thickness by compression molding at 140 °C. To load PS droplets into the HDPE matrix, we used a pin to put a small amount of PS powder onto the HDPE disk, and then covered this with another HDPE disk to form a sandwich. The sandwich was then placed onto the bottom disk and covered with the top disk of the flow cell. The sample was held at the testing temperature until complete melting occurred.

3. Optical Microscopy of Isolated Droplets

Droplet deformation and subsequent relaxation from its deformed ellipsoidal shape were observed using an optical microscope at a magnification that depended on

the droplet size. Around 100 to 200 droplet images were recorded (10-20 seconds per frame).

Since the images of the deformed droplet were captured only in the plane perpendicular to the shear gradient direction, the true length of the major principle axes of the ellipsoidal droplet could not be determined directly. The lengths of all three principle axes can, however, be calculated from a planar image using the known droplet volume provided that we know the orientation angle (θ), i.e., the angle between the major axis and the flow direction. Lacking this orientation angle, we followed our earlier work [Cherdhirankorn *et al.* (2004)] and used the apparent observable lengths of the principle axes to describe the behavior of each droplet by defining a modified deformation parameter Def*:

$$\mathbf{Def^* = (a^*-c) / (a^*+c)} \qquad (6)$$

where the asterisk indicates that the deformation parameter is an apparent one obtained from the droplet image projected into the flow-vorticity plane (see Figure 3).

4. Transient Deformation

Due to the limitation of the flow cell, a single droplet can not be observed continuously from startup until it attains a steady-state shape, since this droplet will move out of the viewing plane after imposing a given strain. Since the behavior of a given isolated droplet is assumed to be reproducible, the complete transient deformation history of an isolated droplet of a particular size was determined, as before [Cherdhirankorn *et al.* (2004)], by combining the results of several

experiments with the droplets of nearly equal sizes. In the experiment of type 1, the droplet was moved out of the viewing window by imposing a strain, typically less than 40 strain units (≈ 1 orbit). The droplet was then left to relax for at least 60 minutes. Then the isolated droplet was deformed at the required strain rate for the same strain but in the opposite direction until it moved back into the viewing window where we could image its deformation. In experiments of type 2, the droplet was deformed continuously at a fixed shear rate and images of the droplet were taken whenever the droplet passed through the viewing window. To obtain clear droplet images, we stopped the flow each time the droplet appeared within the viewing window for a period of less than 1 second and an image was taken. This time interval was sufficiently small enough to avoid droplet relaxation; the typical transient time scale for droplet relaxation in our experiments was of order 10^3 seconds. Then, the flow was then initiated again until the droplet passed through the viewing window again. By repeating this procedure, we could assemble a history of deformation from the initial time to the time at which the droplet attained its steady-state shape. The imposed values of capillary number, Ca, were chosen to be 5, 8, and 11 by using droplets of various sizes at a fixed shear rate of 0.4 s^{-1}. To separate the effects of viscous forces from those of elasticity, some experiments were carried out with the capillary number, Ca, held fixed. The elastic force was varied by changing the shear rate, $\dot{\gamma}$, from 0.10, to 0.17, to 0.40, to 0.63 s^{-1} and the corresponding droplet size, $2r_0$, was varied inversely with the shear rate from 290, to 177, to 85, to 56 μm, respectively, so that $Ca = \eta_m \dot{\gamma} r_0/\Gamma$ was fixed at 8.

5. Steady-State Deformation and Breakup

Here, we describe the procedure used to obtain the steady-state shapes of isolated droplets below the critical capillary number for breakup. Generally, the strain required to reach a steady-state droplet shape increases with the droplet size. From several transient experiments, the required strain to reach steady-state droplet shape was found to be approximately 4000 strain units at Ca = 8 and D_0 = 85 ± 5μm. Therefore a constant shear rate was applied until a strain exceeding 4,000 strain units was attained. To ensure that the steady-state deformation had indeed been attained, when a selected droplet passed through the viewing window, the droplet was imaged many times over a period of 5 to 10 min and Def* was measured and determined until its value became constant. Subsequently, the flow was stopped and the droplet shape relaxation was recorded with the CCD camera at speeds of 10-20 second per frame for approximately 90 minutes.

The critical capillary number was determined by finding the smallest droplet size at which drop breakup was observed at a fixed shearing rate at 0.4 s^{-1} for Systems A and C, and at 0.63 s^{-1} for System B.

For droplets for which no steady-state shape was obtained, the unstable shapes of the droplets were recorded until the droplets broke. The breakup process for System A was studied at a fixed capillary number Ca equal to 11 using a shear rate of 0.40 s^{-1}; and for System B, we selected Ca value of 9.5 with shear rates of 0.20 and 0.63 s^{-1}. These shear rates or capillary numbers were slightly above the minimum values needed to achieve breakup for these systems.

Our experiments were carried out at shear rates at which the viscosities and first normal stress coefficients were mildly shear thinning, so the capillary number and Weissenberg number were calculated using the actual viscosity and first normal stress difference at which the experiments were performed.

III. RESULTS AND DISCUSSION

Figure 4a shows a sequence of optical images during the transient droplet deformation for blend System A, with $\eta_r = 2.6$, $Ca \approx 8$ and $Wi_d \approx 0.30$. Here, the drop stretches at first along the flow direction, and later along the vorticity direction. It nearly recovers its spherical shape at a time of around 6000 s before it stretches again along the flow direction. Finally, it attains its steady state shape by contracting along the flow direction and stretching along the vorticity direction.

A. Transient Deformation in Steady Shear Flow

1 Effect of Imposed Capillary Number on Droplet Deformation

Here we describe the effect of imposed capillary number, Ca, on the transient droplet deformation, over a strain period between 40 and 4000 for blend System A. The conditions of the experiment are: a fixed shear rate of 0.4 s^{-1}, a fixed Weissenberg number, Wi_d, of 0.75, a fixed viscosity ratio of 2.6, and imposed capillary numbers, Ca, of 5, 8, and 11 obtained by choosing droplets of sizes equal to 52 (±5), 85 (±5), and 125 (±7) μm, respectively. The parameters of these experiments are tabulated in Table 3.

Figure 5a displays the transient deformation parameter Def* vs. strain between 40 and 4000 at three capillary numbers: 5, 8, and 11. In these experiments, we can divide the deformation evolution into three regimes. Def* initially decreases

towards a local negative minimum at a strain of around 300, in which its amplitude depends on Ca. In the second regime, 300 < strain < 900, Def* increases towards a local maximum whose value is close to zero, or the state of no deformation, at a strain of approximately 900. For strains > 900, Def* decreases and becomes negative until attaining its steady state negative value which depends on Ca: Def^*_{ss} = -0.065 and -0.205 for Ca ≈ 5 and 8, respectively. In the experiment with Ca ≈ 11, Def* eventually decreases to a value of -0.8 before breakup occurs, and therefore Def^*_{ss} does not exist at or above this capillary number. Qualitatively similar oscillations in droplet deformation were reported in our earlier work [Cherdhirankorn *et al.* (2004)].

Figures 5b and 5c show the corresponding evolution of a^*/D_o and c/D_o vs. strain between 40 and 4000. In the first regime, in which 40 < strain < 300, a^*/D_o first increases above unity and then decreases towards a local minimum of less than unity at a strain of 300. In this regime, there is an initial weak flow elongation followed by a shrinkage of the major principle axis to a value below its initial value. In the second regime with 300 < strain < 900, a^*/D_o increases again towards a local maximum whose amplitude depends on Ca at strain 900. In the third regime, where strain > 900, a^*/D_o decreases towards its steady state value equal to 0.96 for both Ca ≈ 5 and 8, or towards its final value of 0.4 before drop breakup at Ca ≈ 11. In the first regime, the deformation c/D_o along the vorticity axis initially rises to a local maximum whose amplitude depends on Ca at a strain of 300. The stretching along the vorticity direction in this regime coincides with the initial period in which the major principle axis goes through an overshoot and shrinks. In the second regime, c/D_o decreases slightly and then monotonically rises towards its steady state values of 1.09 and 1.34 for Ca ≈ 5 and 8, respectively. For Ca ≈ 11, the final value of c/D_o before breakup is equal to 5.2 at the strain of 4073. In summary, at a value of the

dispersed-phase Weissenberg number, Wi_d, equal to 0.75 and a viscosity ratio of 2.6, the evolution of the droplet deformation with time can be divided into three regimes. In the first regime, there is a weak flow elongation followed by a complete recovery along with a slight stretching in the vorticity direction. In the second regime, a flow elongation reappears along with a slight contraction in the vorticity direction. In the third regime, a contraction occurs in the flow direction along with continuous stretching along the vorticity direction until the droplet attains a steady state condition in which Def^*_{ss} is less than zero. The critical capillary number for System A is approximately equal to 11.

2. Effect of Elasticity on Droplet Deformation

Next we investigate the influence of the droplet elasticity on the droplet transient deformation, for System A, whose viscosity ratio was 2.6, the capillary number Ca was fixed at around 8.0, and the shear rate was varied to be 0.17, 0.40, and 0.63 s^{-1} corresponding to droplet Weissenberg numbers of 0.48, 0.75 and 0.99, respectively. In order to keep Ca fixed at around 8.0, the droplet sizes subject to these shear rates were chosen to be 177, 85, and 56 (±2) μm, respectively.

Figure 6a shows the evolution of Def* vs. strain of droplets subject to three Weissenberg numbers: 0.48, 0.75, and 0.99. Table 3 summarizes the experimental parameters of this experiment. Similar to the results of Figure 5a, there also exist three regimes of the transient deformation when Wi_d is varied with Ca held fixed. The local maxima at a strain of around 900 and the steady state Def* value depends on Wi_d. The negative minimum Def* values at the end of the first regime are equal to -0.10. The positive maximum Def* values at the end of the second regime are 0.109, 0.032 and 0.019, respectively, for Wi_d equal to 0.48, 0.75, and 0.99. The

corresponding steady state negative Def* values are -0.230, -0.205 and, -0.142 respectively. Therefore, it appears that the steady state Def* becomes less negative with increasing droplet elasticity, while the amplitude of the positive maximum Def* decreases with increasing droplet elasticity. Figure 6b shows the corresponding evolution of a^*/D_o vs. strain. The amplitude of the local maximum decreases with increasing Wi_d, but the final steady state value of a^*/D_o is about 0.88, independent of Wi_d. This behavior should be contrasted with the evolution of c/D_o in figure 6c, where the amplitudes of the local maximum and the steady state value of c/D_o decrease with increasing Wi_d.

3. Effect of Viscosity Ratio on Droplet Deformation

To investigate the effect of viscosity ratio on the droplet transient deformation, experiments were carried out with the capillary number, Ca, fixed at 8.0 and the Weissenberg number, Wi_d, fixed at 0.30. The Systems A, B and D were investigated whose experimental conditions and rheological properties are tabulated in Table 4.

Figure 7a compares the evolution of Def* of Systems B, D, and A whose viscosity ratios are 0.5 and 1.0, and 2.6 respectively. The magnitudes of the local minima of Def* for the three experiments appear to be nearly the same at -0.12, and all minima occurred at the strain of 300. However, the locations of the local maxima are at strains of 600, 900, and 1,400, respectively and the corresponding maxima of Def* are 0.16, 0.08, and 0.14, respectively. At first, it may seem surprising that the maxima and their locations are not the same for all three systems, given the fact that the capillary number, Ca, was held fixed at 8.0 and the Weissenberg number, Wi_d,

was also fixed at 0.30. The likely explanation may not lie with the viscosity ratio itself; rather the deformation is controlled by the competition between the matrix shear force which tends to deform the drops, in particular along the flow direction, and the drop elasticity which generally resists droplet deformation and induces a retarded complex flow within droplet. These two competing types of force vary with time presumably at different rates after the startup of shearing. We also find that the steady state Def^*_{ss} value appears to depend somewhat on the viscosity ratio; the Def^*_{ss} values are -0.1, -0.12, and -0.22, respectively for Systems B, D, and A, which are listed in order of increasing viscosity ratio. Figures 7b and 7c show the corresponding evolution of a^*/D_o and c/D_o. We find that the locations for the local maxima in a^*/D_o and the local minima in c/D_o coincide with those of the local maxima in Def* for the three viscosity ratios shown in Figure 7a. Finally, figure 4b shows a sequence of optical images of the transient drop deformation of System B with viscosity ratio equal to 0.5. We may state that a qualitatively similar deformation pattern occurs for both viscosity ratios of 0.5 and 1.0; the only difference appears to be that it takes a shorter time or a smaller strain to reach a steady state for the System B which has a lower viscosity ratio.

B. Steady-State Deformation

The steady-state deformation refers to the final shape of droplets after transient behavior has ceased. Figure 8 shows Def* vs. Ca for Systems A, B, and C and D, corresponding to viscosity ratios of 2.6, 0.5, 1.0, and 1.0, respectively. In these systems, the droplet Weissenberg number, Wi_d, was fixed at 0.35, 0.28, 0.01, and 0.3 respectively. The capillary number of the droplets investigated was varied by

using droplets of various sizes, and thus Wi_d was fixed in each system studied. To determine the steady-state droplet shape as a function of capillary number, a strain sufficient to obtain a steady state shape was imposed. On comparing results for Systems, A, B, and D in Figure 8, it is evident that Def^*_{ss} becomes increasingly negative with increasing Ca and becomes more negative, at a given Ca, with increasing viscosity ratio, η_r. On the other hand, for Systems C and D with the same viscosity ratio equal to 1, we find that Def^*_{ss} becomes more negative with increasing Wi_d. Therefore, droplet elasticity appears to be necessary for droplets to stretch along the vorticity direction, but the viscosity ratio also plays a role in determining the magnitude of the stretching in the vorticity direction. Finally, it is interesting to note that the steady-state values of Def^*_{ss} for System C are quite close to zero and vary slightly as Ca increases from 2 to 8. Thus, it is possible to choose a material system with a fixed viscosity ratio with a corresponding low Wi_d (0.01) value such that droplets do not deform at steady shear rates over a range of values of Ca. For Newtonian fluids (for which $Wi_d = Wi_m = 0$), for $\eta_r = 1$ Def^*_{ss} rises with Ca to a value of around 0.5 at $Ca \approx 0.5$, after which breakup occurs. Thus, even for Wi_d as low as 0.01, droplet deformation in these melts deviates considerably from that in Newtonian fluids.

C. The Critical Capillary Number

The critical capillary number for drop breakup was determined for Systems A, B, and D, corresponding to the viscosity ratios of 2.6, 0.5, and 1.0, respectively. The corresponding fixed Wi_d values are 0.35, 0.28, and 0.30, respectively. In each

system, the shear rate was fixed and drops of various sizes were chosen in order to vary the capillary number.

The critical capillary numbers for droplet breakup, Ca_{crit}, are 10.18, 9.10, and 8.95 for Systems A, D, and B respectively, which have viscosity ratios, η_r, of 2.6, 1.0, and 0.5. The corresponding droplet sizes are 115, 92, and 79 μm, and critical Def^*_c values are -0.40, -0.27, and -0.18. Thus, for comparable Wi_d, Ca_{crit} increases with viscosity ratio over this viscosity ratios. For Newtonian fluids, experimental Ca_{crit} values are 0.5 [Grace (1982)], whereas the predicted Ca_{crit} values are 0.44, 0.46, and 0.47, respectively [Taylor (1932, 1934)]. We were unable to observe the breakup of System C, presumably because the steady state deformation of this system is very small at the shear rates we could access.

D. Droplet Breakup Mechanism

Here, we investigate the droplet breakup sequences of Systems A and B, as shown in Figures 9 and 10. The shear rate applied to System A was 0.40 s^{-1}, $Ca \approx 11$ (slightly above Ca_{crit}) and $Wi_d = 0.75$. For System B, the shear rate used was 0.63 s^{-1}, $Ca \approx 9.5$ (slightly above Ca_{crit}) and $Wi_d = 0.28$. We can see that in both systems, with $\eta_r = 2.6$ and 0.5 under these experimental conditions, the droplets follow oscillation patterns described previously, and eventually break up along the vorticitiy direction. An S shape appears as the final droplet shape before breakup. This S shape presumably arises from the velocity gradient along the radial direction. A minor difference between the breakup patterns of Systems A and B is that, for System B whose viscosity ratio is smaller ($\eta_r = 0.5$), there is a more pronounced stretching along the flow direction.

IV. CONCLUSIONS AND PERSPECTIVE

We reported the transient droplet deformation, under startup of a steady shear flow, for viscoelastic melt blend systems whose viscosity ratios are 0.5, 1.0 and 2.6. The evolution of droplet deformation, Def*, with time can be divided into three regimes: an initial flow elongation followed by contraction, a secondary flow elongation, and a final stretching along the vorticity direction. The magnitudes of the transient maxima and minima of Def* depend on Ca and Wi_d; but the period depends mostly on η_r. For the elastic melt components studied here, the steady-state deformation parameter, Def^*_{ss}, becomes more negative with increasing Ca; it also becomes more negative with increasing Wi_d and η_r at fixed Ca. For η_r fixed at unity, we were able to find suitable experiment conditions, with $Wi_d \approx 0.01$, at which droplets do not deform at steady state, for Ca values ranging up to to 8. Droplets break up along the vorticity direction if Wi_d is sufficiently high.

We also note that the critical value of the capillary number for breakup in the vorticity direction is high, around 8 in our experiments on elastic melt components. As noted in the introduction, for Newtonian fluids, the critical capillary number for breakup in the flow direction is around 0.5, and for weakly elastic droplet fluids with viscosity ratio of unity, this critical capillary number increases to around unity as the dispersed phase Weissenberg number increases to unity. For our melts, and those of Hobbie and Migler (1999), and the solutions of Migler (2000), and Mighri and Huneault (2001), droplet deformation in the vorticity direction is observed and breakup occurs at a much higher critical capillary number, around five or higher. Thus, it appears that viscoelasticity of the droplet phase impedes deformation and

breakup in the flow direction. Elasticity of the droplet and/or matrix phase, if strong enough, can completely block breakup in the flow direction by inducing deformation in the vorticity direction. In this case, breakup can be deferred to much higher capillary numbers, around five or higher.

The conditions required to produce droplet elongation in the vorticity direction are still unclear. For some droplet fluids consisting of dilute or semi-dilute solutions of polymers in a Newtonian matrix (i.e., "Boger fluids"), droplet Weissenberg numbers as high as unity can be reached with no droplet widening, while for the melts studied here, droplet widening is evident for Weissenberg numbers as low as 0.5, and droplet deformation in the flow direction is impeded for one system with a droplet Weissenberg number as low as 0.01. Thus, it seems clear that the droplet Weissenberg number is not the only, or even the most important, variable controlling droplet vorticity stretching. Our studies indicate that the viscosity ratio plays a role, and there have been suggestions in the literatures [Levitt *et al.* (1996); Hobbie and Migler (1999); Migler (2000); Mighri and Huneault (2001)] that the difference in first normal stress difference between the droplet and matrix fluids is important , as are the second normal stress differences of matrix and droplet fluids. To resolve this issue, fluids must be formulated with controlled first and second normal stress differences. Simulation of droplet deformation for viscoelastic droplet and matrix fluids would also help resolve this puzzle. Eventually, correlations of droplet vorticity stretching and breakup with the viscoelastic properties of the fluids are needed so that blends with desired droplet deformation and breakup characteristics can be designed.

ACKNOWLEDGEMENTS

The author, A.S., would like to acknowledge support from the Postgraduate Education and Research Programs in Petroleum and Petrochemical Technology (PTT Consortium), the Conductive and Electroactive Polymers Research Unit (CU-Ratchadapisek), and the financial support from Thailand Research Fund, grant no. BRG4680015.

REFERENCES

1. Arnett RL, Thomas CP. *J. Phys. Chem.* 1980; **84**: 649-652.
2. Bentley BJ, Leal LG. *J. Fluid Mech.* 1986; **167**: 241-283.
3. Brandrup J, Imergut EH. Polymer Handbook, 3rd Ed. New York: 1989.
4. Cherdhirankorn T, Lerdwijitjarud W, Sirivat A, Larson LG. *Rheol Acta* 2004; **43**: 246-256.
5. De Bruijn RA. Ph.D.Thesis, Eindhoven University of Technology, 1989.
6. Elmendorp JJ, Maalcke RJ., *Polym Eng. Sci.*1985; **25**: 1041-1047.
7. Grace HP. *Chem. Eng. Commun.* 1982; **14**: 225-277.
8. Guido S, Villone M. *J. Rheol.*1998; **42**: 395-415.
9. Hobbie EK, Migler KB. *Phys Rev Lett.* 1999; **82**: 5393-5396.
10. Lerdwijitjarud W, Sirivat A, Larson RG. *J. Rheol.* 2004: **48:** 843-862.
11. Levitt L, Macosko CW, Pearson SD. *Polym. Eng. Sci.* 1996; **36**: 1647-1655.
12. Mighri F, Ajji A, Carreau PJ. *J. Rheol.*1997; **41**: 1183-1201.
13. Mighri F, Carreau PJ, Ajji A. *J. Rheol.*1998; **42**: 1477-1490.
14. Mighri F, Huneault MA. *J. Rheol.* 2001; **45**: 783-797.
15. Migler KB. *J. Rheol.* 2000; **44**: 277-290.
16. Rallison JM, Acrivos A. *J. Fluid Mech.* **1978; 89:** 191-200.
17. Taylor GI. *Proc. R. Soc. London*, Ser. A 1932; **138**: 41-48.
18. Taylor GI. *Proc. R. Soc. London*, Ser. A 1934; **146**: 501-523.
19. Varanasri PP, Ryan ME, Stroeve P. *Ind Eng. Chem. Res.* 1994; **33**: 1858-1866.

TABLES

Table 1 Properties of polymers used

Polymer	Suppliers	Grade	M_w
HDPE1	Bangkok Polyethylene	1600J	68,000 [a]
HDPE2	Aldrich	Cat#42,801-9	46,000 [a]
PS1	Polyscience	_	67,000 [b]
PS2	Polyscience	Cat#18544	50,000 [c]
PS3	Polyscience	Cat#23637	800-500[c]

[a] obtained from fitting zero-shear viscosity data with a 3.4-power correlation at 190 °C ($\eta_0 = 5.8 \times 10^{-11} M_w^{3.41}$) as reported by Arnett and Thomas (1980)

[b] measured by gel permeation chromatography based on polystyrene standard calibration

[c] quoted by the manufacturers

Table 2 Polymer blend systems investigated

Blend system	Blend components (Droplet/Matrix)	Temperature (°C)	Viscosity ratio (η_d/η_m)
A	PS1/HDPE1	143	2.6
B	PS2/HDPE1	155	0.5
C	PS3/HDPE2	139	1.0
D	PS2/HDPE1	147	1.0

System D is System A of Cherdhirankorn *et al.* (2004).

Table 3 Experimental parameters for Figure 5, blend System A (PS1/HDPE1), at a shear rate of 0.4 s^{-1}, $W_{i,d}$ = 0.75, and Ca = 5, 8, and 11 obtained by varying the initial droplet size: d_o ≈ 52, 85, and 125 μm; and for Figure 6: blend System A (PS1/HDPE1), Ca ≈ 8, $W_{i,d}$ = 0.48, 0.75 and 0.99 obtained by varying the shear rate, $\dot{\gamma}$ = 0.17, 0.40 to 0.63 s^{-1}.

Shear rate (s^{-1}) / Data	0.17	0.40	0.63
Temperature (°C)	143	143	143
η_d: Viscosity of the droplet phase (Pa.s)	7.620	6.880	6.340
η_m: Viscosity of the matrix phase (Pa.s)	2.870	2.580	2.440
η_r: Viscosity ratio	2.6	2.6	2.6
Γ: Interfacial tension (mN/m)	5.84	5.84	5.84
$N_{1,d}$: First normal stress difference of the droplet phase (Pa)	620	2,080	3,950
$N_{1,m}$: First normal stress difference of the matrix phase (Pa)	208	733	1,230
$N_{1,r}$: First normal stress difference ratio	2.97	2.84	3.21
Ca : Capillary number	≈ 8 [a]	≈ 5, 8, 11 [a]	≈ 8 [a]
D_0 : Initial droplet size (μm)	177	52, 85, 125	56
Wi_d: Weissenberg number of the dispersed phase	0.48 [b]	0.75 [b]	0.99 [b]
Wi_m: Weissenberg number of the matrix phase	0.43 [c]	0.71 [c]	0.80 [c]

[a] $Ca = \frac{D_0 \dot{\gamma} \eta_m}{2\Gamma}$

[b] $Wi_d = N_{1,d}/(\eta_d \dot{\gamma})$

[c] $Wi_m = N_{1,m}/(\eta_m \dot{\gamma})$

Table 4 Experimental parameters for Figures 6 and 8

Blend system(drop/matrix) Data	System A (PS1/HDPE1)	System B (PS2/HDPE1)	System C (PS3/HDPE2)	System D (PS2/HDPE1)
Temperature (°C)	143	155	139	147
Shear rate (s^{-1})	0.10	0.63	0.40	0.50
η_d: Viscosity of the droplet phase (Pa.s)	7,996	964	630	2,323
η_m: Viscosity of the matrix phase (Pa.s)	3,026	2,013	595	2,331
η_r: Viscosity ratio	2.6	0.5	1.0	1.0
Γ: Interfacial tension (mN/m)	5.84	5.60	5.92	5.79
$N_{1,d}$: First normal stress difference of the droplet phase (Pa)	276	168	-	-
$N_{1,m}$: First normal stress difference of the matrix phase (Pa)	78.3	920	-	834
$N_{1,r}$: First normal stress difference ratio	3.53	0.18	-	-
G'_d: Storage modulus of the droplet phase (Pa)	-	-	≈ 1.3	179
G'_m: Storage modulus of the matrix phase (Pa)	-	-	≈ 1.3	248
G'_r: Storage modulus ratio	-	-	1.0	0.72
Wi_d: Weissenberg number of the dispersed phase	0.35	0.28	≈ 0.01	0.31
Wi_m: Weissenberg number of the matrix phase	0.26	0.73	≈ 0.01	0.43

FIGURE CAPTIONS

Figure 1 Viscosity as a function of shear rate of the polymers at the temperatures in which the experiments were carried out: (a) matrix phases; (b) dispersed phases.

Figure 2 The first normal stress difference, N_1, vs. shear rate and the storage modulus, G', vs. frequency for the polymers at the temperatures in which the experiments were carried out: (a) matrix phases; (b) dispersed phases.

Figure 3 Schematic drawing of a single drop observed from the side and top views of the optical microscope; *a* and *b* are the long and short axes of the droplet in the flow-radial plane, *a**, the "apparent axis" is the droplet length projected into the flow direction, and *c* is the principal axis in the radial direction.

Figure 4 Sequence of images of deforming isolated droplets after startup of a steady shear at fixed Ca ≈ 8 and $Wi_d \approx 0.30$: (a) System A, $\eta_r = 2.6$, a shear rate of 0.1 s^{-1}, and $D_0 = 86$ μm; (b) System B, $\eta_r = 0.5$, a shear rate of 0.63 s^{-1}, and $D_0 = 72$ μm.

Figure 5 Transient deformation of isolated droplets of System A vs. strain at a shear rate of 0.4 s^{-1}, $Wi_d = 0.75$, and at various Ca values: Ca ≈ 5, with initial droplet diameter $D_0 = 52$ μm (□); Ca ≈ 8, $D_0 = 85$ μm (○); Ca ≈ 11, $D_0 = 125$ μm (▽). (a) Def* vs. strain; (b) a^*/D_0 vs. strain; and (c) c/D_0 vs. strain.

Figure 6 Transient deformation of isolated droplets of System A vs. strain at fixed Ca ≈ 8, at various shear rates: $\dot{\gamma}$ = 0.63 s^{-1}, $W_{i,d}$ = 0.99 with D_0 = 57 μm (●) and 56 μm (○); $\dot{\gamma}$ = 0.4 s^{-1}, Wi_d = 0.75 with D_0 = 85 μm (▲); $\dot{\gamma}$ = 0.17 s^{-1}, Wi_d = 0.48, D_0 = 177 μm (□). (a) Def* vs. strain; (b) a^*/D_0 vs. strain; and (c) c/D_0 vs. strain.

Figure 7 Transient deformation of isolated droplets of Systems A, B and D vs. strain at fixed Ca ≈ 8 and $W_{i,d}$ ≈ 0.30: η_r = 0.5, $\dot{\gamma}$ = 0.63 s^{-1}, (○): η_r = 1.0, $\dot{\gamma}$ = 0.50 s^{-1}, (●); η_r = 2.6, $\dot{\gamma}$ = 0.40 s^{-1}, (△). (a) Def* vs. strain; (b) a^*/D_0 vs. strain; and (c) c/D_0 vs. strain.

Figure 8 Steady-state deformation parameters vs. capillary number. For Wi_d ≈ 0.30, System A with η_r = 2.6 at a shear rate of 0.1 s^{-1} (△); System D of Cherdhirankorn *et al.* (2004) with η_r = 1.0 at a shear rate of 0.5 s^{-1} (○); and System B with η_r = 0.5 at a shear rate of 0.63 s^{-1} (□). For Wi_d ≈ 0.01, System C, with η_r = 1.0, and a shear rate of 0.4 s^{-1} (▽). Arrows indicate Ca_{crit} of Systems A, B, and D.

Figure 9 Sequence of images of droplet breakup for System A: a shear rate of 0.40 s^{-1}, D_0 = 125 (±7) μm, Wi_d = 0.75, η_r = 2.6, and Ca = 11.

Figure 10 Sequence of images of droplet breakup for System B: a shear rate of 0.63 s^{-1}, D_0 = 82 μm, Wi_d = 0.28 for η_r = 0.5, and Ca = 9.5.

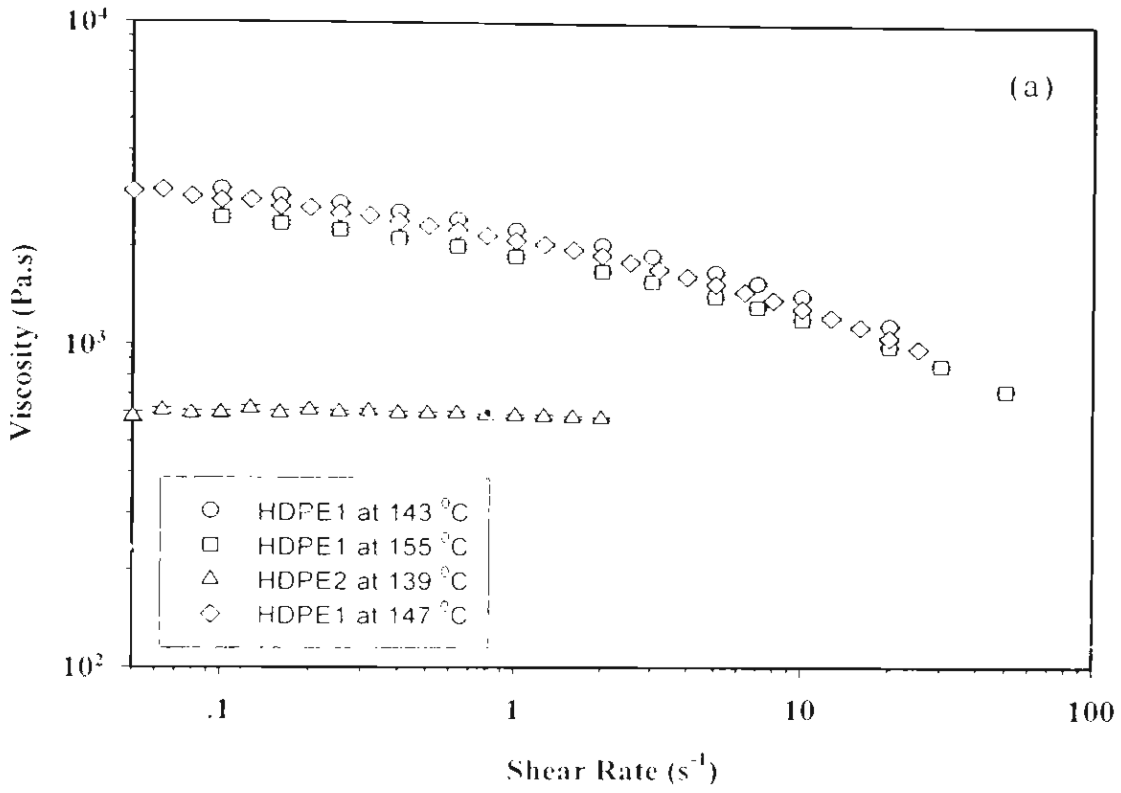
(a)
Viscosity (Pa.s)
Shear Rate (s-1)
HDPE1 at 143 °C
HDPE1 at 155 °C
HDPE2 at 139 °C
HDPE1 at 147 °C

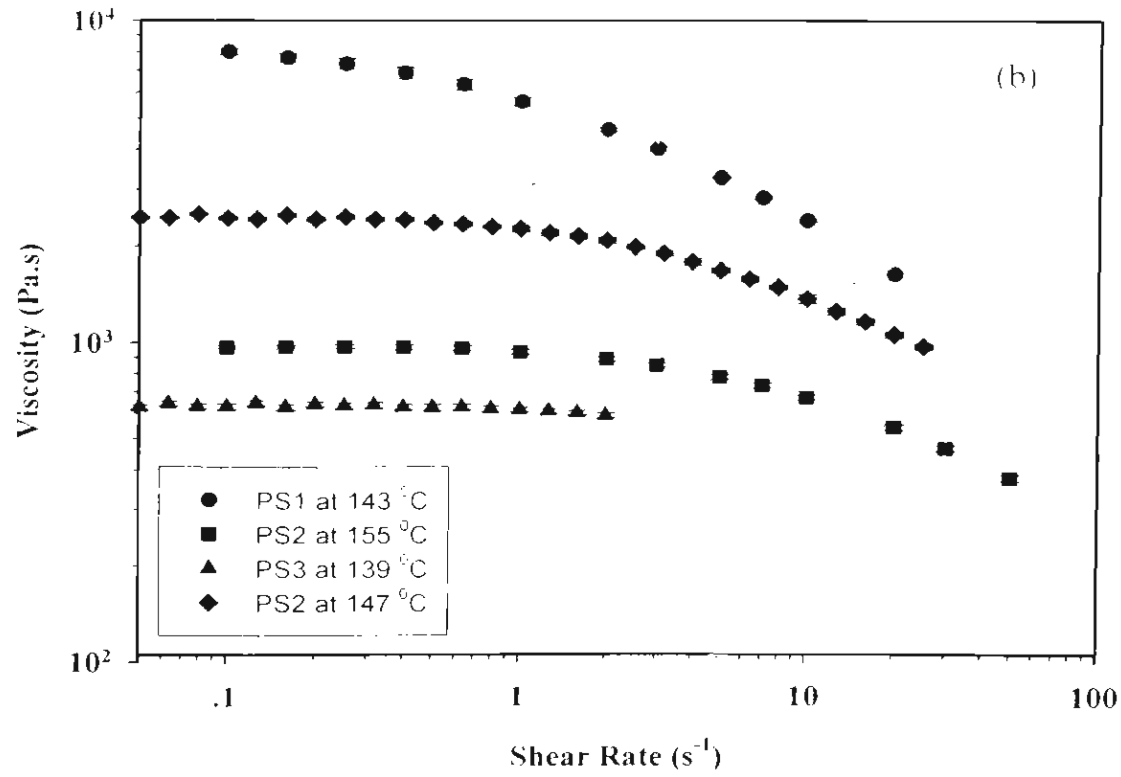
(b)
Viscosity (Pa.s)
Shear Rate (s-1)
PS1 at 143 °C
PS2 at 155 °C
PS3 at 139 °C
PS2 at 147 °C

Figure 1

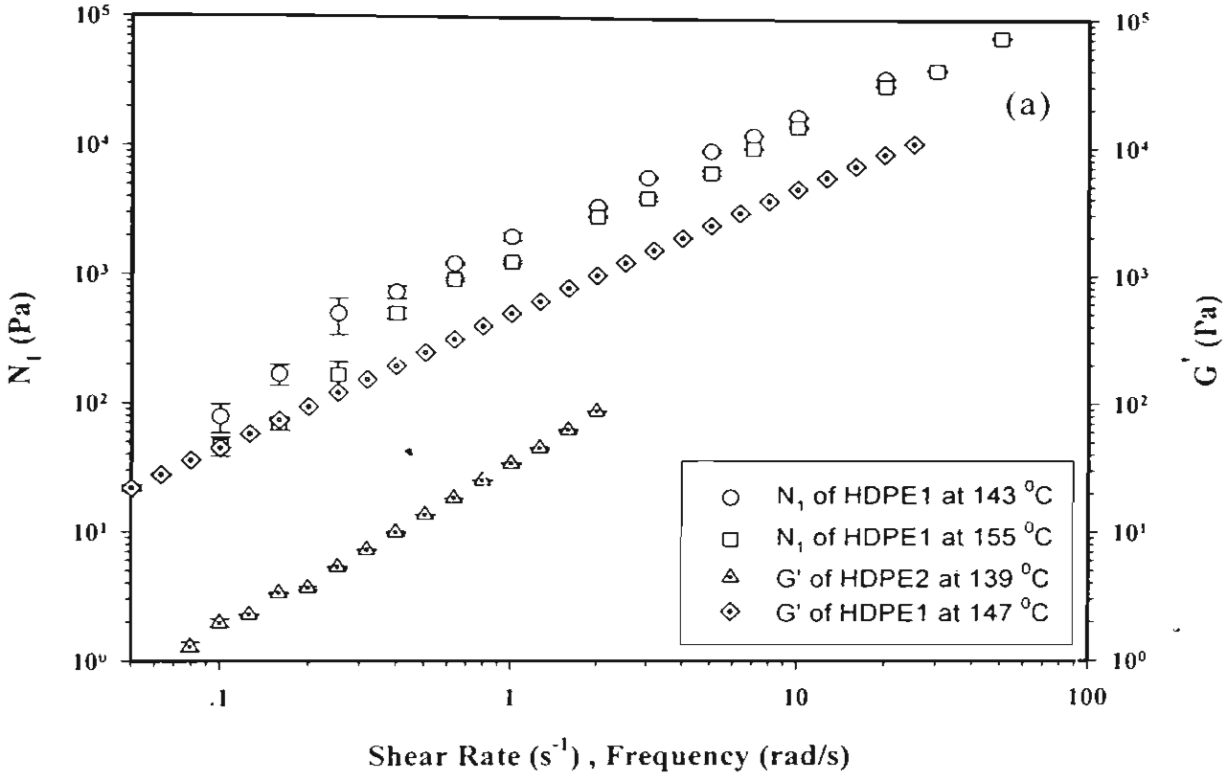
(a)
N1 (Pa)
G' (Pa)
N1 of HDPE1 at 143 °C
N1 of HDPE1 at 155 °C
G' of HDPE2 at 139 °C
G' of HDPE1 at 147 °C
Shear Rate (s-1) , Frequency (rad/s)

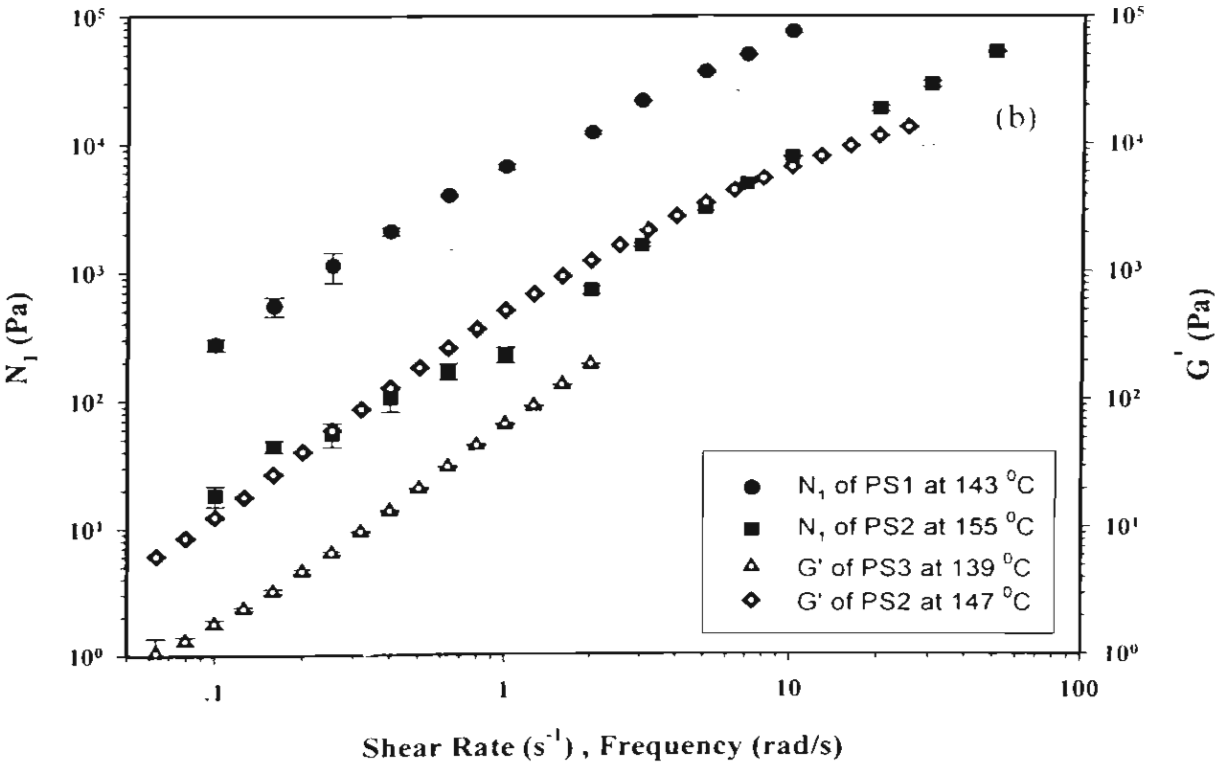
(b)
N1 (Pa)
G' (Pa)
N1 of PS1 at 143 °C
N1 of PS2 at 155 °C
G' of PS3 at 139 °C
G' of PS2 at 147 °C
Shear Rate (s-1) , Frequency (rad/s)

Figure 2

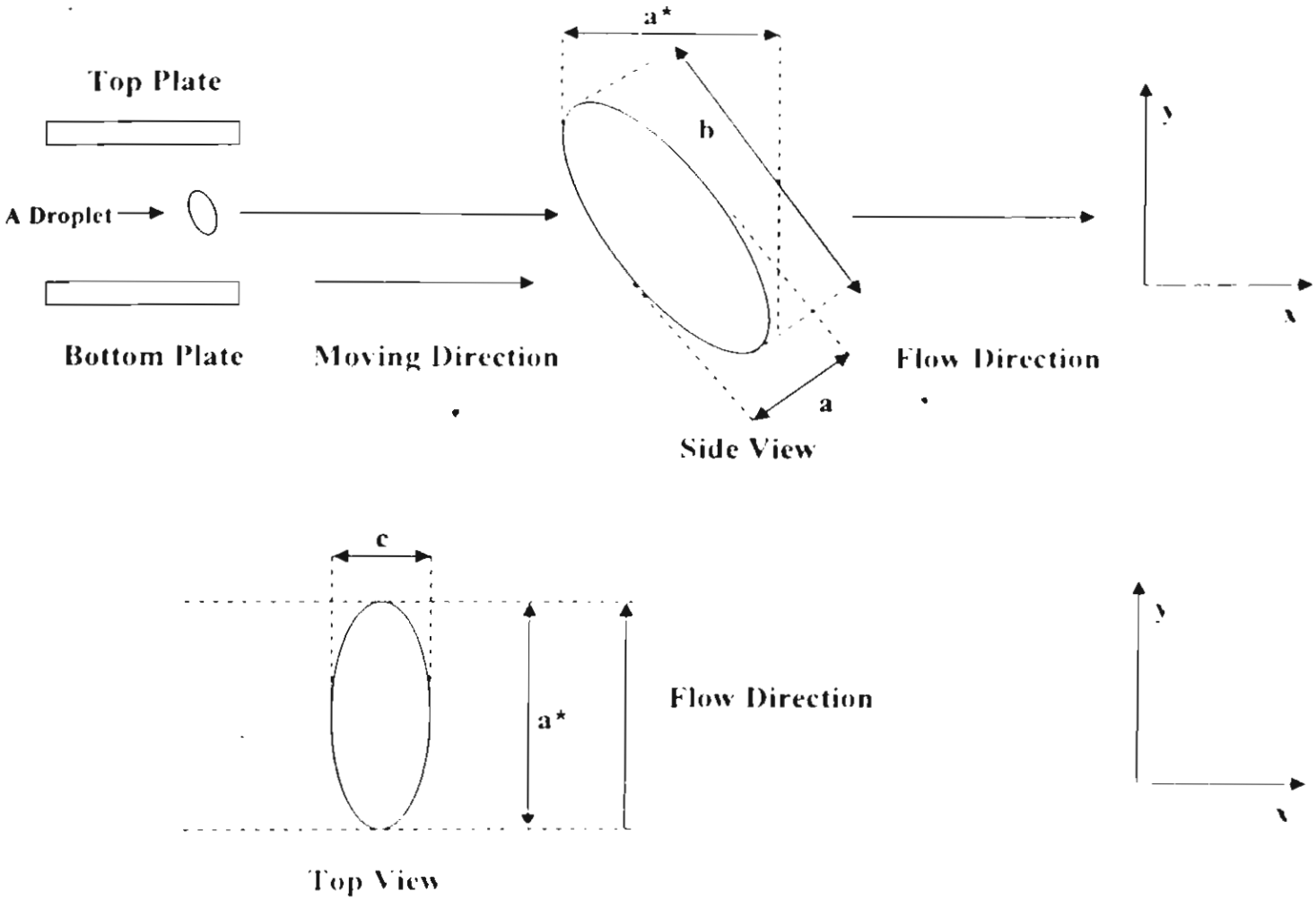
a*
Top Plate
b
A Droplet
y
x
Bottom Plate
Moving Direction
Flow Direction
a
Side View
c
a*
Flow Direction
y
x
Top View

Figure 3

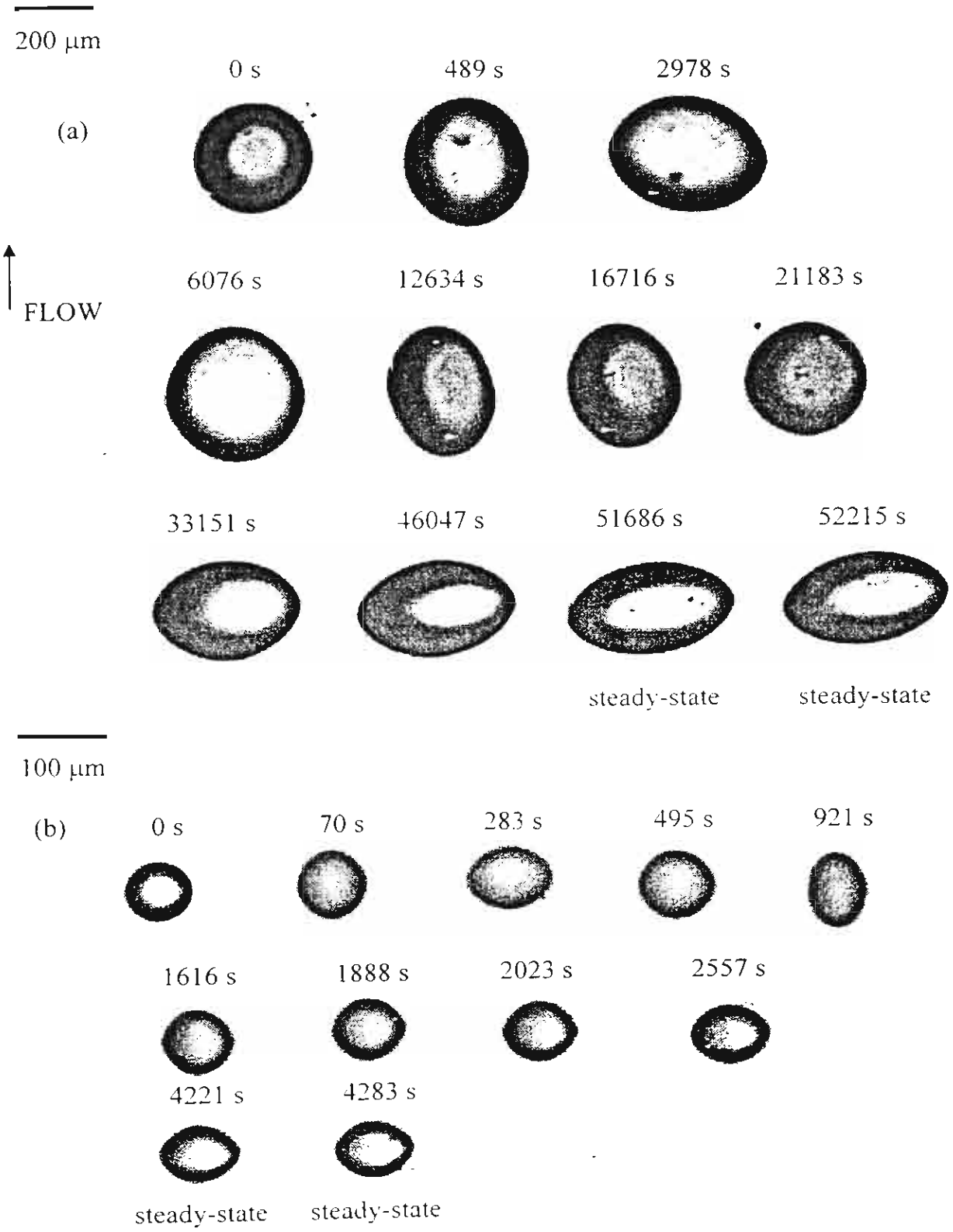
200 μm
(a)
0 s
489 s
2978 s
FLOW
6076 s
12634 s
16716 s
21183 s
33151 s
46047 s
51686 s
52215 s
steady-state
steady-state
100 μm
(b)
0 s
70 s
283 s
495 s
921 s
1616 s
1888 s
2023 s
2557 s
4221 s
4283 s
steady-state
steady-state

Figure 4

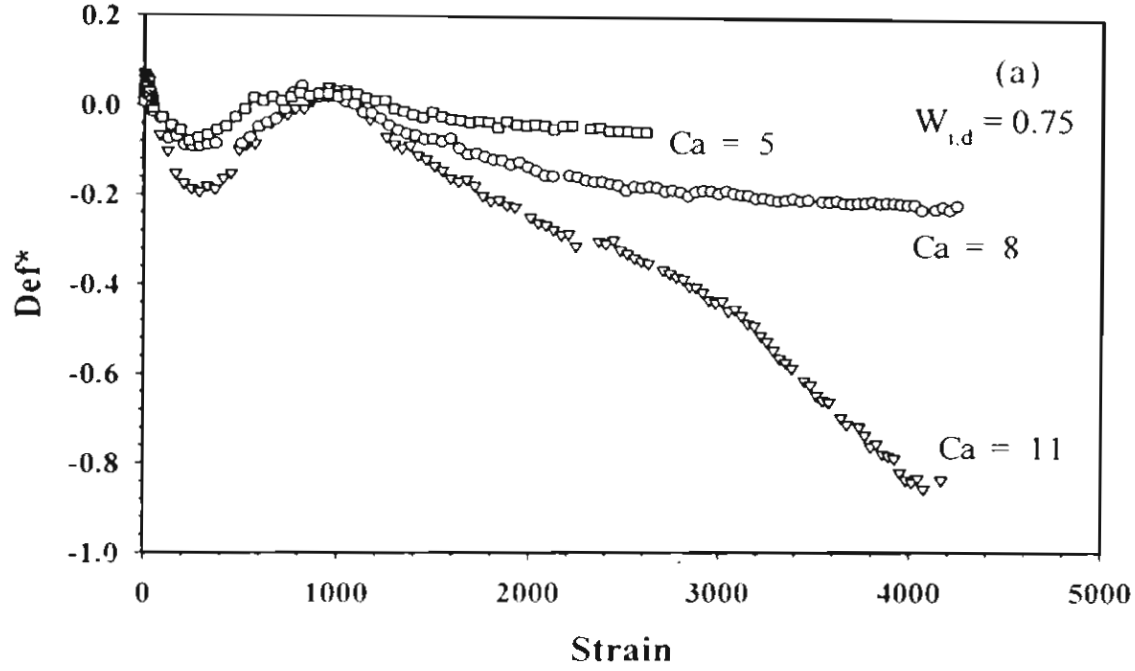

Figure 5a

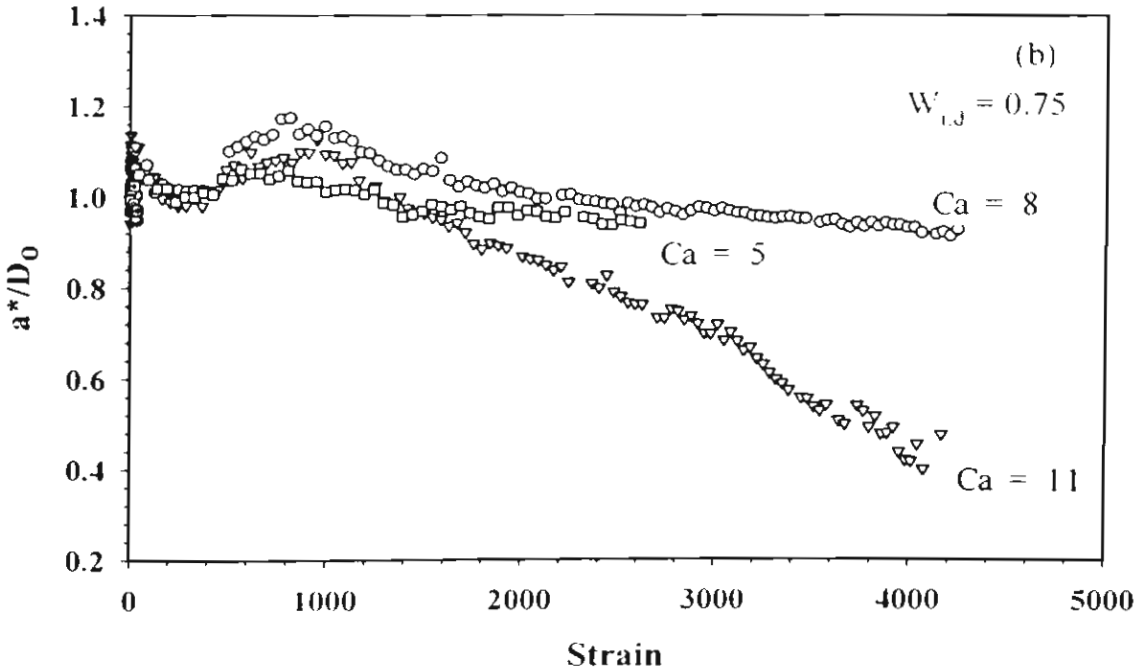

Figure 5b

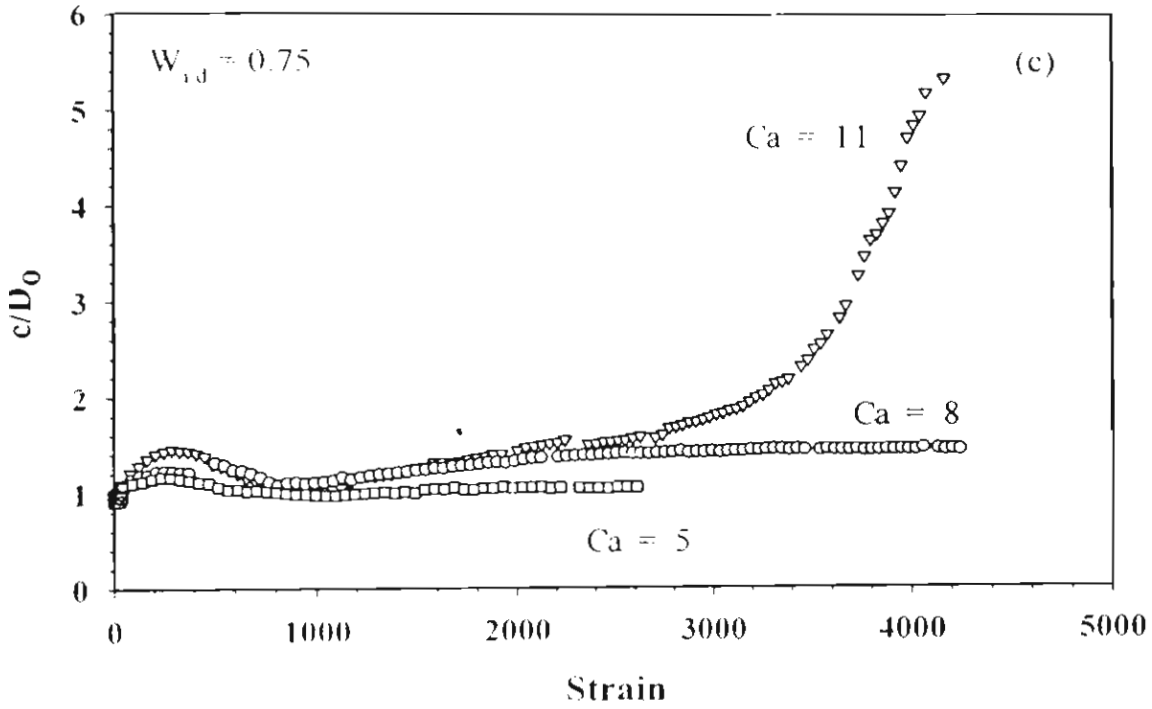
W_{rd} = 0.75
(c)
Ca = 11
Ca = 8
Ca = 5
c/D$_0$
Strain
0
1
2
3
4
5
6
0
1000
2000
3000
4000
5000

Figure 5c

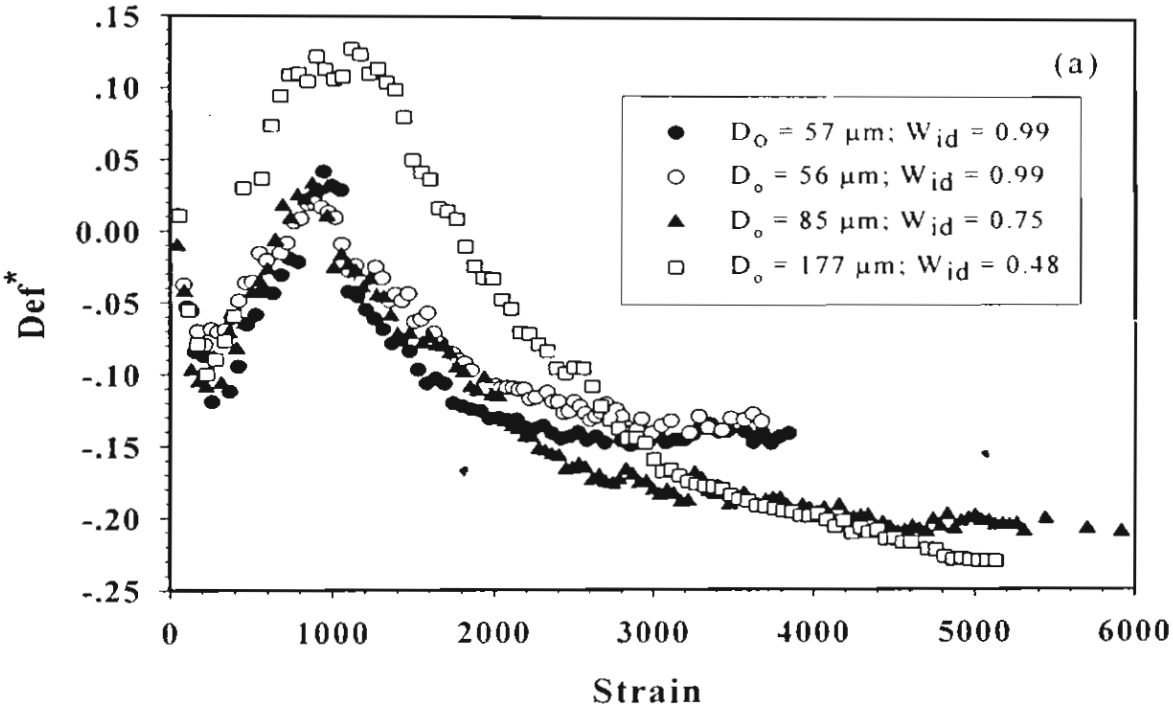

Figure 6a

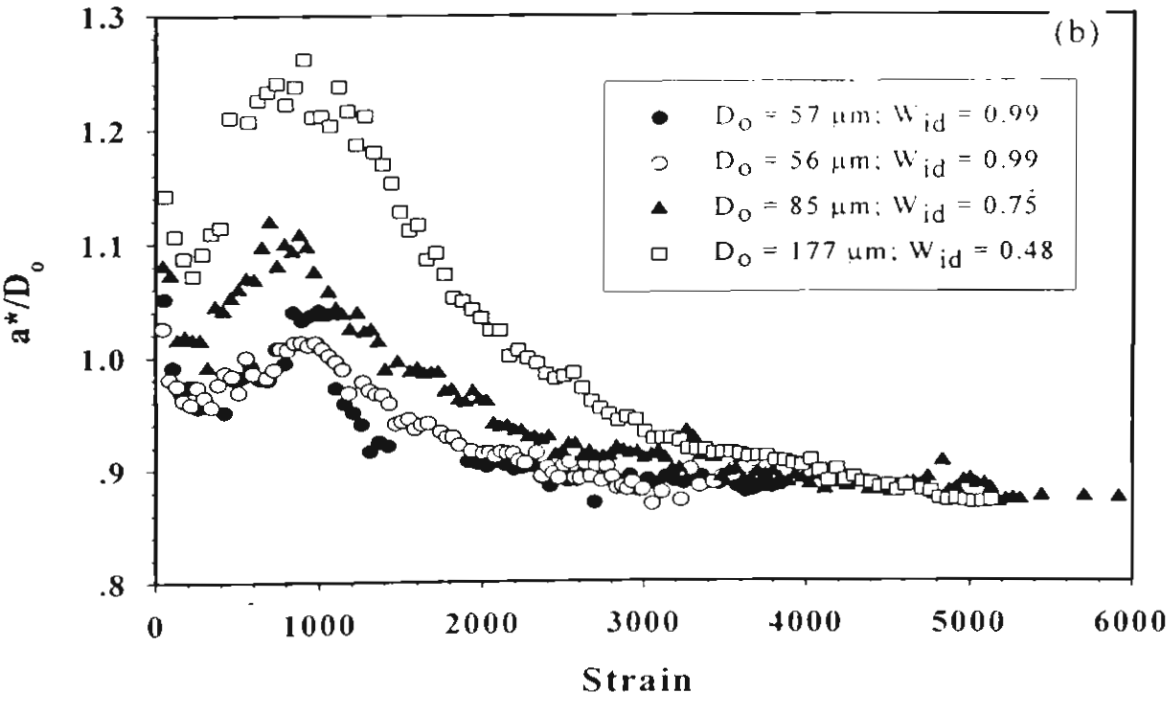

Figure 6b

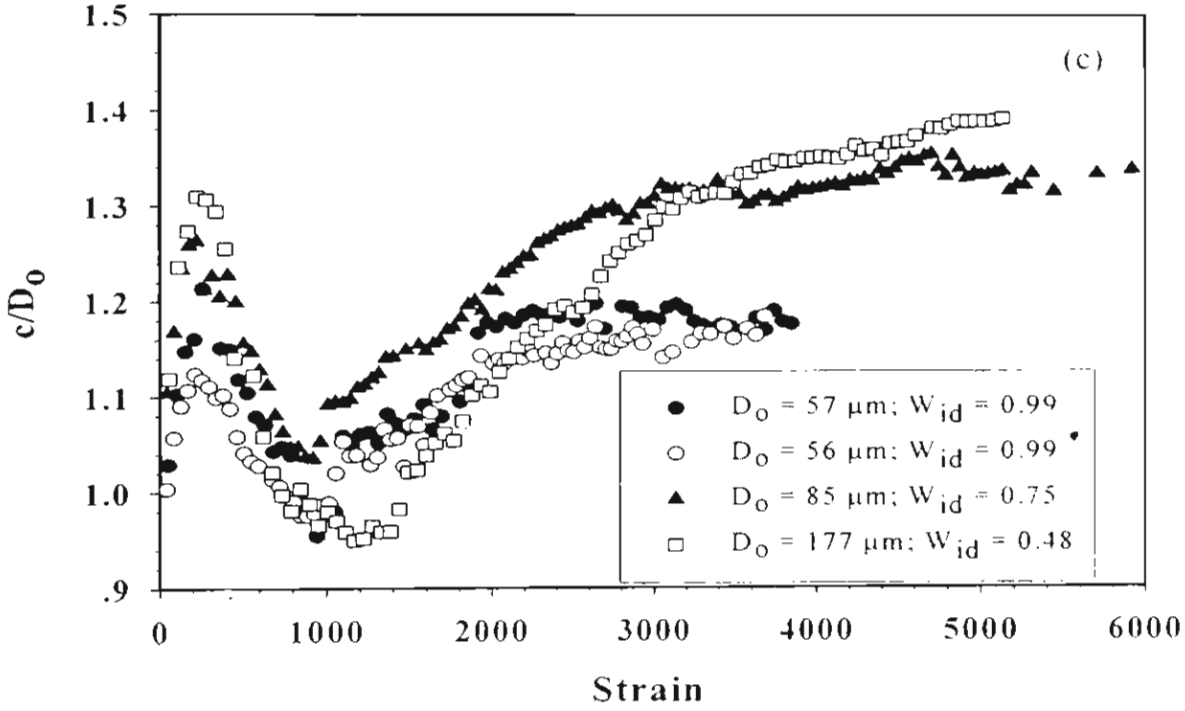
(c)
1.5
1.4
1.3
1.2
1.1
1.0
.9
c/D0
0
1000
2000
3000
4000
5000
6000
Strain
D0 = 57 µm; Wid = 0.99
D0 = 56 µm; Wid = 0.99
D0 = 85 µm; Wid = 0.75
D0 = 177 µm; Wid = 0.48

Figure 6c

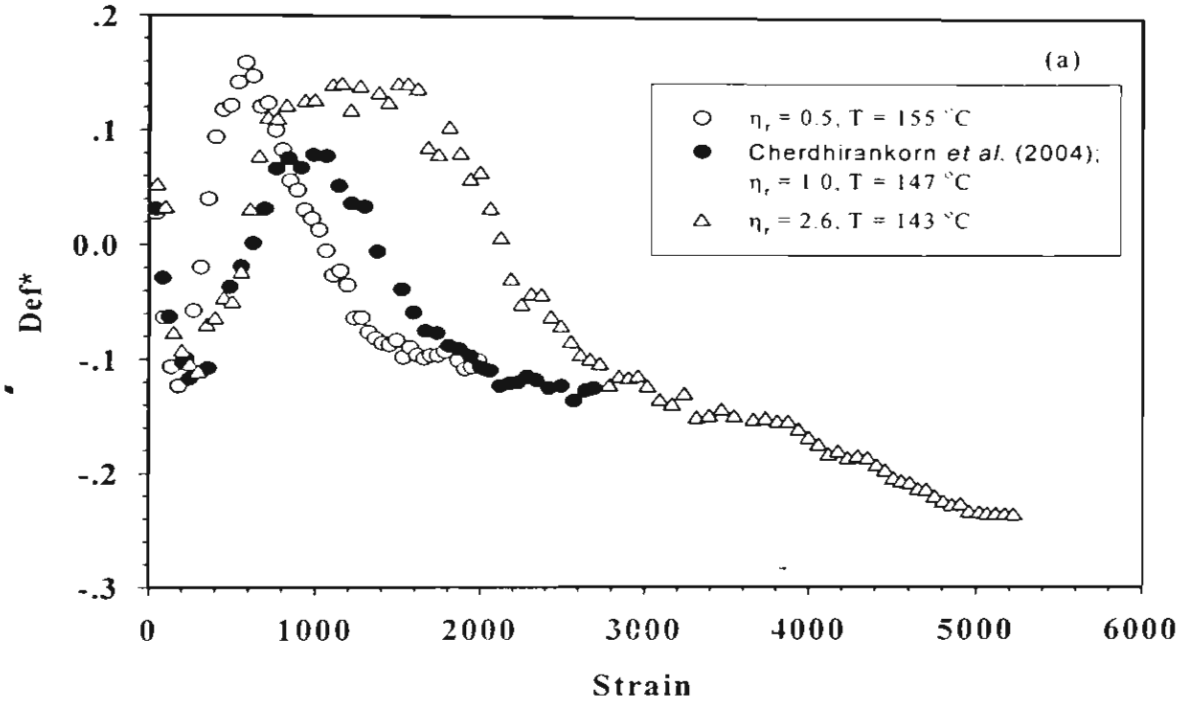

Figure 7a

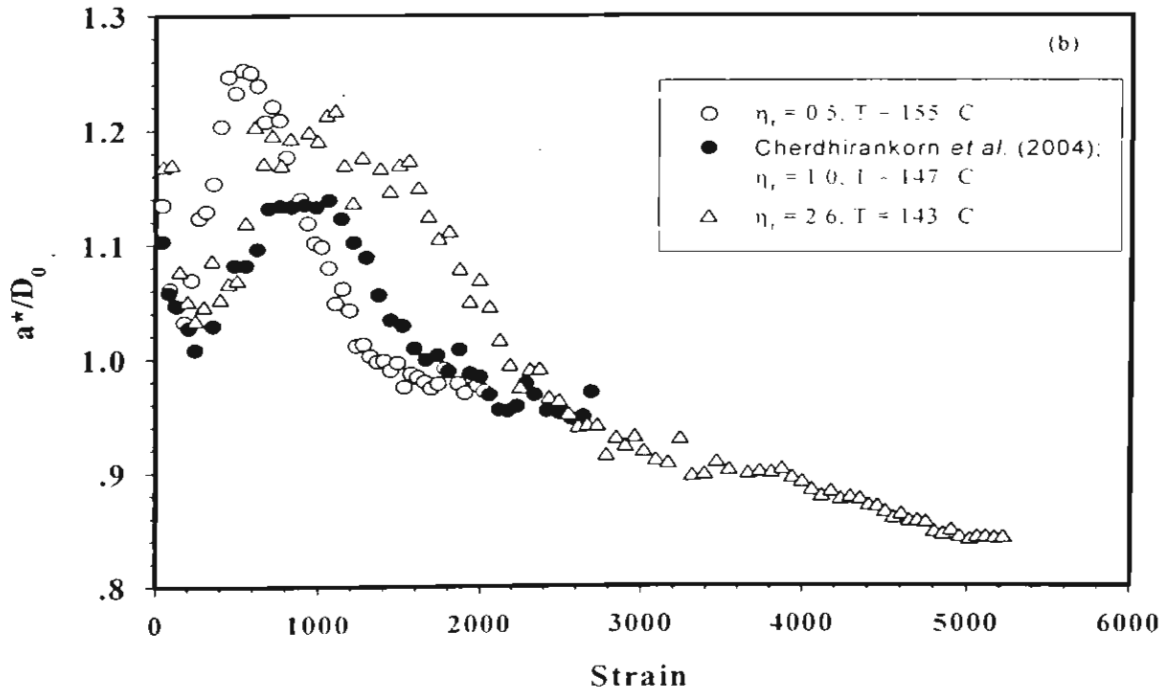

Figure 7b

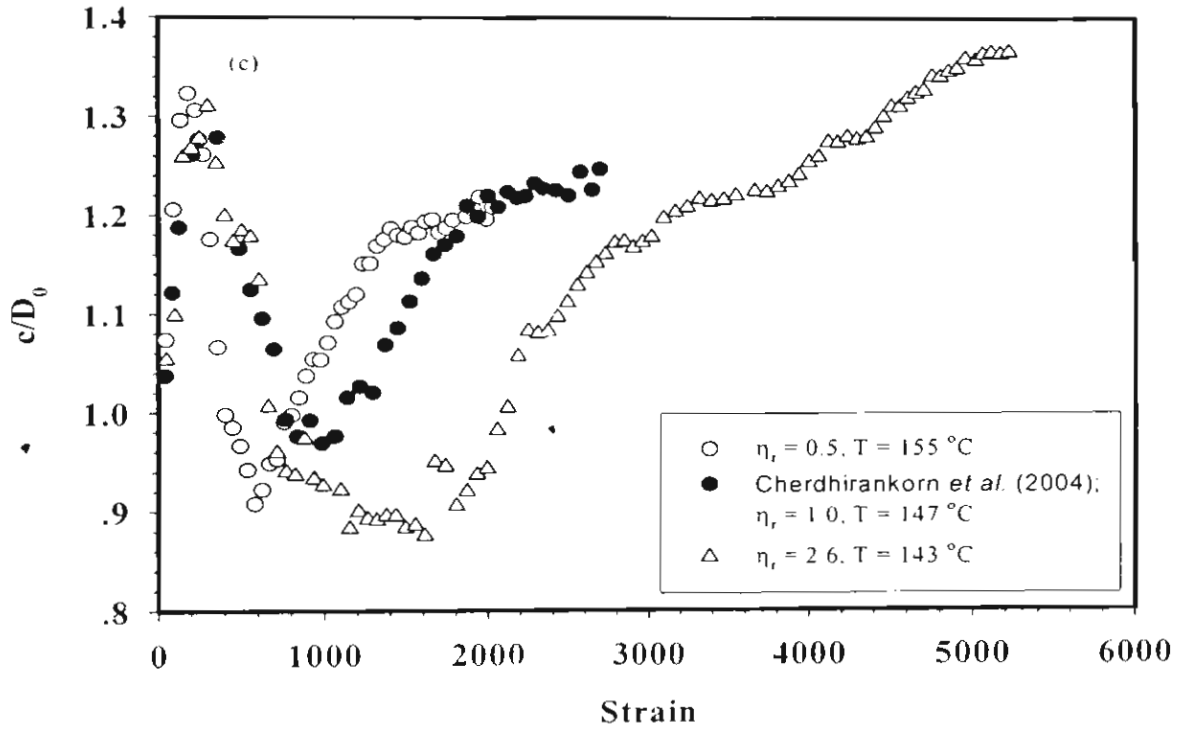
(c)
1.4
1.3
1.2
1.1
1.0
.9
.8
c/D0
0
1000
2000
3000
4000
5000
6000
Strain
ηr = 0.5, T = 155 °C
Cherdhirankorn et al. (2004);
ηr = 1.0, T = 147 °C
ηr = 2.6, T = 143 °C

Figure 7c

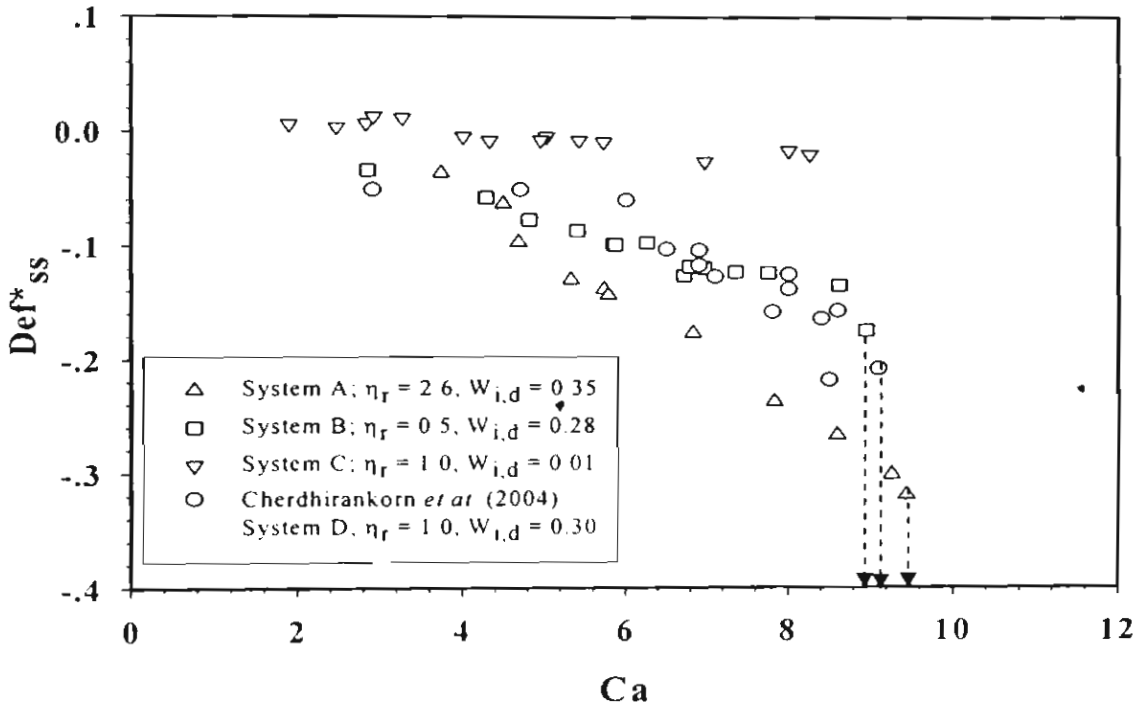
.1
0.0
-.1
-.2
-.3
-.4
Def*ss
0
2
4
6
8
10
12
Ca
System A; ηr = 2.6, Wi,d = 0.35
System B; ηr = 0.5, Wi,d = 0.28
System C; ηr = 1.0, Wi,d = 0.01
Cherdhirankorn et al (2004)
System D, ηr = 1.0, Wi,d = 0.30

Figure 8

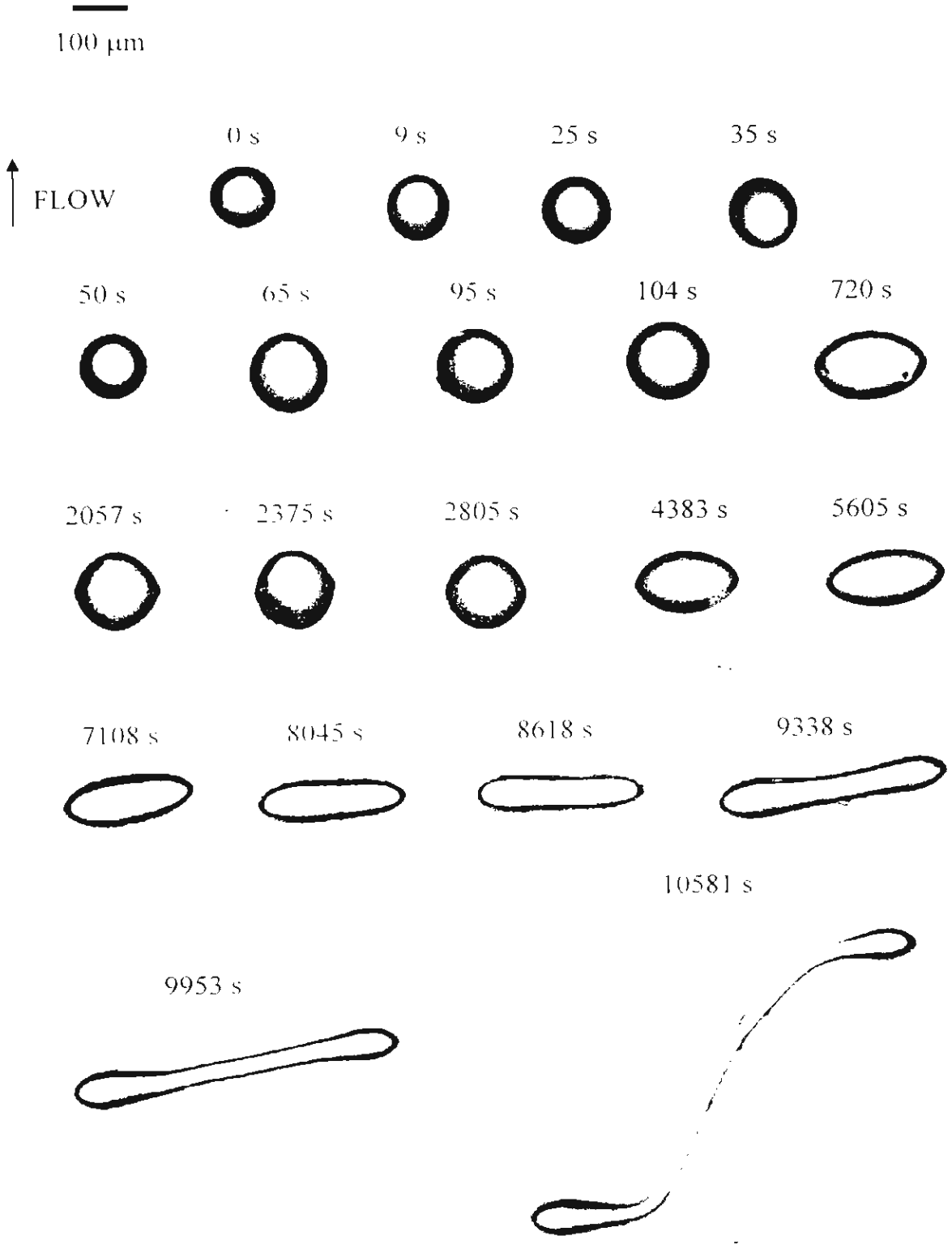
100 μm
FLOW
0 s
9 s
25 s
35 s
50 s
65 s
95 s
104 s
720 s
2057 s
2375 s
2805 s
4383 s
5605 s
7108 s
8045 s
8618 s
9338 s
10581 s
9953 s

Figure 9

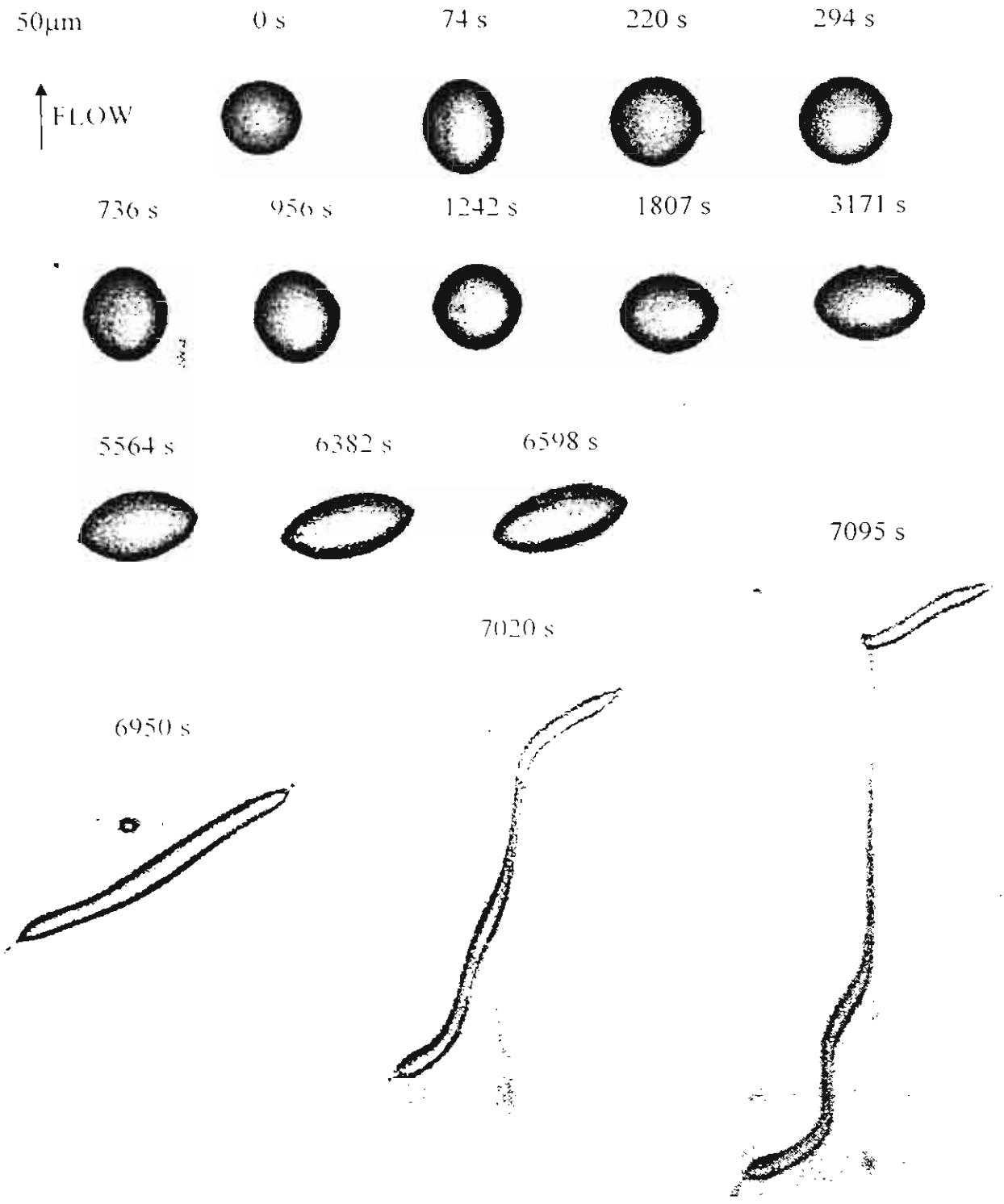
50μm
0 s
74 s
220 s
294 s
FLOW
736 s
956 s
1242 s
1807 s
3171 s
5564 s
6382 s
6598 s
7095 s
7020 s
6950 s

Figure 10

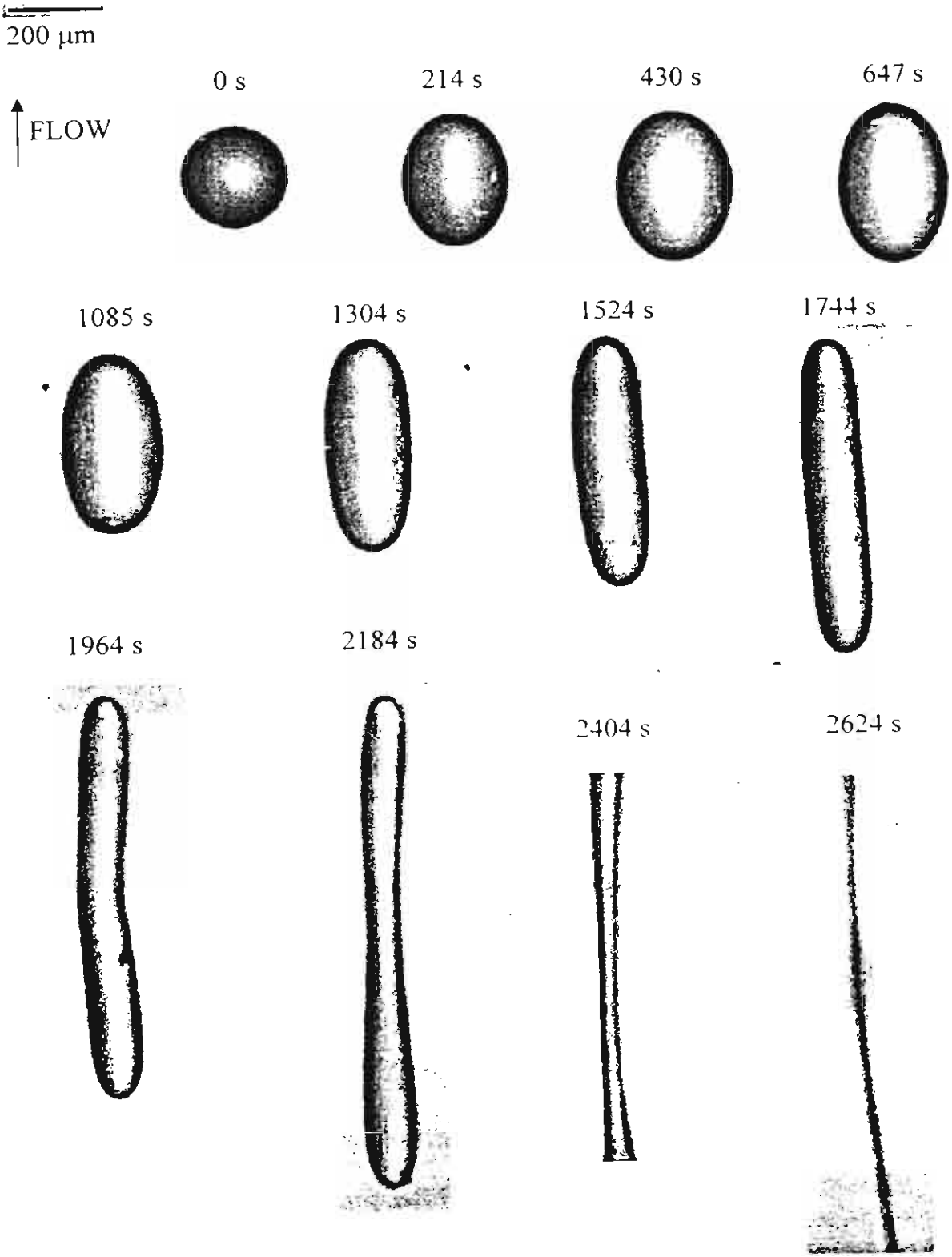
200 μm
FLOW
0 s
214 s
430 s
647 s
1085 s
1304 s
1524 s
1744 s
1964 s
2184 s
2404 s
2624 s

Figure 11

Chapter 5: Influence of Dispersed-phased Elasticity on Steady-state Deformation and Breakup of Droplets in Simple Shearing Flow of Immiscible Polymer Blends

Wanchai Lerdwijitjarud [a], Anuvat Sirivat [b], and Ronald G. Larson [c,*]

[a] Department of Materials Science and Engineering, Faculty of Engineering and Industrial Technology, Silpakorn University, Nakhon Pathom 73000, Thailand

[b] Petroleum and Petrochemical College, Chulalongkorn University, Bangkok 10330, Thailand

[c] Department of Chemical Engineering, University of Michigan, Ann Arbor, Michigan 48109, USA

* Corresponding Author

Influence of Dispersed-phased Elasticity on Steady-state Deformation and Breakup of Droplets in Simple Shearing Flow of Immiscible Polymer Blends

Abstract

The effect of dispersed-phase elasticity on steady-state deformation and breakup of isolated droplets for polybutadiene/poly(dimethyl siloxane) blends in simple shearing flow is investigated systematically for values of the dispersed-phase Weissenberg number (Wi_d) ranging up to around 3, where the Weissenberg number is defined as the ratio of the first normal stress difference to twice the shear stress at the imposed shear rate. The dependence on droplet elasticity of steady-state morphology for 10%-dispersed phase blends is also studied. The polybutadiene droplet phase is an elastic "Boger" fluid prepared by dissolving a high-molecular-weight polybutadiene into low-molecular-weight Newtonian polybutadiene. To isolate the contribution of droplet elasticity, all experiments were done on a fixed viscosity ratio of around unity, achieved by adjusting the temperature appropriately for each blend. When the droplet elasticity increases, the steady-state deformation of isolated droplets decreases for fixed capillary number. The critical capillary number for breakup (Ca_{crit}) increases linearly with the Weissenberg number of the droplet phase (Wi_d) up to a value of Wi_d of around unity. When Wi_d is greater than unity, Ca_{crit} seems to approach an asymptotic value of 0.95 for high values of Wi_d. For 10%-dispersed phase blends, the steady-state capillary number (Ca_{ss}) calculated from a volume-averaged droplet diameter is less than the Ca_{crit} for isolated droplets for the same blend. Ca_{ss} increases monotonically with the first normal stress difference of the droplet phase (N_{1d}). Droplet widening in the vorticity direction is not observed even at droplet

Weissenberg numbers much in excess of those for which widening is observed in blends of melts, suggesting that widening is strongly influenced by factors other than the first normal stress difference, such as shear thinning or second normal stress differences.

Keywords: immiscible blend, droplet elasticity, droplet deformation, Capillary number, Weissenberg number

INTRODUCTION

The dispersal of one fluid in another immiscible fluid phase is important in industrial processes, such as emulsion formulation, polymer blending, and also to create interface for heat transfer, mass transfer, and chemical reactions. The size and size distribution of droplets in the matrix phase are crucial for controlling the reactivity of these processes and/or the properties of the final products. For example, the impact strength of a polymer blend is significantly improved when the size of rubbery dispersed-phase inclusions is smaller than a critical value [Wu (1985)]. The droplet size distribution is controlled by deformation, relaxation, breakup, and coalescence of droplets during mixing.

The investigation of deformation and breakup of an isolated Newtonian droplet in an immiscible Newtonian matrix was pioneered by Taylor (1932, 1934). He observed that droplet deformation and breakup of isolated droplets in a Newtonian blend under quasi-steady conditions (i.e., gradually increasing deformation rate) are controlled by two dimensionless parameters, namely the capillary number (Ca), which is the ratio of matrix viscous stress to interfacial stress, and the viscosity ratio (η_r), of the dispersed (η_d) to the matrix phase (η_m). For viscosity ratios near unity, the steady-state three-dimensional shape of an isolated deformed Newtonian droplet sheared in a Newtonian matrix can be represented by an ellipsoid having three different principal axes, the longest of which orients at an angle 0 with respect to the flow direction, (Guido and Villone 1998). When the matrix viscous stress ($\eta_m \dot{\gamma}$ where $\dot{\gamma}$ is the applied shear rate) overcomes the interfacial stress (Γ/r_0, where Γ and r_0 are the interfacial tension and the undeformed droplet radius, respectively), the droplet will break. This occurs when the ratio of the viscous to the interfacial stress, which is the

capillary number $Ca \equiv \eta_m \dot{\gamma} r_0/\Gamma$, exceeds a critical value, Ca_{crit}. Ca_{crit} is a minimum when η_r is around unity [Grace (1982); De Bruijn (1989)]. The flow type (shear vs. extensional flow) was also found to effect the correlation between Ca_{crit} and η_r [Rallison and Acrivos (1978), Bentley and Leal (1986)].

For polymer blends, non-Newtonian behavior, including elasticity and shear-thinning, is expected to influence the deformation and breakup of droplets. Wu (1987) studied the steady-state average droplet size in extruded viscoelastic polymer blends containing 15% of dispersed phase and compared the results with those of Newtonian blends. Like the Newtonian blend, the minimum in Ca for these polymer blends was found at a viscosity ratio of around unity; however the value of Ca at η_r = 1 for Wu's polymer blends was around ten times greater than that of a Newtonian system. Many experimental results on immiscible viscoelastic blends when either one phase or the other is viscoelastic have been reported in the literature [Flumerfelt (1972); Elmendrop and Maalcke (1985); Milliken and Leal (1991); Tretheway and Leal (2001)]. An unusual phenomenon, transient and steady-state droplet widening along the vorticity axis [Levitt *et al.* (1996); Hobbie and Migler (1999); Migler (2000); Mighri and Huneault (2001)], was observed for a viscoelastic droplet sheared in a viscoelastic matrix.

Most of the experimental evidence shows that elasticity of the droplet fluid inhibits droplet deformation, causing the droplet to break at a higher capillary number, while elasticity of matrix phase tends to destabilize the droplet, making it break at a lower capillary number. However, quantitative correlations between Ca and elasticity of droplet or matrix phase are rare. Varanasri *et al.* (1994) studied the breakup of isolated viscoelastic droplets sheared in purely viscous Newtonian fluids in a cone-and-plate device and found a linear relationship between Ca_{crit} and the first normal

stress difference of the dispersed phase fluid at a fixed viscosity ratio. However, for any fixed viscosity ratio there was a critical value of the shear rate, $\dot{\gamma}^*$, below which the breakup of a viscoelastic droplet was easier than that of Newtonian droplet. The reasons for these results are still unclear. Mighri *et al.* (1998) investigated the deformation and breakup of isolated droplets under a simple shear flow for a blend prepared from "Boger" fluids (in which each blend component is a dilute polymer in a Newtonian matrix) and also constructed a correlation between Ca_{crit} and elasticity contrast, as measured by the ratio λ_d/λ_m of the relaxation time of the droplet phase ($\lambda_d \equiv N_{1d}/2\eta_d\dot{\gamma}^2$) to that of matrix phase ($\lambda_m \equiv N_{1m}/2\eta_m\dot{\gamma}^2$), where N_{1d} and N_{1m} are the first normal stress differences of dispersed and matrix phase, respectively. The correlation between Ca_{crit} and λ_d/λ_m was found to be nonlinear, in which Ca_{crit} sharply increased with increasing λ_d/λ_m when $\lambda_d/\lambda_m < 4$, but for $\lambda_d/\lambda_m > 4$, Ca_{crit} reached an asymptotic value of Ca_{crit} around 0.9.

In most previous work, both droplet elasticity and viscosity ratio were varied simultaneously. However, the study of droplet behavior when droplet elasticity is the sole manipulated valuable has been recently reported [Lerdwijitjarud *et al.* (2003)]. In that work, the deformation and breakup of isolated droplets of weakly elastic fluid ($Wi_d \leq 0.02$, $Wi_d \equiv(\Psi_{1,d}/2\eta_d)\cdot\dot{\gamma}_c$; where $\Psi_{1,d}$ is the first normal stress difference coefficient of dispersed phase), sheared in a Newtonian matrix, were microscopically investigated at a fixed viscosity ratio of unity. Elasticity of the droplet produced a reduction in the degree of deformation at any given imposed Ca, and correspondingly resulted in greater value of Ca_{crit} for droplet breakup compared with a Newtonian droplet. The breakup mechanism appeared to be similar to that in a Newtonian fluid; i.e., the droplet deformed increasingly in the flow direction as the shear rate was

gradually increased, until breakup occurred. A quantitative relationship linking Wi_d to Ca_{crit} was established. Ca_{crit} increased linearly with increasing Wi_d, but a downward deviation from linearity was found for the blends with highest Wi_d, i.e., for $Wi_d \approx 0.02$.

This paper is devoted to finding a quantitative relationship between the critical capillary number for breakup, Ca_{crit}, and elasticity of dispersed phase, as measured by Weissenberg number, Wi_d, for the blend systems with a fixed viscosity ratio of unity and a much higher degree of droplet phase elasticity than in our previous work [Lerdwijitjarud *et al.* (2003)], in order to move toward more realistic commercial high-molecular-weight polymer blends with high elasticity.

EXPERIMENTAL METHODS

A. Materials

The materials used as the matrix and dispersed phases of the blends in this study were polydimethylsiloxane (PDMS) (Viscasil 100M donated by General Electric) and low-molecular-weight, Newtonian, polybutadiene (PBd) (Sartomer R150 donated by Sartomer Inc.), respectively. The properties of both fluids are listed in Table I. A high-molecular-weight polybutadiene (M_w = 1.43 x 10^6, M_w/M_n ~ 1.13) was also used as a flexible polymer component added to the low-molecular-weight PBd to make "Boger" fluids with elasticity but low shear thinning [Boger and Binnington (1977)].

B. Blend Preparation and Characterization

To remove all volatile components, both PDMS and PBd were placed in a vacuum oven at 50 ^{0}C until no further weight change was observed. The polybutadiene "Boger" fluids were prepared by thoroughly dissolving high-molecular-weight polybutadiene into methylene chloride. The solution was gently mixed with low-molecular-weight PBd by the rolling-bottle technique at ambient conditions for at least 7 days to ensure that a homogeneous solution was achieved. The mixture was then vacuum dried at 50 ^{0}C to eliminate the methylene chloride and other volatile materials until the weight loss ceased. The weight percentages of high-molecular-weight flexible polymer in the polybutadiene "Boger" fluid for this work are 0.1, 0.2, 0.5, and 1.0. The steady-state viscosities and first normal stress differences, N_1, of all fluids were measured by a cone-and-plate rheometer with 25-mm. plate diameter and cone angle of 0.1 rad. (Rheometrics Scientific, ARES). The

temperature at which both PDMS and low-molecular-weight PBd have the same viscosity is 18.3 °C. At this equiviscosity temperature of these two fluids, the PBd shows Newtonian behavior at shear rates of 0.1-10 s^{-1}, whereas weak shear thinning and a small value of N_1 at high shear rates are observed for PDMS (see Figure 3a). Figure 1 depicts the dependence of steady-state viscosity and N_1 of all PBd "Boger" fluids on shear rate at a temperature of 18.3 °C. The zero-shear viscosities, η_0, and also the elasticities, as measured by the N_1 values, of the "Boger" fluids increase with increasing concentration of high-molecular-weight polymer component in the solution. Unfortunately, shear thinning also increases with increasing concentration of long-chain species, which is especially evident in the "Boger" fluids containing the high-molecular-weight PBd at concentrations of 0.5% and 1.0%. The dependence of η_0 on weight percent of long-chain polymer in PBd "Boger" fluid is shown in Figure 2. For the "Boger" fluids containing 0.1%, and 0.2% of long-chain polymer, the solutions are believed to be dilute in high-molecular-weight PBd because we observe an approximately linear relation between the concentration of high-molecular-weight polymer and the increment in zero-shear viscosity over that of low-molecular-weight PBd. However, the linear relation is no longer valid for the solutions containing 0.5%, and 1.0% of high-molecular-weight polymer, evidently because of the onset of entanglements at these higher concentrations.

The blends used in this study are presented in Table II. To clearly isolate the contribution of elasticity, the viscosity ratios of the blends were fixed at around unity. The testing temperature, therefore, was varied from blend to blend to compensate for the effect of long-chain polymer on the viscosity of PBd dispersed phase. For A0, A1, and A2 blends, the viscosity ratios could be set to around unity using only a single value of temperature for each blend (see Figure 3). Due to the shear-thinning

characteristics of the 0.5% and 1.0% high-molecular-weight PBd solutions, however, different testing temperatures were used for these blends over different ranges of shear rate to better satisfy the equiviscosity condition (see Figures 4 and 5). The steady-state viscosities and the first normal stress differences of the PDMS matrix and the PBd dispersed phase at the temperature at which both phases have the same viscosity are shown for all blends in Figures 3, 4, and 5. The viscosity ratios of all blends were well controlled to be unity ± 5% at the testing conditions, whereas the elasticity of the dispersed phase monotonically increases with concentration of high molecular weight Pbd in blends A0, A1, A5, A10, as indicated by the increasing values of N_1 of the droplet fluid.

C. Experiments on Isolated Droplets

1. Instruments and sample loading

An optical flow cell (Linkam CSS450, Linkam Scientific Instruments Inc.), consisting of two parallel quartz disks, i.e. a rotatable lower one and a fixed upper one, mounted on an optical microscope (Leica DMRXP, Leica Imaging Systems Inc.) was used to conduct the experiments. The temperature of the flow cell was controlled by the cell-heating elements and circulating water from a water bath. Images were captured by a CCD camera (Cohu 4910, Cohu Inc.) in the flow-vorticity plane and transferred to a PC computer via a frame-grabber card (LG3-128, Scion Corporation Inc.). The images were analyzed by the Scion Image software.

The PDMS matrix phase was loaded into the flow cell, and the fluid was allowed to level. Several PBd droplets were then immersed into the matrix using a small needle. The upper plate of the flow cell was gradually lowered until the quartz

disk touched the sample and the desired gap was reached. For the experiments on isolated droplets, the total amount of dispersed phase in the blend was less than 0.2%.

II. Optical microscopy of an isolated droplet

Droplets located near the center of the gap and separated from their neighboring droplets by a distance more than three times the diameter of the biggest neighboring droplet were considered to be isolated droplets and were chosen for observation and measurement. Since hydrodynamic interactions with the solid surfaces disappear if the distance between the closest surface and the droplet center is more than five times the droplet radius [Kennedy *et al.* (1994); Uijittewaal and Nijhof (1995)], the gap in all our experiments was at least ten times larger than the diameter of the chosen droplet. Since the images of the deformed droplet were taken only in the flow-vorticity plane, which is the plane perpendicular to the shear gradient direction, the lengths of all three principle axes of the ellipsoidal droplet could not be obtained unless the orientation angle (θ), the angle between the major axis of deformed droplet in the flow-flow gradient plane, was known. This orientation angle can be predicted from either the affine deformation model for step strains or the Chaffey and Brenner relation for steady-state shearing [Chaffey and Brenner (1967)], and these formulas will be used here to obtain the orientation angle, which then allows the lengths of all three droplet axes to be determined. For a step-strain or startup flow experiment, if the imposed Ca is at least three times higher than Ca_{crit}, the orientation angle predicted from the affine deformation model has been found to be close to the experimental value obtained from microscopy for both Newtonian and viscoelastic blends in experiments that imaged the droplet from two different directions [Yamane *et al.* (1998); Okamoto *et al.* (1999)]. For $Ca \leq Ca_{crit}$, Chaffey

and Brenner (1967) found that for isolated Newtonian droplet sheared in immiscible Newtonian matrix, the orientation angle of the steady-state deformed droplet depended on the applied Ca and the viscosity ratio of the system. Guido and Villone (1998) compared the predictions of the Chaffey and Brenner relation with the experimental results obtained from microscopy for polydimethylsiloxane droplets sheared in polyisobutylene at η_r of 1.4 and 2, and found good agreement between the two.

III. Interfacial tension determination

The interfacial tensions of all blend systems studied were determined by the deformed-droplet retraction technique [Luciani *et al.* (1997); Guido and Villone (1999); Mo *et al.* (2000); Xing *et al.* (2000)]. The shape evolution of a deformed isolated droplet during relaxation from an ellipsoidal back to a spherical shape was recorded. The characteristic relaxation time for an isolated droplet, τ, can be obtained from the slope, $-1/\tau$, of a straight line fit to the data in the linear relaxation regime of semilogarithemic plots of the deformation parameter, Def (Def $\equiv (a-b)/(a+b)$, where a is the major axis of the ellipsoid oriented at a particular angle (θ) within a flow-gradient plane, b is the minor axis in the shear-gradient direction), versus relaxation time. The interfacial tension, Γ, can be calculated from the Palierne Model [Palierne (1990); Graebling *et al.* (1993)] in the limit of zero volume fraction of the dispersed phase:

$$\tau = \frac{(3 + 2\eta_{r,0})(16 + 19\eta_{r,0})r_0\eta_{m,0}}{40(1 + \eta_{r,0})\Gamma}$$

where $\eta_{r,0} \equiv \eta_{d,0}/\eta_{m,0}$ is the ratio of zero-shear viscosities of dispersed to matrix phase, and r_0 is the radius of the spherical drop. For viscoelastic systems, the

contribution of both droplet and matrix elasticity to the relaxation of the droplet shape may lead to errors if this equation is used. However, the relation can still be used to determine the interfacial tension of viscoelastic materials if the relaxation of the nonNewtonian elastic stress of the blend constituents is relatively fast compared with the droplet shape relaxation and the droplet retraction rate is sufficiently slow to ensure that the materials behave as Newtonian during the droplet shape relaxation [Luciani *et al.* (1997), Xing *et al.* (2000)]. For large enough droplets, relaxation should become slow enough that viscoelastic stresses relax too quickly to influence droplet shape relaxation and hence the rate of relaxation is then governed by the interfacial tension alone. In this study, the interfacial tension values obtained using the Palierne formula applied to experiments on 180-μm and 100-μm droplets are the same within an experimental error for all blend systems, which implies that the true interfacial tension was obtained. The interfacial tension of all blends is presented in Table II.

IV. Steady-state deformation and breakup of isolated droplet

For steady-state deformation experiments, a suitable isolated droplet with desirable size was selected. The chosen droplet was then driven out of the field of view by applying a relatively small shear rate until the desired magnitude of the strain to be subsequently imposed strain was reached. The shear flow was stopped to allow the droplet to completely relax into a spherical shape. The same strain in the opposite direction was then applied at the desired shear rate, thus deforming the droplet and simultaneously bringing it back into viewing window. The droplet images were recorded by using a CCD camera at the maximum capturing speed (25 frames/ second). The capturing process was begun before the sheared droplet moved into the

viewing window and continued until the shear flow was stopped and the deformed droplet started to relax. To ensure that a steady-state deformation had been established, the strain required to reach a steady-state droplet shape was determined. This was done by finding a strain high enough that an increase of this strain by at least 20 strain units did not change the droplet shape. After determining the steady-state shape at a fixed shear rate, the applied shear rate was gradually increased from low to high in small incremental steps until the critical shear rate required for breaking the droplet was reached.

D. Experiments on Concentrated Blends

The concentrated blend compositions are 10% by weight PBd dispersed phase and 90% by weight PDMS matrix phase. The blend constituent components were weighed and mixed together with a spatula for around 20 min. resulting in a white-creamy product. The sample was placed in the vacuum oven at room temperature for about 1 hr to remove all bubble generated during the mixing step. The bubble-free sample was loaded into the flow cell. The upper plate of the flow cell was gradually reduced until the gap reached 500 microns. The testing temperature was set to a value at which both the matrix and dispersed phases had the same viscosity. After the loading process, the sample was pre-conditioned by shearing at a shear rate of 0.3 s^{-1} for a strain of 20,000 units. During this step, coalescence dominated, leading to a relatively coarse morphology.

After the pre-conditioning process, the shear rate was stepped up to 0.5 s^{-1}. A strain of 20,000 units was used to ensure that the steady-state morphology at this shear rate was reached. The flow was then stopped to allow the deformed droplets to relax back into spherical shapes. Due to the high viscosity of the matrix fluid and low

temperature of our blend systems, the diffusion coefficient associated with Brownian motion of the droplets is small (~10^{-6} $\mu m^2/s$ for droplets with diameter of 5 μm at 20 ^{0}C). Thus, the coalescence effect should be negligible in quiescent blends since the time waiting for droplet relaxation is less than 30 s. The blend images were then captured. The shear rate was subsequently increased in small steps, i.e. 0.7, 1.0, 2.0, 3.0 and 5.0 s^{-1}, from the previous steady-state shear rate. For each shear rate, a strain of 20,000 was allowed to attain a steady-state morphology before capturing images.

The blend images were transferred to a Photoshop program (Adobe Systems, Inc) to outline the droplets. The images were brought back to the Scion-Image software to determine the droplet diameter. From the droplet size distributions, the volume-average droplet diameter, D_v, was calculated by using the following equation:

$$D_v = \sum_i \Phi_i D_i$$

where Φ_i is the volume fraction of the droplets with diameter D_i relative to the total volume of the droplets. Typically, data from 400-600 droplets were used to calculate D_v.

RESULTS AND DISCUSSION

A. Steady-State Deformation and Breakup of Isolated Droplet

Newtonian Blend

When a steady shear flow is applied to an isolated spherical droplet, the droplet simultaneously moves and deforms. If the imposed shear rate is less than the critical shear rate for droplet breakup, a steady-state deformed droplet shape is eventually obtained after sufficient strain. The strain required to reach a steady-state deformation shape increases with increasing applied shear rate and droplet size. For Newtonian droplets sheared in Newtonian matrix at viscosity ratios near unity, Guido and Villone (1998) verified that the steady-state deformed shape of the droplet can be approximated as an ellipsoid having three different principle axes, i.e. a is the major axis of the ellipsoid oriented at a particular angle (θ) within a flow-gradient plane, b is the minor axis in the shear-gradient direction, and c is the minor axis in the vorticity direction.

Figure 6a shows the dependence of the steady-state shape of the droplet in terms of deformation parameter, $\text{Def} \equiv (a-b)/(a+b)$, on the imposed capillary number for blend A0 (low-molecular-weight PBd/PDMS blend), for various droplet sizes, i.e. 180 μm ± 10%, 100 μm ± 10%, 50 μm ± 10%, and 20 μm ± 10% in diameter. As depicted in Figure 6a, the curves for all droplet sizes coincide well with each other, and are also close to Taylor's prediction ($\text{Def} = \text{Ca}\,[(19\eta_r+16)/(16\eta_r+16)]$). The last data point in each curve can be estimated to be the critical point above which the steady-state deformed shape no longer exists and droplet breakup finally occurs. The critical capillary number, Ca_{crit}, for droplet breakup for blend A0 is equal to 0.50 for

droplets with diameter of 180μm ± 10%, 0.52 for diameter 100μm ± 10%, 0.51 for diameter 50μm ± 10%, and 0.54 for diameter 20μm ± 10%. The value of Ca_{crit} obtained from Taylor's prediction is 0.5, which is similar to these results. The good agreement of our results on blend A0 with Taylor's prediction is obtained in both the dependence of Def on the imposed Ca, and in the value of Ca_{crit} for droplet breakup.

Elastic Droplet

As in the A0 blend containing Newtonian components, for the A1 blend containing isolated slightly elastic droplets, the dependence of the deformation parameter on capillary number was the same for various droplet sizes, as shown in Figure 6b, although the capillary number at which breakup occurred monotonically increased with decreasing droplet size. For the A5 blend, however, as shown in Figure 6c, the droplet diameter influences both the capillary number at breakup and the deformation before the breakup condition is reached. As shown in Figures 6b, and 6c, Ca_{crit} monotonically increases with decreasing droplet size for blends A1 and A5. In order to obtain the same value of Ca for a given blend, the applied shear rate has to be higher for a smaller droplet and the degree of elasticity also increases with increasing shear rate. Thus, at the same Ca, the smaller droplet has a higher elasticity, leading to a higher shear rate required for breakup.

To better characterize this elastic effect, the correlation between Def and the imposed Ca for different blends having comparable droplet sizes is plotted on the same graph in Figure 7. For each droplet size, the more elastic droplet deforms less and Ca_{crit} for droplet breakup increases with increasing droplet elasticity. The degree of elasticity of the fluid can be represented by a Weissenberg number (Wi), a ratio of elastic stress to viscous stress. Therefore, we try to determine a quantitative

correlation between the Weissenberg number of the droplet fluid, $Wi_d(\dot{\gamma}) \equiv [\Psi_{1d}(\dot{\gamma})/2\eta_d(\dot{\gamma})].\dot{\gamma}$, and Ca_{crit} for droplet breakup. We obtain the values of the first normal stress difference coefficient, Ψ_1, directly from the measured N_1 or from extrapolated values, if breakup occurred at a shear rate too low to accurately measure the value of N_1. The relationship between Wi_d and Ca_{crit} obtained in this way is shown in Figure 8a, where the closed symbols represent the data obtained from the directly measured N_1 value and the open symbols represent data from extrapolated N_1 values. It should be noted that the shear rate inside the droplet is in general different from the imposed shear rate; it is not uniform and depends on the shape of deformed droplet. The N_1 value inside the droplet, thus, will not be uniform and will be a complex function of shear rate and droplet size. However, for simplicity, we used the nominal N_1 values at the imposed shear rate to calculate Wi_d. As shown in Figure 8a, Ca_{crit} increases linearly with Wi_d up to a value of Wi_d of around 1.0. Interestingly, the Ca_{crit} value of 0.5 is obtained from the extrapolation of the linear regression line to Wi_d equal to zero, which recovers the droplet breakup condition from Taylor's prediction for Newtonian blend. When Wi_d is greater than unity, a downward curvature from linearity is observed, and the Ca_{crit} seems to reach a constant value of 0.95 for a high value of Wi_d. Surprisingly, the asymptotic value of Ca_{crit} of our results is close to the asymptotic value of Ca_{crit} around 0.9 (or 1.8 in the plot of $\eta_m \dot{\gamma}_{crit} D/\Gamma$ versus λ_d/λ_m) reported by Mighri *et al.* (1998). The general conclusion drawn from Figure 8a is that the elasticity of the droplet resists its deformation; however the effect seems to saturate at a value of Ca_{crit} around 0.95 for high values of Wi_d. However, another possible reason for saturation in Ca_{crit} is the shear-thinning behavior of the dispersed phase fluids because all the data at Wi_d above unity are obtained from blend

systems A5 and A10, in both of which the dispersed phase is shear-thinning (see Figures 4, and 5).

Fig. 8a also includes data from our earlier study (Lerdwijitjarud *et al.* 2003), which was limited to a droplet Weissenberg number no higher than 0.02, because of the lower molecular weight of the high-molecular-weight Pbd component in the Boger fluid used in that study. Fig. 8b shows the same data with a logarithmic x axis.

We note that although our blends contained elastic droplets with Wi_d up to around 3, all droplets stretched and broke in the flow direction, as the case with Newtonian droplets. Steady-state droplet vorticity widening (or "vorticity stretching") was not observed in our experiments. Table III shows the rheological data for blend systems in this studied compared with those data taken from literature that reported steady-state vorticity stretching of droplets. From Table III, it seems that we need Wi_d greater than 20 to get steady-state droplet widening in the vorticity direction for blends of "Boger" fluids, which is beyond the range of Wi_d studied here. For blends of high-molecular weight polymer *melts*, however, droplet widening has been detected at Wi_d somewhat lower than unity. Since all of the "Boger" fluid blends have matrix fluids that are Newtonian or only weakly elastic, an alternative explanation may be that the highly elastic matrix fluid boosts up droplet widening. Another relevant point is that the minimum capillary number for which widening occurs has been reported is around 7, which is much greater than the critical capillary number for droplet breakup of the blends studied here. We also point out that the viscosity ratio has been found to play an important role in droplet widening [Jackson and Tucker (2003)], and this parameter was often not well controlled in previous experiments.

B. Steady-State Droplet Size of 10%-dispersed Phase Blend

When the 10%- dispersed phase blends were sheared to a sufficiently high strain, a steady-state morphology was obtained, representing a dynamic equilibrium between droplet breakup and coalescence. From images of the steady-state morphology of concentrated blends containing 10% by weight of the dispersed phase, the steady-state volume-averaged droplet diameter (D_v) and steady-state capillary number (Ca_{ss}) calculated from D_v were determined. Figure 9 shows that Ca_{ss} increases monotonically with increasing elasticity of the dispersed phase for blends A0, A1, A2, A5, and A10. Figure 9 also shows that Ca_{ss} depends on shear rate, even for a nearly Newtonian blend (A0 blend). Possible reasons may include the effect of weak elasticity of the PDMS matrix fluid, or a dependence on shear rate of the critical thickness of the lubricating layer between droplets at which coalescence occurs.

It is also interesting to note that Ca_{ss} obtained from a 10%-dispersed phase blend is smaller than Ca_{crit} obtained from an isolated droplet for the same blend system; that is, the average droplet size in the blend is smaller than the critical size for breakup of an isolated droplet at the same shear rate. This result is initially surprising, since coalescence can occur in the 10% blend, but not for an isolated droplet, and this would tend to make the average droplets bigger in the blends, not smaller, as is actually seen in the experiments. This phenomenon, i.e., droplets in a blend that are smaller on average than the droplet size at which breakup occurs for an isolated droplet at the same shear rate, was previously found when comparing Ca_{ss} of a 20%-dispersed phase blend with Ca_{crit} for an isolated droplet, where both fluids were Newtonian [Lerdwijitjarud *et al.* (2003)]. Jansen *et al.* (2001) used a small concentration of dye-containing droplets added to a blend of the same droplet phase in an immiscible matrix, and observed that the critical capillary number Ca_{crit} for

breakup decreases with increasing concentration of dispersed phase. One possible reason for this phenomenon is that the flow in the blend is locally highly nonuniform and non-steady due to the presence of many other droplets in the vicinity of any one droplet, and this can lead to droplet breakup at a lower average shear rate than occurs for an isolated droplet [Lerdwijitjarud *et al.* (2003)].

We also tried to find a relationship between the degree of droplet elasticity and Ca_{ss} for the blend systems containing 10%-dispersed phase. Since the matrix phase used for all blends is the same pure PDMS, which shows only a very weakly elastic behavior even at high shear rates and its rheological properties do not change much with temperature, the $N_1(\dot{\gamma})$ value of the dispersed phase was chosen to be the index of blend elasticity. Figure 10 depicts the correlation between the steady-state capillary number (Ca_{ss}) and N_1 of dispersed phase ($N_{1d}(\dot{\gamma})$) as a semi-logarithmic plot. This plot shows that Ca_{ss} increases monotonically with N_{1d}, which implies that the elasticity of the dispersed phase resists droplet breakup. However, the maximum value of Ca_{ss} achieved in these experiments is only around 0.6, much less than the value of around five or so observed in experiments with polymer melts [Wu (1985); Cherdhirankorn *et al.* (2003); Lerdwijitjarud *et al.* (2002)], possibly because related to absence of droplet widening which can forestall the breakup process. The scatter in Figure 10 indicates that Ca_{ss} may be affected by factors other than N_{1d}, even though all data were obtained at a viscosity ratio of unity. Other factors that might affect Ca_{ss} might include shear thinning, the second normal stress differences of either phase, or the time-dependent elasticity, as well as interactions of these phenomena with coalescence or breakup. While Figure 10 does provide a clearer correlation of average droplet size with droplet elasticity under better controlled conditions than has heretofore been achieved, more experiments, and especially numerical simulations of

droplet breakup and coalescence for fluids modeled by well defined constitutive equations, will be needed to provide further clarification and more precise correlations.

Conclusions

We studied the contribution of droplet elasticity to steady-state deformation and breakup of isolated polybutadiene (PBd) droplets in a sheared poly(dimethyl siloxane) (PDMS) matrix fluid and on steady-state droplet size in blends of 10%-dispersed Pbd in PDMS under conditions at which both matrix and droplet fluid has the same viscosity. The steady-state deformation of isolated droplets decreases with increasing dispersed phase elasticity for the same imposed capillary number. A linear relationship between critical capillary number for droplet breakup (Ca_{crit}) and dispersed-phase Weissenberg number (Wi_d) holds up to a value of Wi_d around unity, with a saturation of Ca_{crit} at around Ca_{crit} = 0.95 for high Wi_d. The steady-state capillary number (Ca_{ss}) obtained from the average steady-state droplet size in blends containing 10% by weight of dispersed phase is less than the value of Ca_{crit} obtained for an isolated droplet of the same fluid in the same matrix fluid used in the blend. Ca_{ss} increases monotonically with the first normal stress difference of dispersed phase (N_{1d}).

TABLES

Table I: Properties of materials

Materials	Molecular Weight (M_n) (g/mol)	Density at 25 ^{0}C
PDMS	139 000	0.97
PBd	3 900	0.89

Table II: Blend systems studied

Blend	Blend Components (matrix : dispersed)	Testing Temp. (^{0}C)	Γ (mN/m)
A0	PDMS : low-MW PBd	18.3	2.89 ± 0.19
A1	PDMS : 0.1% high-MW PBd solution	19.5	2.80 ± 0.19
A2	PDMS : 0.2% high-MW PBd solution	20.7	2.72 ± 0.22
A5	PDMS : 0.5% high-MW PBd solution	22.0 – 28.0	2.81 ± 0.17 – 2.66 ± 0.28
A10	PDMS : 1.0% high-MW PBd solution	26.0 – 40.0	3.68 ± 0.42 – 2.74 ± 0.13

Table III: The rheological data of blend systems in this studied compared to that from literature.

System	Shear Rate (s^{-1})	Matrix				Droplet				η_r	N_1 ratio (N_{1r})	G' ratio (G'_r)	Ca_1‡	Ca_2§	Ref.
		η*	N_1†	G'	W_i	η	N_1	G'	W_i						
"Boger" Fluids															
A0	1.4	108.1	< 2¶	-	~ 0	108.4	< 1¶	-	~ 0	1.00	-	-	Droplet widening or vorticity stretching is **not** observed.		Verdvijitjarud *et. al.* (present work)
A1	1.8	105.3	< 2¶	-	~ 0	104.7	149	-	0.39	0.99	-	-			
A2	1.8	102.6	< 2¶	-	~ 0	100.6	226	-	0.62	0.98	-	-			
A5	2.2	96.4	< 2¶	-	~ 0	92.5	545	-	1.35	0.96	-	-			
A10	3.9	90.9	< 2¶	-	~ 0	86.4	1943	-	3.14	0.95	-	-			
PIB/ PDMS	5	29.7	5.5	-	0.04	17.8	1200	-	13.5	0.60	185	-	-	-	Migler (2000)
	20	29.7	63	-	0.11	17	19200	-	56.5	0.57	305	-	-	7	
	80	27.3	664	-	0.3	16	307200¶	-	240	0.59	462	-	-	7	
D1/M1	4.6	10	Newtonian		-	13	700	-	11.7	1.3	-	-	5.5	-	Mighri an Huneault (2001)
	9	10			-	13	2350¶	-	20.1	1.3	-	-	-	12	
D2/M2	6.4	30	Newtonian		-	10	74490¶	-	1162	0.33	-	-	5.5	-	
	7.7	30			-	10	100000¶	-	1300	0.33	-	-	-	6.5	
D2/M1	48.2	10	Newtonian		-	2	500000¶	-	5185	0.2	-	-	9	-	
Polymer Melts															
PS1/PE2	280	175	288000¶	-	5.88	303	460000¶	-	5.42	1.73	1.60	-	53	-	Hobbie and Migler (1999)
	320	170	300000¶	-	5.51	278	560000¶	-	6.29	1.64	1.87	-	-	60	
PS1/PE1	290	22	41780	-	6.55	288	14497	-	0.17	13	0.35	-	13	-	
	700	14.5	57288	-	5.64	207	31041	-	0.21	14	0.54	-	-	31	
A	0.28	2524	403	135	0.38	2370	205	70	0.21	0.94	0.51	0.52	-	-	Cherdhirankorn *et. al.* submitted to Rheologica acta
	0.3	2505	435	145	0.39	2360	226	78	0.22	0.94	0.52	0.54		12	
	0.5	2340	772	250	0.43	2270	468	181	0.32	0.97	0.61	0.72			
	0.8	2170	1310	410	0.47	2133	912	395	0.46	0.98	0.70	0.96	-	-	
B	1.0	603	-	34.2	0.11	619	-	64.7	0.21	1.03	-	1.89	-	28	

* η [=] Pa.s
† N_1, G' [=] Pa
‡ Ca at which droplet first contracts in the flow direction after having stretched in the flow direction.
§ Ca at which droplet reorients to the vorticity alignment
¶ Extrapolated values

FIGURE CAPTIONS

Figure 1. The dependence on shear rate of steady-state viscosity (open symbols) and of the first normal stress difference (closed symbols) for low-molecular-weight PBd and PBd "Boger" fluids at 18.3 ^{0}C.

Figure 2. The dependence of zero-shear viscosity on the weight percentage of high-molecular-weight PBd added to low molecular-weight Pbd. The filled symbols are in the range where the viscosity depends linearly on concentration.

Figure 3. The shear-rate dependence of the viscosity of PDMS (O) and of low-molecular-weight PBd or PBd "Boger" fluids(!) as well as the shear-rate dependence of the first normal stress difference of PDMS (1), and of PBd "Boger" fluids (+) for (a) blends A0, (b) A1, and (c) A2 at temperatures chosen such that the PDMS and Pbd fluids have nearly the same viscosity.

Figure 4. The shear-rate dependence of the viscosity of PDMS (O), and of PBd "Boger" fluids (!), and the shear-rate dependence of the first normal stress difference of PDMS (1), and of PBd "Boger" fluid (+) for blend A5 at a series of temperatures.

Figure 5. The same as Figure 4, except for blend A10.

Figure 6. The dependence of the deformation parameter on capillary number for blends (a) A0, (b) A1, and (c) A5 for various droplet sizes.

Figure 7. The dependence of deformation parameter on capillary number for blends A0, A1, A2, A5, and A10 for droplet diameters of (a) 180μm ± 10%, (b) 100μm ± 10%, (c) 50μm ± 10%, and (d) 20μm ± 10%.

Figure 8. The dependence of critical capillary number for droplet breakup (Ca_{crit}) on Weissenberg number of the dispersed phase (Wi_d) (a) linear plot, and (b) semi-log plot. The closed symbols represent the data obtained from the measured N_1 values and the open symbols from extrapolated N_1 values. Data from earlier work (Lerdwijitjarud, et al. 2003) are also included.

Figure 9. The shear-rate dependence of steady-state capillary number (Ca_{ss}) for all 10%-dispersed phase blends studied.

Figure 10. The dependence of the steady-state capillary number (Ca_{ss}) on the first normal stress difference of dispersed phase (N_{1d}) for blends A1, A2, A5, and A10.

REFERENCES

1. Bentley, B.J., and L. G. Leal, "An experimental investigation of drop deformation and breakup in steady, two-dimensional linear flows," *J. Fluid Mech.*, **167**, 241-283 (1986).
2. Boger, D. V. and R. J. Binnington, "Separation of elastic and shear thinning effects in the capillary rheometer", *Trans. Soc. Rheol.* **21**, 515-534 (1977).
3. Chaffey, C. E. and H. Brenner, "A second-order theory for shear deformation of drops", *J. Colloid Interface Sci.* **24**, 258-269 (1967).
4. Cherdhirankorn T., W. Lerdwijitjarud, A. Sirivat, and R. G. Larson, "Dynamics of Vorticity Stretching and Breakup of Isolated Viscoelastic Droplets in an Immiscible Viscoelastic Matrix" submitted to *Rheologica Acta* (2003).
5. De Bruijn, R. A., "Deformation and breakup of drops in simple shear flow", Ph.D.Thesis, Eindhoven University of Technology, 1989.
6. Elmendorp, J. J. and R. J. Maalcke, "A study on polymer blending microrheology: Part 1", *Polym Eng. Sci.* **25**, 1041-1047 (1985).
7. Flumerfelt, R. W."Drop breakup in simple shear fields of viscoelastic fluids", *Ind. Eng. Chem. Fundam.*, **11**, 312-318 (1972).
8. Grace, H. P., "Dispersion phenomena in high viscosity immiscible fluid systems and application of static mixers as dispersion devices in such systems", *Chem. Eng. Commun.* **14**, 225-277 (1982).
9. Graebling, D., R. Muller, and J. F. Palierne, "Linear viscoelastic behavior of some incompatible polymer blends in the melt. Interpretation of data with a model of emulsion of viscoelastic liquids", *Macromolecules* **26**, 320-329 (1993).

10. Guido, S., and M. Villone, "Three-dimensional shape of a drop under simple shear flow", *J. Rheol.* **42**, 395-415 (1998).

11. Guido, S., and M. Villone. "Measurement of interfacial tension by drop retraction analysis", *J. Colloid and Interface Science*, **209**, 247-250 (1999).

12. Hobbie, E. K. and K. B. Migler, "Vorticity elongation in polymeric emulsions," *Phys. Rev. Lett.* **82**, 5393-5396 (1999).

13. Jackson, N. E. and C. L. Tucker III, "A model for large deformation of an ellipsoidal droplet with interfacial tension", *J. Rheol.* **47**, 659-682 (2003).

14. Jansen, K. M. B., W. G. M. Agterof, and J. Mellema, "Droplet breakup in concentrated emulsions", *J. Rheol.* **45**, 227-236 (2001).

15. Kennedy, M. R., C. Pozrikidis, and R. Skalak, "Motion and deformation of liquid drops, and the rheology of dilute emulsions in simple shear flow", *Comput. Fluids* **23**, 251-278 (1994).

16. Lerdwijitjarud, W., A. Sirivat, and R. G. Larson, "Influence of elasticity on dispersed-phase droplet size in immiscible polymer blends in simple shearing flow", *Polym. Eng. Sci.* **42**, 798-809 (2002).

17. Lerdwijitjarud, W., R. G. Larson, and A. Sirivat, "Influence of weak elasticity of dispersed phase on droplet behavior in sheared polybutadiene/ Poly(dimethylsiloxane) blends," *J. Rheol.* **47**, 37-57 (2003).

18. Levitt, L., C. W. Macosko and S. D. Pearson, "Influence of normal stress difference on polymer drop deformation", *Polym. Eng. Sci.* **36**, 1647-1655 (1996).

19. Luciani, A., M. F. Champagne, L. A. Utracki, "Interfacial tension coefficient from the retraction of ellipsoidal drops", *J. Polym. Sci. Pol. Phys.* **35**, 1393-1403 (1997).

20. Mighri, F., P. J. Carreau, and A. Ajji, "Influence of elastic properties on drop deformation and breakup in shear flow" *J. Rheol.* **42**, 1477-1490 (1998).

21. Mighri, F. and M. A. Huneault, "Dispersion visualization of model fluids in a transparent Couette flow cell," *J. Rheol.* **45**, 783-797 (2001).

22. Migler, K. B., "Droplet vorticity alignment on model polymer blends," *J. Rheol.* **44**, 277-290 (2000).

23. Milliken, W. J., and L. G. Leal, "Deformation and breakup of viscoelastic drops in plannar extensional flows", *J. Non-Newtonian Fluid Mech.*, **40**, 355-379 (1991).

24. Mo, H., C. Zhou, and W. Yu, "A new method to determine interfacial tension from the retraction of ellipsoidal drops", *J. Non-Newtonian Fluid Mech.* **91**, 221-232 (2000).

25. Okamoto, K., M. Takahashi, H. Yamane, H. Kashihara, H. Watanabe and T. Masuda, "Shape recovery of a dispersed droplet phase and stress relaxation after application of step shear strains in a polystyrene/polycarbonate blend melt", *J. Rheol.* **43**, 951-965 (1999).

26. Palierne, J. F., "Linear rheology of viscoelatic emulsions with interfacial tension", *Rheol. Acta* **29**, 204-214 (1990).

27. Rallison J. M., and A. Acrivos, "numerical study of deformation and burst of a viscous drop in an extensional flow", *J. Fluid Mech.*, **89**, 191-200 (1978).

28. Taylor, G. I., "The viscosity of a fluid containing small drops of another fluid", *Proc. R. Soc. London*, Ser. A **138**. 41-48 (1932).

29. Taylor, G. I., "The formation of emulsions in definable fields of flow", *Proc. R. Soc. London*, Ser. A **146**, 501-523 (1934).

30. Tretheway D. C., and L. G. Leal, "Deformation and relaxation of Newtonian drops in planar extensional flows of a Boger fluid" *J. Non-Newtonian Fluid Mech.* **99**, 81-108 (2001).

31. Uijittewaal, W. S. J. and E. J. Nijhof, "The motion of a droplet subjected to linear shear flow including the presence of a plane wall", *J. Fluid Mech.* **302**, 45-63 (1995).

32. Varanasri, P. P., M. E. Ryan, and P. Stroeve, "Experimental study on the breakup of Model viscoelastic drops in uniform shear flow", *Ind. Eng. Chem. Res.* **33**, 1858-1866 (1994)

33. Wu, S., "Phase structure and adhesion in plymer blends: A criterion for rubber toughening", *Polymer* **26**, 1855-1863 (1985).

34. Wu, S., "Formation of Dispered phase in incompatible polymer blends-interfacial and rheological effects." *Polym. Eng. Sci.* **27**, 335-343 (1987).

35. Xing, P., M. Bousmina, and D. Rodrigue, "Critical experimental comparison between five techniques for the determination of interfacial tension in polymer blends: model system of polystyrene/polyamide-6", *Macromolecules* **33**, 8020-8034 (2000).

36. Yamane, H., M. Takahashi, R. Hayashi, K. Okamoto, H. Kashihara and T. Masuda, "Observation of deformation and recovery of poly(isobutylene) droplet in a poly(isobutylene)/poly(dimethyl siloxane) blend after application of step shear strain", *J. Rheol.* **42**, 567-580 (1998).

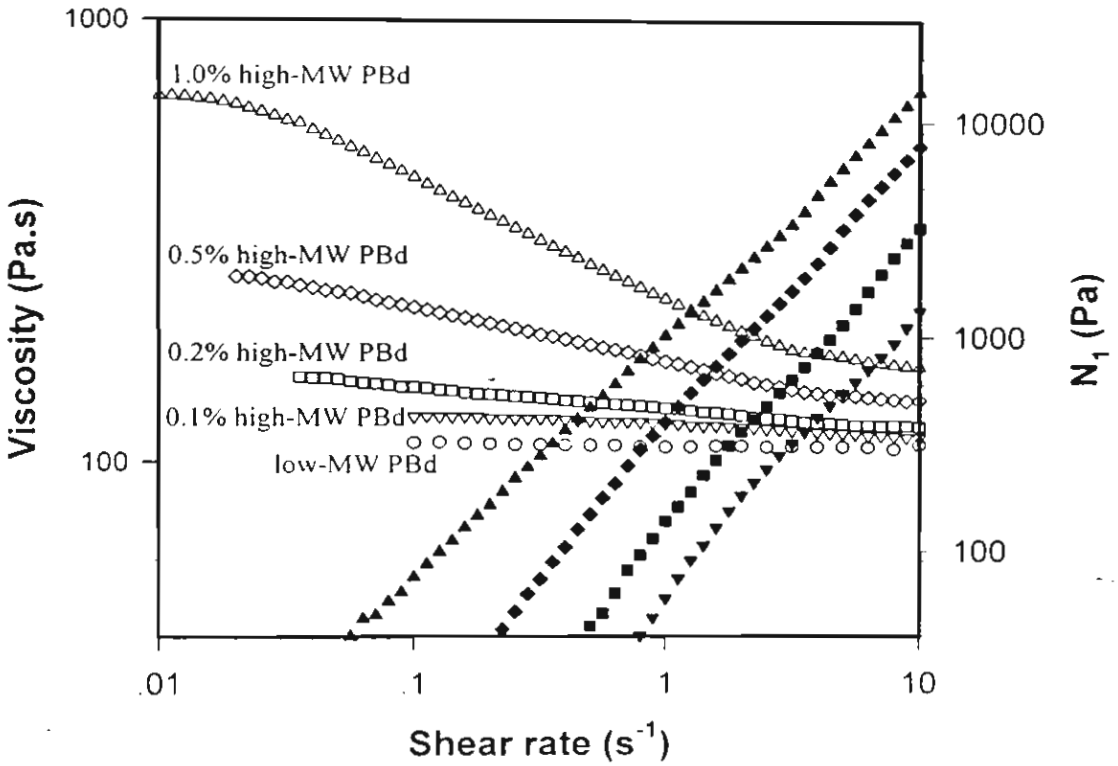

Lerdwijitjarud *et al.*, Figure 1

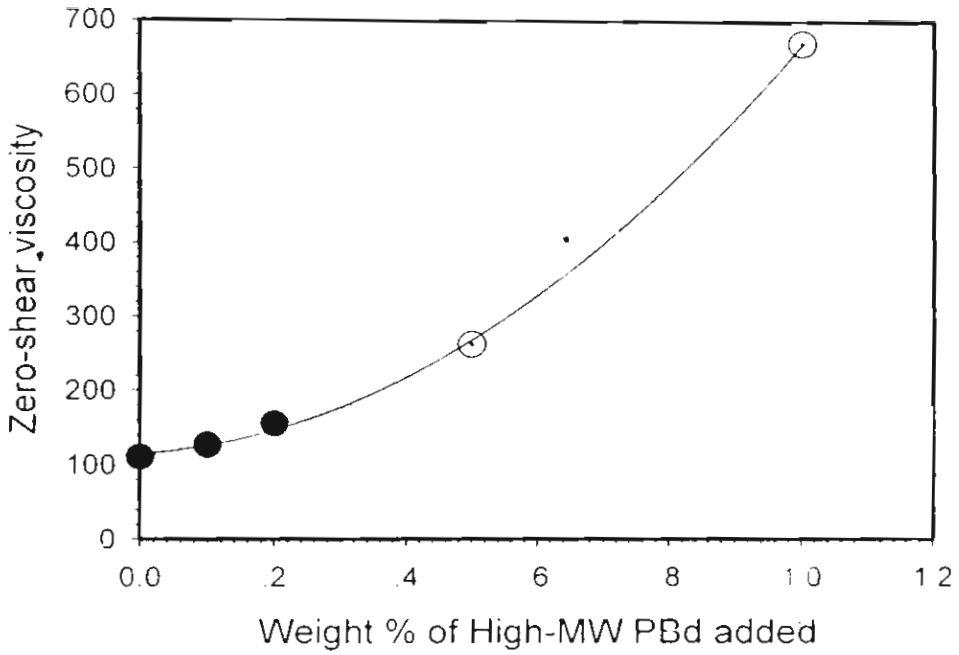

Lerdwijitjarud *et al.*, Figure 2

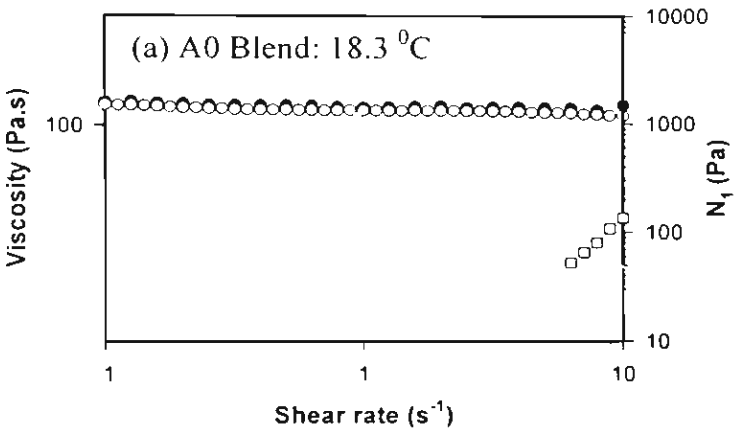

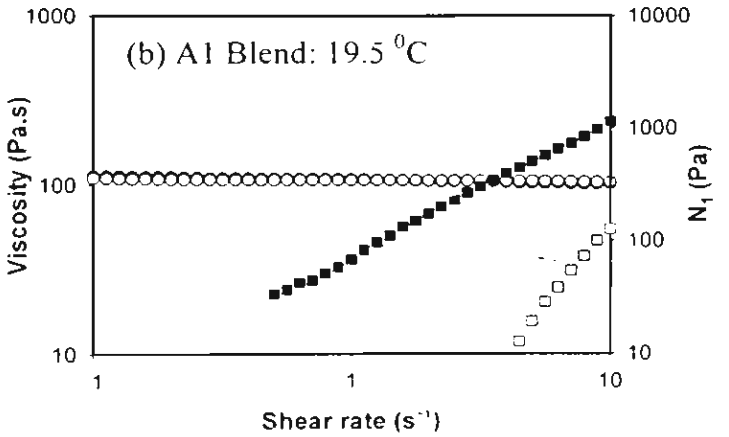

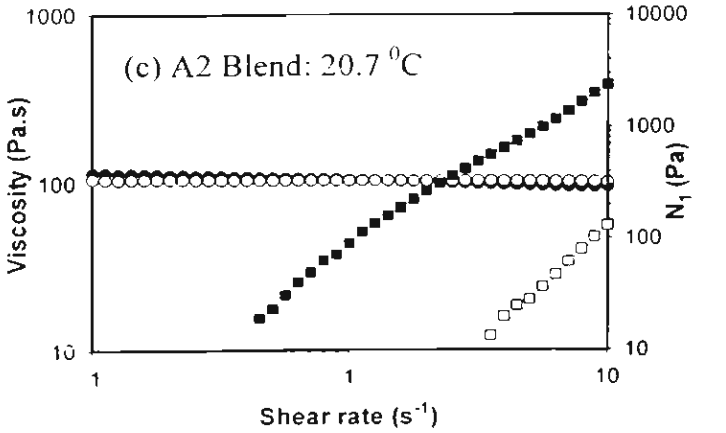

Lerdwijitjarud *et al.*, Figure 3(a), 3(b), and 3(c)

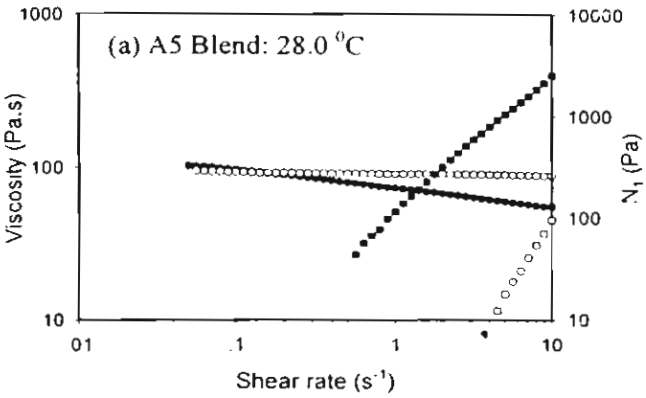

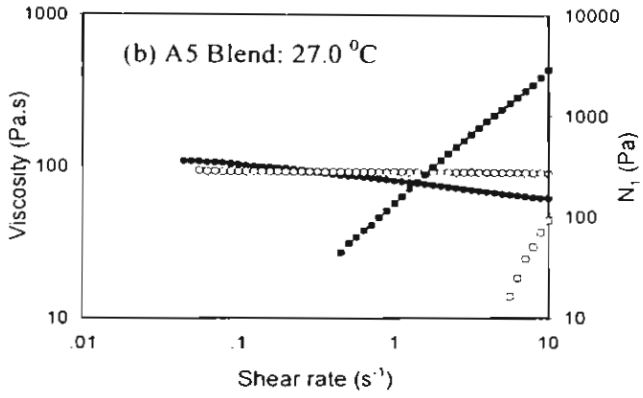

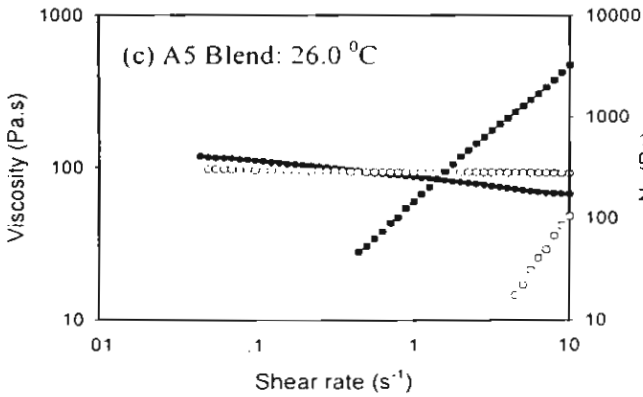

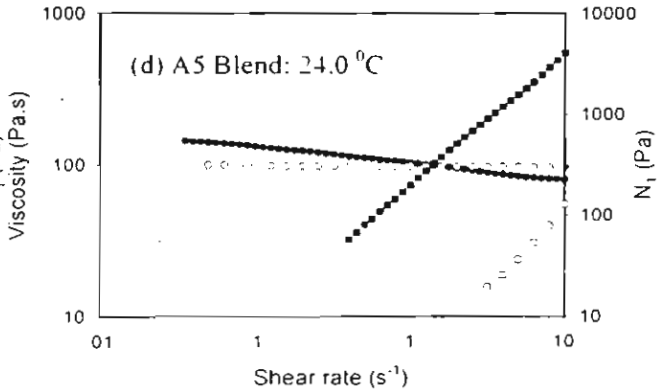

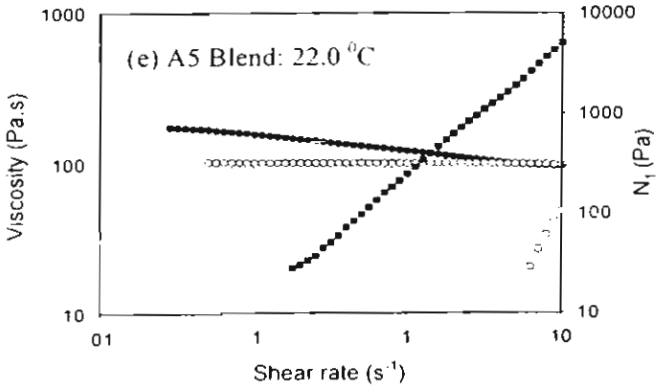

Lerdwijitjarud *et al.*, Figure 4(a), 4(b), 4(c), 4(d), and 4(e)

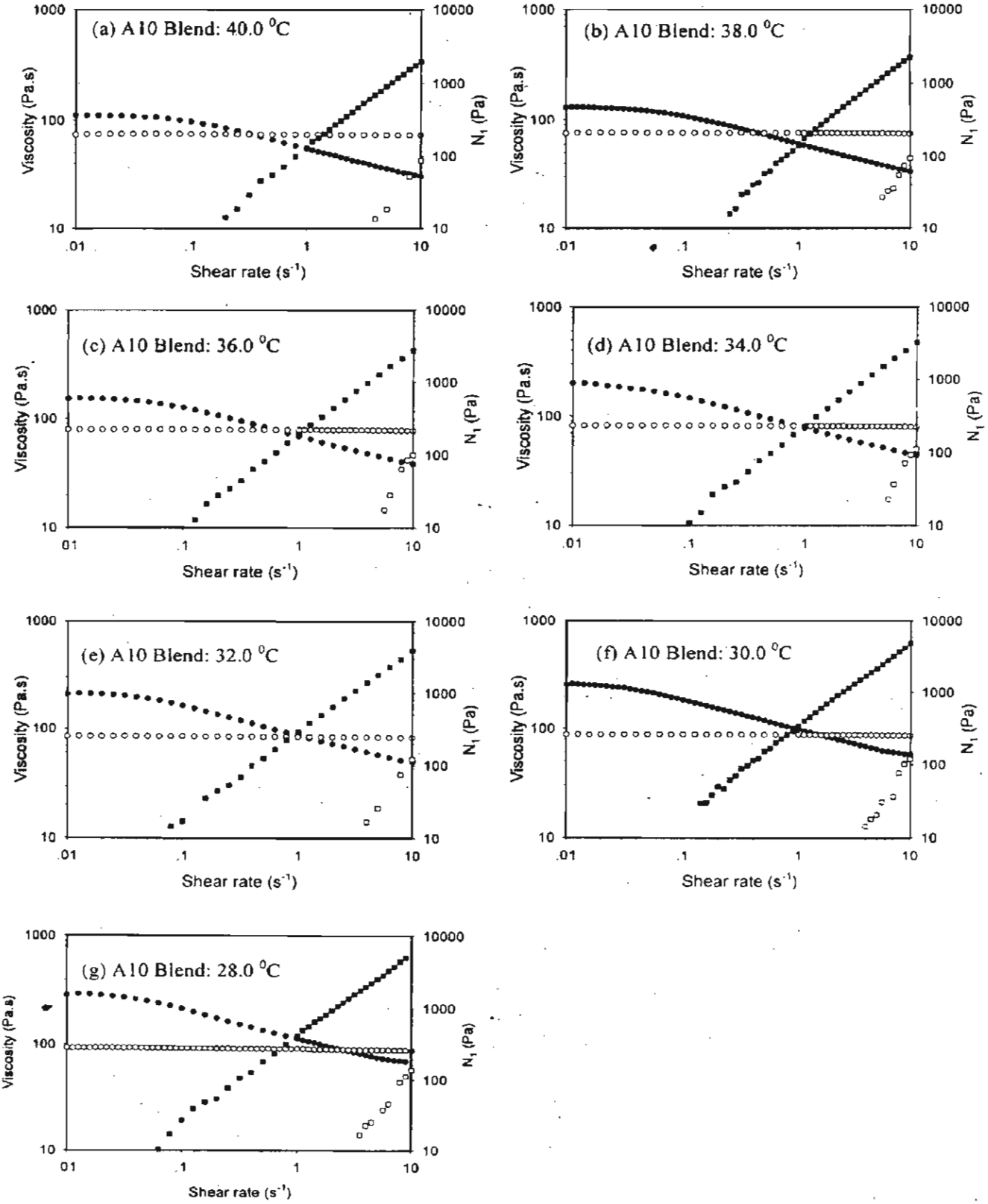

Lerdwijitjarud *et al.*, Figure 5(a), 5(b), 5(c), 5(d), 5(e), 5(f), and 5(g)

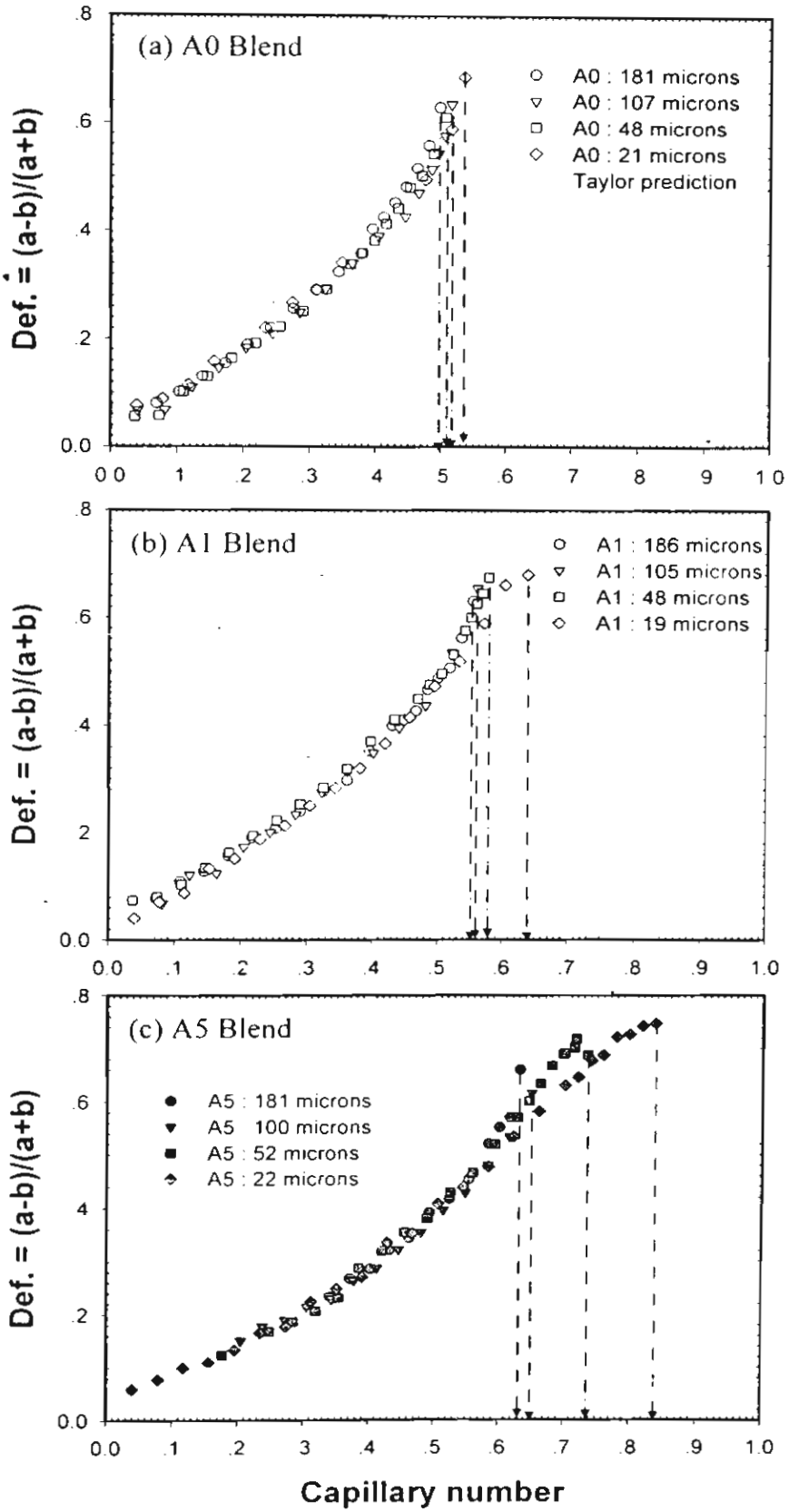

Lerdwijitjarud *et al.*, Figure 6(a), 6(b), and 6(c)

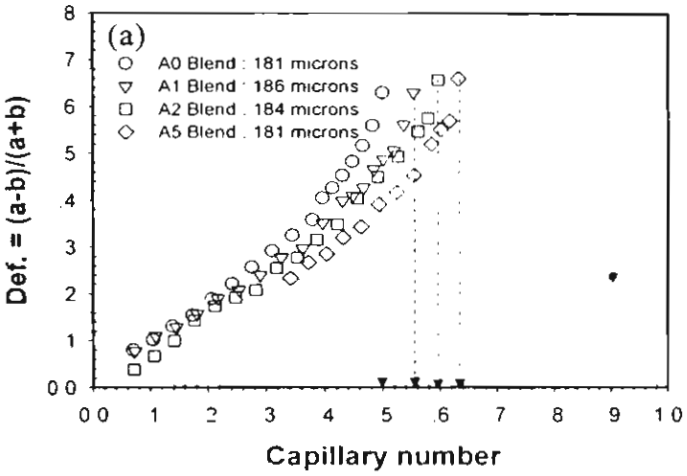

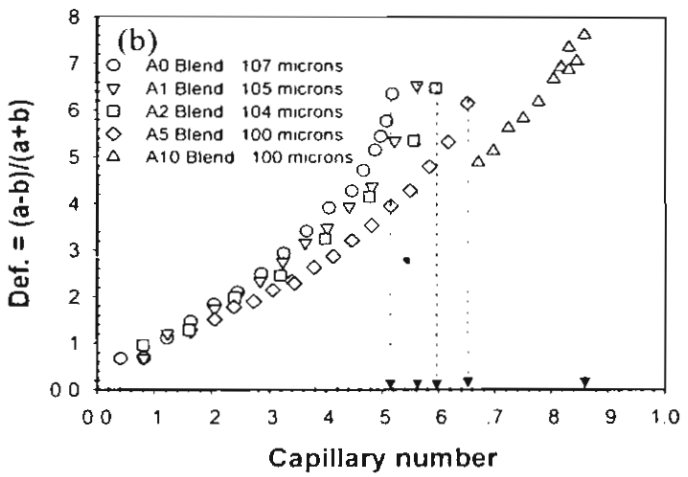

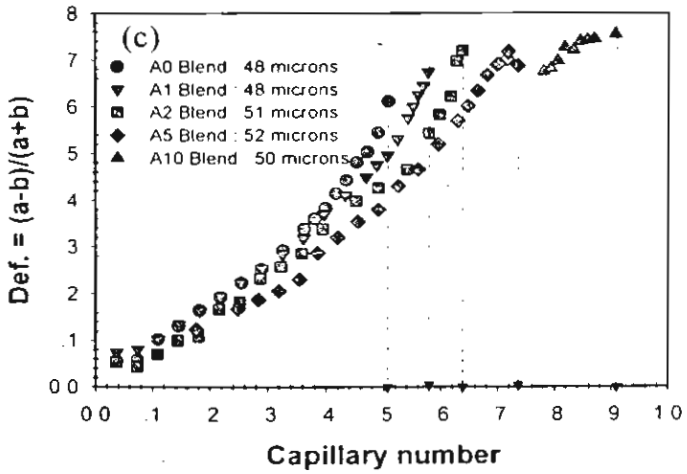

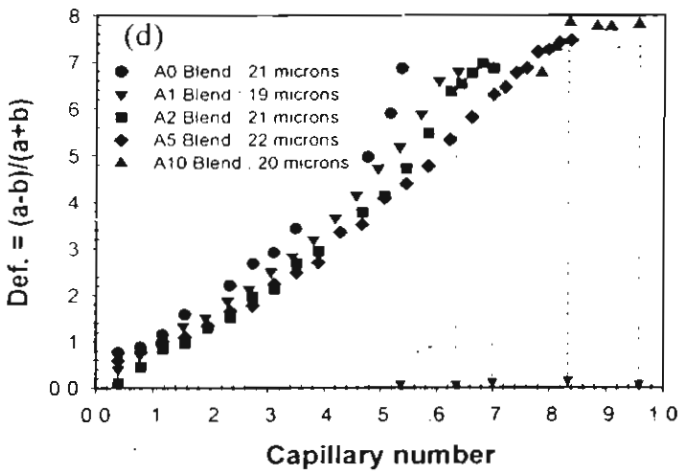

Lerdwijitjarud *et al.*, Figure 7(a), 7(b), 7(c), and 7(d)

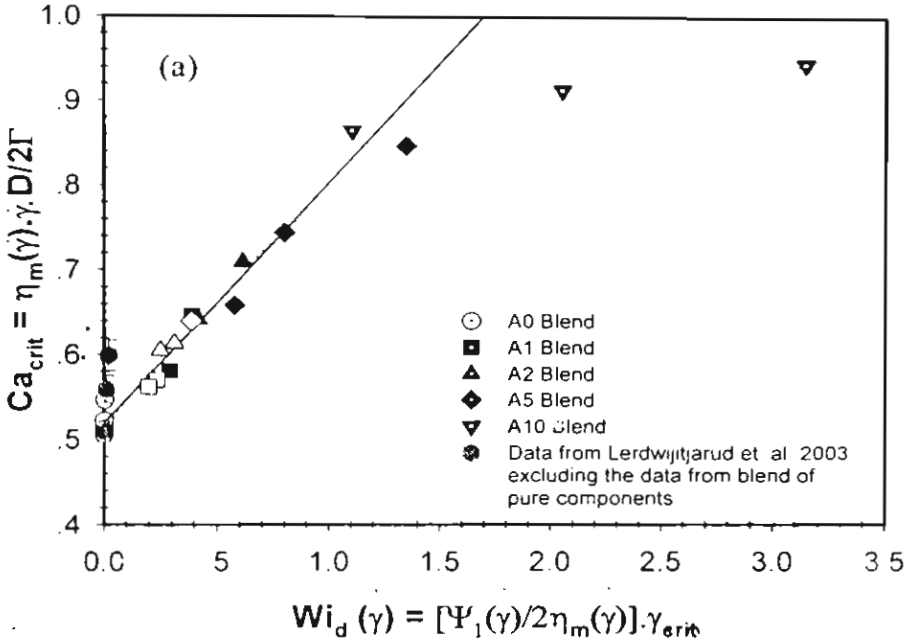

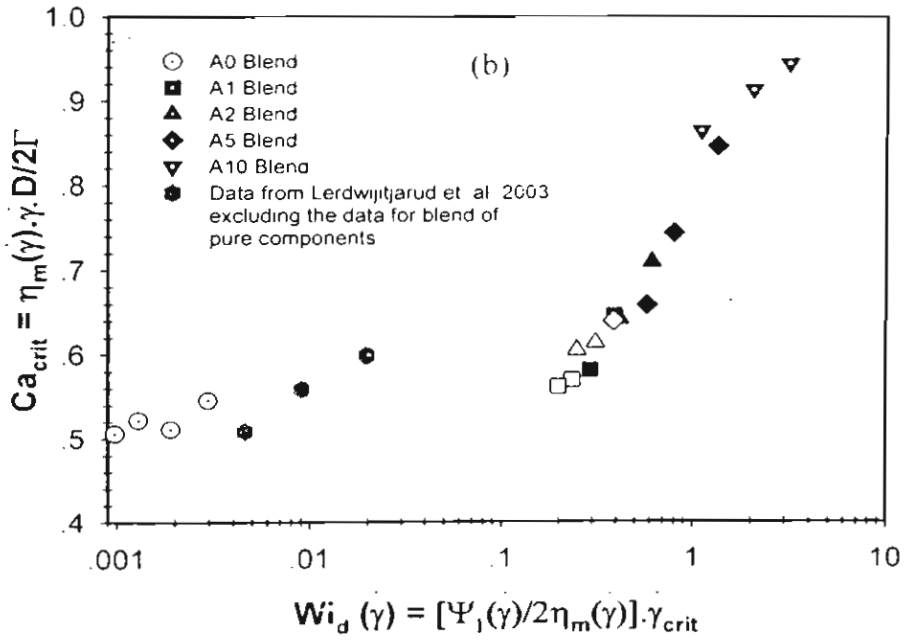

Lerdwijitjarud *et al.*, Figure 8(a), and 8(b)

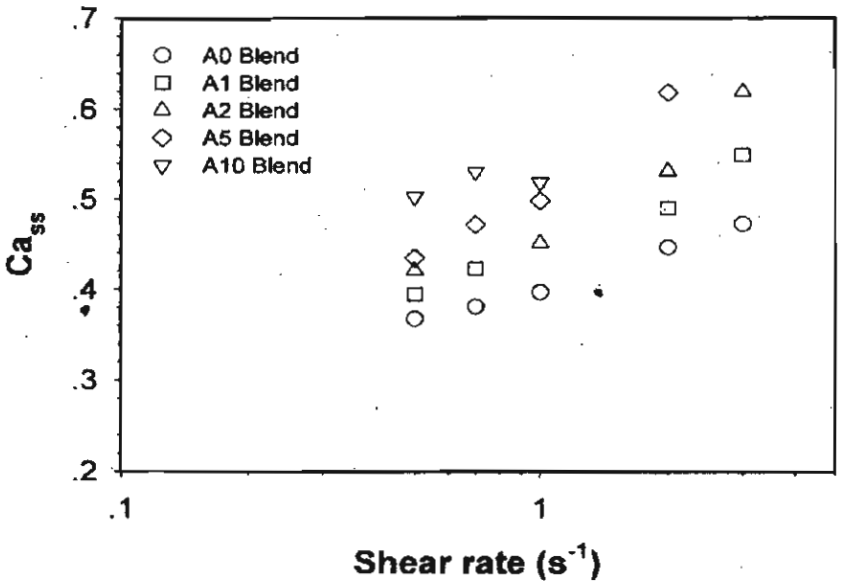

Lerdwijitjarud *et al.*, Figure 9

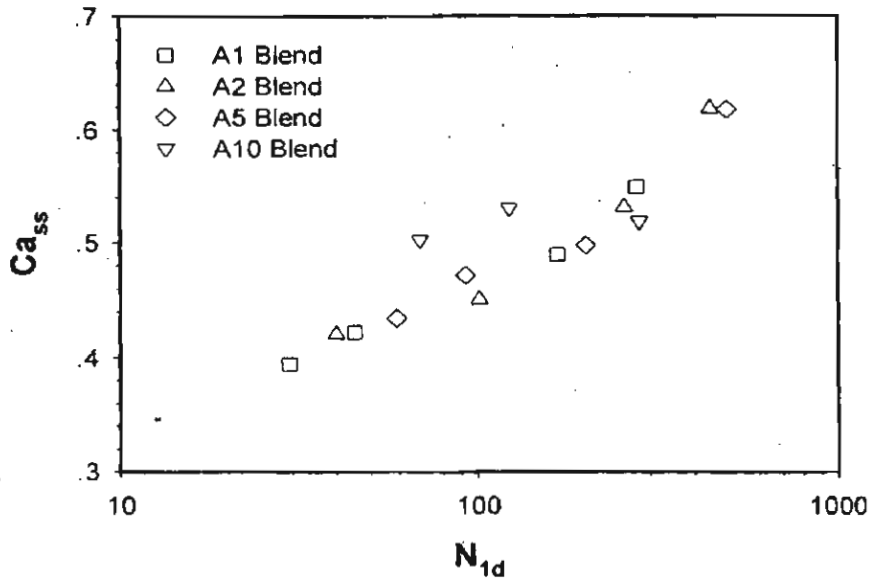

Lerdwijitjarud *et al.*, Figure 10